Brain Signal Processing and Neurological Therapy

Pan Yaozhang

Email:yaozhang.pan@nus.edu.sg

Tel:96587036

(B.Eng, Harbin Institute of Technology)

(M.Eng, Harbin Institute of Technology)

A THESIS SUBMITTED

FOR THE DEGREE OF DOCTOR OF PHILOSOPHY

DEPARTMENT OF ELECTRICAL & COMPUTER ENGINEERING

NATIONAL UNIVERSITY OF SINGAPORE

Sep. 2009

Acknowledgements

I am grateful to all the people who have encouraged and supported me during my PhD study, which has led to this thesis.

Firstly, I am deeply gratitude to my supervisor, Professor Shuzhi Sam Ge, for his constant and patient guidance, inspiration, and support, especially for the selfless sharing of his invaluable experiences and philosophies in and beyond research. I sincerely thank my co-supervisor, Professor Abdullah Al Mamun, for his constant support and help during my PhD program. I thank both my supervisors for their passion and painstaking efforts in training me, without which I would not have honed my research skills and capabilities as well as I did in my Ph.D studies. My appreciation goes to Professor Cheng Xiang and Professor Woei Wan Tan in my thesis committee, for their kind help and advice.

At work I have had the great fortune of working with brilliant people who are generous with their time and friendship. Special thanks must be made to Dr. Feng Guan, with whom a number of discussions on research have been made. Thanks to Mr. Qing Zhuang Goh, who worked closely with me and contributed much valuable programming and experiment during his final year project. Thanks to Mr. Chengguang Yang and Ms. Beibei Ren, my fellow adventurers in the research course, for their encouragement and friendship. Many thanks to my seniors, Dr. Pey Yuen Tao, Dr. Keng Peng Tee, Dr. Cheng Heng Fua, Dr. Thanh Trung Han, Dr Xuecheng Lai, Dr Zhuping Wang, Dr Fan Hong and Mr. Yong Yang for their generous help since the day I joined the research team. To Dr. Bingbing Liu, Dr Hongbin Ma, Dr Rongxin Cui, Dr Mou Chen, Mr Voon Ee How, and Dr Yu Kang for many

enlightening discussions and help they have provided in my research. I would also like to thank Mr Qun Zhang, Mr Yanan Li, Mr Hongsheng He, Mr Wei He, Mr Zhengcheng Zhang, Mr Hewei Lim, Mr Sie Chyuan Law, Dr. Jing Liu, Dr. Kok Zuea Tang and many other fellow students/colleagues for their friendship, valuable help and the happy time we have enjoyed together.

To my family, for their generous and unconditional support through the good times and the bad.

Finally, I am very grateful to the National University of Singapore for providing me with the research scholarship to undertake the PhD study.

Contents

Abstract

Advances in cognitive neuroscience, brain imaging and signal processing technologies provide us with an increasing array of diagnostic and therapeutic technologies for neurological disorders. Some important application areas of neurological therapy include: brain tumors, developmental disorders, epilepsy, motor neuron diseases, muscular dystrophies, neurogenetic disorders, pain, Parkinson's pathology and stroke.

In this thesis, neurological therapies which consist of advanced engineering technologies such as brain imaging, signal processing, pattern recognition, intelligent control, and advanced robotics are presented for motivating future development of neurological therapies. Three major neurological disorders - epilepsy, stroke, and autism are studied, and neurological therapies are proposed as aid in the treatment of these neurological disorders. By investigating the characteristics of these neurological disorders, pattern recognition based brain signal processing approaches, and multimodal human robot interaction (HRI) based advanced robotics are presented for neurological therapies of these neurological disorders.

The first application is the detection and prevention of epilepsy. For detection of epileptic seizures, a new electroencephalography (EEG)-based brain state identification method is presented. Several statistical features which are specifically suited for detection of epileptic

spike waves are derived and support vector machine (SVM) is used to classify the low-dimensional features. It is illustrated by experimental evaluation that the proposed method is a promising way for automatic seizure detection. Once epileptic states are identified from normal states of epilepsy patients, the problem of controlling the synaptic plasticity to constrain bursting activity in epileptic seizures can be addressed by a direct drug injection or electrical stimulation of related brain region. With a good understanding of dynamical changes in the brain during seizures onset and the mechanisms that cause these changes, a model based control is designed to develop close-loop stimulation system for brain states restoration in epileptic seizures onset. Numerical simulations are carried out to illustrate the effectiveness of the proposed controls.

Another important application is stroke rehabilitation. Clinical studies have shown that robotic rehabilitation helps to improve impairment of the upper limb after chronic stroke. Recently, brain computer interface (BCI)-based robotic rehabilitation is introduced which directly translates brain signals that involve motor or mental imagery into commands for controlling the robot and bypasses the normal motor output neural pathways. In this work, a human-friendly interactive robot is developed as a visual and motion feedback for BCI system to help the patients to be more cognitively engaged in rehabilitative training process. For the BCI system, a feature fusion of common spatial pattern (CSP) and autoregressive (AR) spectral analysis is proposed to extract features from EEG signal with left hand movement imagination or right hand movement imagination for further classification of these two brain states. Quadratic discriminant analysis (QDA) is utilized as classifier for the combined feature vectors. The feature fusion method is proved to outperform each of the single-feature extraction algorithms in motor imagery BCI system through both off-line

and real-time experiments.

Finally, social therapy of autism is studied based on some well-developed hypothesis of cognitive and social science. An interactive robot, RoBear, is developed with multimodal HRI to help autistic children become more socially engaged. Under the multimodal HRI framework we proposed in this study, RoBear is able to identify the face and voice, and sensitive to the emotional change of the human working with it. Scale invariant neighborhood linear embedding (SINLE) is proposed for sound source recognition motivated by neighborhood linear embedding (NLE) and scale adaptation of human's perception. Weighted locally linear embedding (WLLE) motivated by weighted distance measurement and locally linear embedding (LLE) is proposed for feature extraction of face images to obtain more compact and low-dimensional representations. WLLE is demonstrated to outperform several well-known face recognition algorithms through extensive experiments. For the social rehabilitation process, training scenarios are designed based on hypotheses of cognitive science and social psychology, in the form of games between child and robot. During the interaction between child and robot, the robot will elicit physical and psychological states of the child, followed by therapy of management according to social norms.

Through these neurological therapies based on brain signal processing and advanced robotics, how advanced engineering technologies such as brain imaging, signal processing, pattern recognition, intelligent control, and advanced robotics allow for effective design of therapeutic schemes achieving brain states restoration are shown for motivating future development concerning the spectrum of neurological therapy.

List of Figures

List of Tables

List of Abbreviations

AED	antiepileptic drugs
ANN	artificial neural networks
AR	autoregressive
ASD	autism spectrum disorders
BCI	brain computer interface
BPNN	back propagation neural network
CCBs	calcium channel blockers
CKFD	complete kernel fisher discriminant
CSP	common spatial pattern
DBS	deep brain stimulation
DLDA	direct linear discriminant analysis
ECoG	electrocorticography
EEG	electroencephalography
ELM	extreme learning machine
ERP	event related potential
ERD	event-related desynchronization
ERS	event-related synchronization
fMRI	functional magnetic resonance imaging

HRI	human robot interaction
I-EEG	intracranial EEG
KDDA	kernel direct discriminant analysis
KNN	K nearest neighbors
KPCA	kernel principal components analysis
LDA	linear discriminant analysis
LLE	locally linear embedding
MEG	magnetoencephalographic
MI-BCI	motor imagery brain-computer interface
NIRS	near infrared spectroscopy
NLE	neighborhood linear embedding
PCA	principal components analysis
PET	positron emission tomography
PSD	power spectral density
QDA	quadratic discriminant analysis
RBFNN	radial basis function neural network
RNS	responsive neurostimulation system
SE	status epilepticus
SINLE	scale invariant neighborhood linear embedding
SLFN	single hidden layer feedforward network
SPECT	single photon emission computed tomography
SVM	support vector machine
VNS	vagus nerve stimulation
WLLE	weighted locally linear embedding

Chapter 1

Introduction

1.1 Background and Motivation of Research

In recent years, brain signal processing has received much attention and many significant advances have been made in this field. Brain signal processing refers to investigations on analysis, extraction, enhancement, detection, localization, recognition and classification of brain signals and patterns. Due to the complexity and nonlinear characteristic of brain signal, research on brain signal processing is still focusing on development of the fundamental data analysis methodologies. A great number of research articles, books, reporting algorithms, and applications within the fields of analysis and recognition of brain signals and patterns have been published in various journals and conferences. How to make a good use of brain signal sensing and processing technologies in real world for practical applications is still an open problem.

Among the well-known applications of brain signal processing, neurological therapy is

one of the most important and promising areas. Neurological therapy, also called neurological rehabilitation, refers to a series of diagnostic and therapeutic technologies for neurological disorders. Advances in cognitive neuroscience, brain imaging and engineering technologies such as signal processing and pattern recognition provide us with an increasing array of necessary technologies for novel neurological therapy. However, because many aspects of neurological functioning and illness are not yet fully understood, it is still challenging to aid the treatment of neurological diseases by the available brain signal processing and pattern recognition technologies for obtaining optimal effect of neurological therapy.

This research aims to develop fundamental brain signal processing and pattern recognition algorithms. Furthermore, based on current advances in robotics, interactive robot with multimodal HRI is developed and applied for designing novel neurological therapeutic schemes. Through presentation of three different applications in neurological therapy, how advanced engineering technologies such as brain imaging, signal processing, pattern recognition, intelligent control, and advanced robotics allow for effective design of therapeutic schemes that achieve brain states restoration are shown for motivating future development concerning the spectrum of neurological therapy.

1.2 Brain Imaging Techniques

During the past decade, a number of techniques have been developed for brain activities monitoring and recording based on different bio-sensors, and can be classified into two main classes of invasive or non-invasive.

Invasive methods refer to intracranial methods for measuring brain activities, which

is called electrocorticography (ECoG) or intracranial EEG (I-EEG). In these methods, electrodes are implanted intracranially in either single cortical area or multiple areas simultaneously. A single area method records neuronal activity from a specific area. These methods are usually used in some BCI applications [1,2] or some medical diagnosing applications [3–6]. These methods suffer from instability related to variability of neuronal activity and changes in the sampled populations of neurons. This problem can be conquered by utilizing a multiple recording method, which can take in the advantages of distributed information of the whole brain, so that it can provide stable signals for controlling prosthesis with multiple degree of freedom and other complicated mechatronics systems [7–14], or gaining fundamental knowledge for analysis of the human neural network mechanism [15, 16]. However, the invasive methods for monitoring brain activity are not easily acceptable for their possible dangers caused by brain intrusion. Furthermore, the huge quantity of data to be processed bring in computational complexity for implementation.

The non-invasive ways include, but are not limited to: EEG that directly measures the electrical activity of the brain; magnetoencephalographic (MEG) that measures the magnetic fields produced by electrical activity in the brain; functional magnetic resonance imaging (fMRI) and near infrared spectroscopy (NIRS) which detect changes of blood oxygen levels in active brain areas; and a series of nuclear medical imaging techniques such as positron emission tomography (PET) and single photon emission computed tomography (SPECT). Different from intracranial methods, most of the non-invasive methods are only brain function tests and gross correlates of brain activity. Compared to the invasive brain imaging techniques, the major advantage of non-invasive techniques is that it requires no brain surgery operation, and avoids the risk of possible dangers. The spatial resolution, time

resolution [17–19], hardware complexity and cost [18] of these brain imaging techniques are briefly presented in Fig. 1.1.

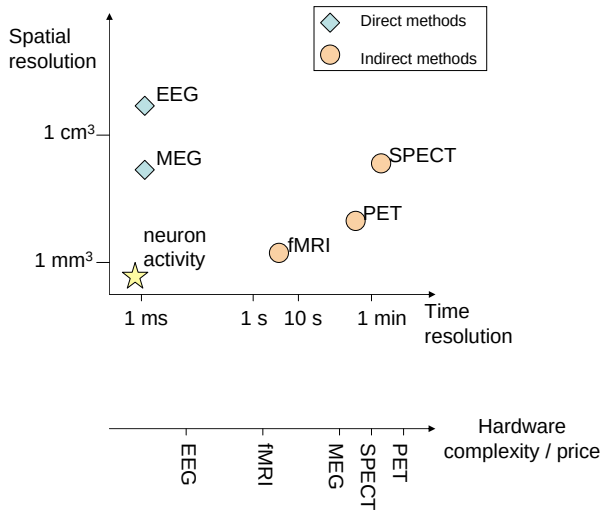

Figure 1.1: Core features comparison of brain imaging techniques

Among these methods, PET as well as SPECT is partially invasive as it requires radioactive injection which may have potential harm to human, though no surgery operation is needed [20, 21]. fMRI does not require radioactive injection but still causes exposure to X-rays. It can record on a spatial resolution in the region of 3-6 millimeters, but with relatively poor temporal resolution compared to EEG. This may result from that fMRI measures blood activity which has a slower response while EEG measures electrical/neural activity directly with fast response.

NIRS is typically used in pharmaceutical, medical diagnostics such as blood sugar and oximetry, food and agrochemical quality control, and combustion research. To apply NIRS as an alternative and direct way of brain functional imaging is a relatively novel idea. NIRS has a few merits like high degree of flexibility, high biochemical specificity, and high

sensitivity in detecting small substance concentrations [22]. Similar to EEG, NIRS also has the disadvantage of low spatial resolution. Despite this limitation, the advantages of NIRS make it a promising way of brain functional imaging. Recently, it was claimed in [23–25] that the optical response of NIRS denoting brain activation can be used as an alternative to electrical signals as EEG, with the intention of developing a more practical and user-friendly BCI.

MEG hardware is helmet-shaped and contains as many as 300 sensors, covering most of the head. Because the MEG, like EEG, measures the electrical activity of the neurons directly, it promises extremely high temporal resolution (better than 1 ms), which is comparable with that of intracranial electrodes. Additionally, MEG offers better spatial resolution than EEG, although not as good as PET, SPECT and fMRI. It is completely non-invasive, and there is no possible damage by radioactive injection or exposure to X-rays and magnetic fields as opposed to PET and SPECT. Moreover, the biosignals measured by MEG do not depend on head geometry as much as EEG does. Because of these merits, MEG becomes a rapidly growing and increasingly popular brain imaging technique. MEG shares several disadvantages with EEG. The unique disadvantage of MEG compared with EEG is that MEG hardware is extremely expensive, and it requires a magnetically shield room, adding to the expense and hindering the feasibility of this imaging technique.

Compared to the techniques mentioned above, EEG has several strong features as a tool for exploring brain activity. Compared to fMRI, which has time resolution between seconds and minutes, EEG has a much higher temporal resolution and is capable of detecting electrical activity changes in the brain on a millisecond time scale. Furthermore, EEG measures the brain's electrical activity directly, while other methods are indirect markers

of brain electrical activity by recording changes in blood flow (e.g., SPECT, fMRI, NIRS) or metabolic activity (e.g., PET). The need for subject to hold still in EEG experiment is perhaps less stringent than in fMRI and NIRS. Compared to MEG, EEG is inexpensive and has no requirement for shield environment, so that it holds promises for developing low cost and portable brain monitoring system.

EEG used to be an important clinical tool for diagnosing, monitoring and managing neurological disorders such as epilepsy, stroke, brain tumours, migraine headaches, Parkinson's disease, etc. Recently, because of its non-invasive characteristic and less stringent requirement for experiment subject, EEG has become a popular tool for neuroscience research. For example, a lot of cognitive research is conducted with EEG using the event related potential (ERP), which is obtained by averaging the EEG signal from each of the trials within a certain condition. Besides, a lot of research has been done to transfer this former medical technique to novel BCIs development [26–28].

The disadvantages of EEG include the poor spatial resolution, inability to measure activity in subcortical structures, the constraint of assuming a single source of brain activity at any time instant, and the impossibleness to reconstruct a unique intracranial current source for a given EEG signal since EEG is a measurement of the combined electrical activities of massive neuronal populations. Despite these limitations, the advantages of EEG such as non-invasiveness, relatively low cost and portability make it well suited for brain monitoring in the case that high spatial resolution and sensitivity are not required. Consequently, EEG is commonly used in neurological therapies to reduce the cost, enhance convenience and improve the feeling of patients.

1.3 Neurological Therapy

Neurological therapy, also called neurological rehabilitation, refers to a series of diagnostic and therapeutic technologies which can be used in rehabilitation of neurological disorders.

Although many aspects of neurological functioning and illness are not yet fully understood, neurologists have an increasing array of diagnostic and therapeutic technologies from which to choose. Clinical study generally applies directly to mechanisms of the diseases of the nervous system which may then be translated into studies of brain imaging techniques, brain signal processing techniques, and discovery of revolutionary therapies such as electrical stimulation for epilepsy treatment and robotic rehabilitation for motor recovery. Some important neurological therapy include: epilepsy, stroke, motor neuron diseases, muscular dystrophies, brain tumors, developmental disorders, pain, Parkinson's pathology and etc.

In following subsections, three major neurological disorders and their therapeutic related issues are introduced and discussed.

1.3.1 Epilepsy Treatment

Epilepsy is a common chronic neurological disorder characterized by recurrent unprovoked seizures [29]. These seizures are transient signs and symptoms of abnormal, excessive or synchronous neuronal activity in the brain [30]. About 50 million people worldwide have epilepsy.

The diagnosis of epilepsy typically includes neurological examination, routine EEG, Long-term video-EEG monitoring, neuropsychological evaluation, and neuroimaging such as MRI, SPECT, PET. fMRI and MEG are also used as supplementary tests in some

epilepsy centers. Among these methods, because of its non-invasiveness, relatively low cost and portability, EEG monitoring is commonly used as a helpful tool for seizures diagnosis and detection [3, 5, 6, 31–33].

The mainstream treatment of epilepsy is anticonvulsant medications. Often, anticonvulsant medication treatment will be lifelong and can have major effects on quality of life. Since the introduction of the first antiepileptic drug, bromides, in 1857, many effective antiepileptic drugs have been found, such as Primidone, Carbamazepine, Clonazepam, Ethoxuximide, Valproate, etc. Unfortunately, epilepsy is usually only controlled, but not cured with medication. Even worse, over 30% of people with epilepsy do not have seizure control even with the best available medications [34, 35]. Moreover, it was reported in a European survey [36] that there is at least one anticonvulsant related side effect in 88% of patients with epilepsy.

Surgical treatment may be considered as an alternative way to cure epilepsy by removing a focal abnormal part of the brain tissue through surgery operation. Neurosurgical operations for epilepsy can be palliative, reducing the frequency or severity of seizures. For some patients, an operation can be curative. It is a good option for patients whose seizures remain resistant to treatment with anticonvulsant medications and have a focal abnormality that can be located and therefore removed. The goal of epilepsy surgery is to locate the loci of the epileptic abnormality and remove the relative brain tissue, yet whether the removal of brain tissue will affect normal brain function has not been fully investigated.

Recently, several electrical stimulation treatments have been developed [37–39] to be reasonable alternatives of surgical treatment when the patient is reluctant to any required invasive monitoring, or when there are multiple epileptic foci, although the success rates are not usually equal to that of epilepsy surgery. Vagus nerve stimulation (VNS) which

involves implanting a computerized electrical stimulator of the vagus nerve was reported to be helpful for patients with localization-related epilepsies and patients with certain generalized epilepsies like Lennox-Gastaut syndrome [37]. Responsive neurostimulation system (RNS) consists of a computerized electrical device implanted in the skull with electrodes implanted in presumed epileptic foci within the brain [38, 39]. The RNS contains several brain electrodes and device with seizure-detection software. Different from the VNS that stimulates the vagus nerve at preset intervals and intensities of current, the RNS only delivers a small electrical charge to the epileptic focus when the seizure-detection device detects abnormal signal transmitted from the brain electrodes. As such, it was claimed that the RNS is a more effective method with less side effects to brain. Deep brain stimulation (DBS) [40] consists of computerized electrical device implanted in the chest in a manner similar to the VNS, but electrical stimulation is delivered to deep brain structures through depth electrodes implanted through the skull. The efficacy of the VNS, RNS and DBS in localization-related epilepsies is still under investigation.

Besides, there are many other treatments for epilepsy. A special high fat, low carbohydrate diet can be helpful in the treatment of children with severe, medically-intractable epilepsies, but the mechanism of action is unknown. Avoidance therapy consists of minimizing or eliminating triggers in patients whose seizures are particularly susceptible to seizure precipitants. The warning system contains a seizure response dog trained to summon help or ensure personal safety when a seizure occurs. Rarely, a dog may develop the ability to sense a seizure before it occurs, but this is not suitable for every one and not all dogs can be so trained. A possible alternative is the electronic form of seizure detection which is currently under investigation [5, 6, 31, 33, 41].

1.3.2 Stroke Rehabilitation

Stroke is the third leading cause of death and the leading cause of severe disabilities all over the world [42]. About 40% of stroke survivors are left with some degree of impairment, which creates a burden for the stroke survivors and to societies. In Singapore, stroke has an estimated prevalence rate of 4.05% [43]. About 25% of people who suffered stroke will survive for at least a year, but around 50% of stroke survivors will have moderate to severe disabilities relating to movement, cognition, speech and activities of daily living. Stroke affects the quality of life of the survivors in their daily functioning in the workplace, home, and community.

Recovery from stroke can be distinguished in terms of motor recovery and functional recovery [44]. Motor recovery refers to improvements in the strength, speed or accuracy of arm and leg movements. Functional recovery refers to improvement in performance such as self-care and walking. Motor recovery is the basis of function recovery. It can occur as a result of natural recovery and stimulated recovery involving rehabilitation interventions.

The principle behind motor recovery is brain plasticity - the reorganization of brain tissue [45, 46]. In the past, the complex wiring of the adult human brain was thought to be fixed. Presently, it is known that the human brain is dynamically changing at all times throughout its lifespan [47]. Based on the key aspects of brain plasticity, the fundamental functions of the healthy brain are no different from those in stroke patients who have a lesser complement of intact neural pathways. Hence, the brain is capable of adjusting itself and undergoes plastic changes in reaction to brain injury.

With effective rehabilitation, stroke patients could partially regain their functional impairment and continue with their activities of daily living. Rehabilitation is the processes involving professionals such as doctors, nurses, therapists, social service staff and psychologists to improve the quality of life for people facing daily living difficulties caused by chronic diseases [48]. Physical therapy is the de facto motor rehabilitation [49], which involves human therapists to assist patients in recovering their motor ability. However, physiotherapies are currently labor intensive and expensive [50]. Furthermore, the maximum effectiveness of the existing physiotherapy approaches is rapidly being reached. This has resulted in a pressing need for new therapeutic strategies to take advantage of recent advances in technology in order to optimize productivity and functional outcome on the rehabilitation of stroke patients.

The infancy of therapeutic robotics began around the last decade. Although the application of robotics to rehabilitation has a longer history, the substantial increase of research in the recent years is due to a significant shift away from assistive technology for people with disabilities towards therapeutic technology to support and enhance clinicians productivity and effectiveness to facilitate the patients recovery [51]. The robotic rehabilitation devices offer a way to precisely control and measure rehabilitation therapy. Modern robotic stroke rehabilitation alleviates the labor-intensive aspects of physical rehabilitation by human therapists [52]. Studies have shown that effective movement therapy can be delivered from robots [51]. Rehabilitation programs that incorporate robotic and information technology can ameliorate the increasing burden on manpower by automating parts of the process that are repetitive and time-consuming. Additionally, robots are able to provide consistent training in an efficient manner, and pervasive and accurate monitoring of the progress of

patients.

In current robotic rehabilitation approaches, the robot provides assistive actions based solely on the motor output variables such as the position of the robot but not the cognitive processes that drive and monitor voluntary movements [51]. The assumption is that the patient is well motivated towards the therapy and fully utilizing the neural mechanisms pertaining to motor intention and attention. For typical robot-aided rehabilitation involving reaching movements of the paretic limb, in the absence of any motor output from the patients within a time limit, the robot automatically moves the patients' limb to the target and back. In this case, it is difficult to judge objectively whether the patient is cognitively involved in the process.

For a more holistic approach, the mind robot approach synergizes non-invasive BCI technology with robot-assisted rehabilitation to enable relevant cognitive processes to be detected and monitored [53]. This is motivated by the recent advent of BCI technology that enables the translation of thoughts and intents of humans to actions by machines.

1.3.3 Autism Therapy

Autism is a brain development disorder characterized by impaired social interaction and communication, and by restricted and repetitive behavior. These signs all begin before a child is three years old. Autism involves many parts of the brain but how this occurs is not well understood [54]. About 0.1 % of people worldwide have autism, with about four times as many males as females.

Social deficits distinguish autism and the related autism spectrum disorders (ASD) from other developmental disorders [55]. People with autism have social impairments and

often lack the intuition about others that many people take for granted. Unusual social development becomes apparent early in childhood. Parents usually notice signs in the first two years of their child's life [56]. The signs usually develop gradually, but some autistic children first develop more normally and then regress [57].

The main goals of treatment of ASD are to lessen associated deficits and family distress, and to increase quality of life and functional independence. No single treatment is best, and treatment is typically tailored to the child's needs [56]. Available approaches include applied behavior analysis, developmental models, structured teaching, speech and language therapy, social skills therapy, and occupational therapy [56].

Besides behavioral treatment, many medications are used to treat ASD symptoms that interfere with integrating a child into home or school when behavioral treatment fails [55, 58–60]. But the medications may have adverse effects [56], and there is no known medication relieves autism's core symptoms of social and communication impairments [61].

Many alternative therapies and interventions are available, but few of them are supported by scientific studies [62, 63]. Treatment approaches have little empirical support in quality-of-life contexts, and the success measures of the treatment lack predictive validity and real-world relevance [64]. Furthermore, although most alternative treatments have only mild adverse effects, some may place the child at risk [65, 66]

Recently, robot assisted autism therapies were proposed. Studies showed that individuals with social-cognitive disabilities, including autistic children, tend to be more receptive to robots than to human beings [67]. In [68], some mobile and interactive robots, including *Roball* and *Tito*, were used for building interaction between autistic children and robots for fostering children's selfesteem. A creature-like robot, *Muu*, has been developed in [69] for

observing how autistic children spontaneously collaborate with the robot in shared activities such as arranging colored blocks. In [70], social robots have been used for the study of children's social development, and found that autistic children interacting with a robot showed positive proto-social behaviors such as touching, vocalizing, smiling, which were rare in their daily life.

1.4 Objectives and Scope of the Thesis

There is a long history of investigation on neurological disorders. A variety of treatments like medication, surgery and physical therapy have been developed for neurological disorders. However, most of the existing neurological therapies are labor intensive and expensive, and the maximum effectiveness of the existing approaches is rapidly being reached. Furthermore, because many aspects of neurological functioning and illness are not yet fully understood, there is no clear design target for treatment of neurological disorders nor any reliable standard to gauge its effectiveness. These resulted in a pressing need for new therapeutic strategies to take advantage of recent advances in engineering technologies in order to optimize productivity and functional outcome in the neurological therapy. It is promising and challenging to involve the available advanced engineering technologies in the treatment of neurological disorders.

The general objectives in this thesis are to develop preliminary works using advanced engineering techniques for future development concerning the spectrum of neurological therapies and to investigate the most important modules of the neurological therapy in three

different real-world applications: detection and treatment of epilepsy; mind robotic rehabilitation for stroke; and social therapy for autism.

Specifically, this thesis aims to

(i) design a detection and prevention scheme for treatment of epilepsy. Statistical methods and effective machine learning algorithms such as feature extraction and classification are utilized in EEG signal processing for automatic seizures detection. After detection of seizures, a nonlinear closed-loop control scheme is designed for automatic drug delivery or electrical stimulation to prevent seizures based on a good understanding of dynamical changes of brain in seizures onset and the mechanisms that cause these changes.

(ii) develop a mind robotic rehabilitation system for recovery of stroke. This novel rehabilitation is based on advanced robotics and BCI technology. A human-friendly robot is designed for motor rehabilitation to help the stroke patients with regular training at home in a more convenient way. In addition, the robotic rehabilitation is combined with motor imagery based BCI technology to let the patients be cognitively involved in the training process.

(iii) investigate child robot interaction and develop an interactive pet robot for social therapy of autism. The interactive pet robot is developed based on multimodal HRI which consists of real-time vision system for human face detection and recognition, and audio system for sound source recognition. Based upon these human identification technologies, an individualized treatment plan can be applied for each patient after in-depth

evaluation of the patients' needs and goals. A training scheme of child robot interaction is designed for social therapy of autistic children to help them communicated better in social life.

The work presented in this thesis is problem oriented and dedicated to the fundamental academic exploration of pattern recognition algorithms and control designs for brain signal processing and multimodal HRI in developing interactive robot for neurological therapy.

For the fundamental academic research on pattern recognition, we mainly focus on feature extraction, and propose several manifold learning algorithms like CSP, WLLE, NLE and SINLE for novel feature extraction of (i) EEG signal for detecting brain state and (ii) image and sound data for multimodal HRI. Classification is also an important aspect in pattern recognition. A well-designed classifier may significantly improve the final results of pattern recognition, but since the optimization of classifier is not within the scope of the thesis, we do not propose nor utilize more effective classifier in our study. Instead, we use some simple and standard classifiers such as SVM, BPNN and QDA to evaluate our feature extraction algorithms.

Practical implementation of these algorithms to develop effective neurological therapeutic schemes is also discussed for three neurological disorders - epilepsy, stroke and autism. These applications are chosen to be presented because their treatments cover most of the important modules in neurological therapy like medical diagnosis, medication optimization, motor rehabilitation and social therapy. Many other neurological disorders like brain tumors, developmental disorders, muscular dystrophies, neurogenetic disorders, pain, Parkinson's pathology are also worth investigating, but these are not within the scope of this

thesis.

1.5 Thesis Outline

This thesis is organized as follows:

In **Chapter 2**, with the review and extension of existing methods for detection of epileptic seizures, a novel EEG based brain-state identification method is presented for automatically detecting epileptic seizure. The automatic detection of seizures is realized by feature extraction algorithms and classification algorithms. Numerous statistical features from both time domain and frequency domain are extracted. SVM and BPNN are used as classifier. These algorithms are evaluated and compared through experiments on two-channels I-EEG data obtained from Swiss mice.

In **Chapter 3**, the problem of controlling the synaptic plasticity to constraint bursting activity in epileptic seizures is addressed by designing a closed-loop control strategy for a direct drug injection or electrical stimulation of related brain region. The control strategy is designed on the basis of a good understanding of dynamical changes in seizures onset and the mechanisms that cause these changes. Dynamic properties of the model describing interaction between synaptic strength and the intracellular calcium concentration $[Ca^{2+}]_i$ are explored, and nonlinear control design is presented through backstepping.

In **Chapter 4**, a human-friendly mind robotic rehabilitation is developed for regular training of stroke rehabilitation. The mind robotic rehabilitation is developed based on non-invasive motor imagery based BCI technology. For the BCI system, the usage of a spatial filtering algorithm, CSP, is proposed for feature extraction which maximize the

discrimination of two different brain states, left hand movement imagination and right hand movement imagination. Furthermore, a feature fusion of feature vectors from both CSP and AR spectral analysis can obviously improve the performance of the BCI. QDA is applied to classify the combined feature vectors into left or right motor imagery categories. An interactive robot is developed as a visual and motion feedback for BCI to make the user more cognitively engaged into rehabilitative training process.

In **Chapter 5**, social therapy of autism is studied for research and development of an interactive robot pet, RoBear, to help autistic children becoming more socially engaged. RoBear is developed based on well understanding of autism from neuroscience and cognitive science point of view and advanced robotics technology with multimodal HRI. Under a multimodal HRI framework, RoBear is able to identify the face and voice and sensitive to the emotion change of the patients working with it. The RoBear with multimodal HRI is responsive to the physical and psychological states of the patients and detects both implicit and explicit communication from the human to determine its own behavior.

In **Chapter 6**, under the multimodal HRI framework proposed in Chapter 5, an intelligent audio human detection system that is able to recognize user's voice is introduced. The sound sources recognition is realized using an unsupervised learning algorithm, NLE, which is able to extract the intrinsic features such as neighborhood relationships, global distributions and clustering property of a given data set. Additionally, motivated by the scale adaptation of human's perception, several scale invariant metrics are designed to enhance the intrinsic feature extraction performance of NLE.

In **Chapter 7**, under the multimodal HRI framework proposed in Chapter 5, a real-time vision system for detecting and recognizing human face from real environment is introduced.

Firstly, the human face is detected using Adaboost-based Haar-Cascade classifier, and then extreme learning machine (ELM) is used to improve the real human face detection. Secondly, feature extraction algorithm like LLE and WLLE are proposed and utilized for finding compact and distinctive descriptors of face image for face recognition.

Finally, **Chapter 8** summarizes the work presented in this thesis. It concludes this thesis and highlights the major contributions. It also discusses the limitations of this thesis and suggests future research directions that can be extended from the current research results.

Part I

Detection and Prevention of Epilepsy

Chapter 2

Automatic Detection of Epileptic Seizures in EEG Signal

2.1 Introduction

Epilepsy is one of the most common neurological disorders affecting almost 1% of the population worldwide. This disorder is normally characterized by the abnormal synchronized firing of a large number of neurons. The large synchronized event is known as a seizure, paroxysmal discharge, or ictal event.

Initially, the epilepsy research community shared low confidence in the prediction of seizures because that seizures were highly random phenomena without any prior indication of occurrence. But over time, many research groups have observed clinical symptoms and quantitative measures that foreshadow seizure onsets. With the intent to foster more proactive means of treating epilepsy, such findings have invoked interesting discussion and methods for seizure prediction. To date, precursor detection schemes have been focused

on spikes, sharp waves, or combinations of spikes and sharp waves as an event of interest. Prospective studies on prediction of epileptic seizures have been published in peer-reviewed journals. These methods include time-domain analysis of EEG signal by statistical analysis and characteristics computation [33], frequency-domain analysis by decomposing the EEG signal into components of different frequencies [5, 6, 71], non-linear dynamics and chaos theory [41, 72], and intelligent systems such as artificial neural network and other artificial-intelligence structures [31]. Over the past 30 years, seizure detection technology has matured. Despite impressive advances, all reported approaches suffer from some problems, such as the requirements of careful patient-specific tuning; the requirement of a priori localization of the seizure focus; and the need of large quantity of seizure data, which is expensive to collect.

Techniques for overcoming some or all of these limitations hold promise for developing more precise and widely applicable methods to control or eliminate seizures. In this work, we propose a technique for automatic seizures detection. Numerous energy based features revealed in the literature are used to serve as possible inputs to the classification algorithm, such as SVM and BPNN. SVM classification is an unsupervised approach, which is one of its most important advantages. An unsupervised approach allows for uniform treatment of seizure detection and prediction, and offers many advantages for implementation [3]. For the unsupervised approach, there is no need to perform supervised, patient-specific tuning during training. Furthermore, the assumption that seizures are electrographically homogeneous, which is often needed in training of classifier due to very small data sets, is relaxed.

We evaluate the proposed feature extraction algorithms using two-channels I-EEG data

obtained from Swiss mice. A comparison of classifiers between SVM and BPNN is presented to show the advantages of SVM algorithm for detecting epileptic spike wave discharge in EEG time series.

The contributions in this Chapter lies in

(i) thoroughly analyzing the long term EEG signal recording from experiment mice, labeling EEG signal according to revised criteria of kindling model, and windowing the raw data with the stationary unchanged;

(ii) feature extraction for the time series of EEG signal based on numerous features derived from time domain analysis, frequency domain analysis, and nonlinear dynamics; and

(iii) utilizing unsupervised SVM classifier to automatically detect seizures onset. It is compared to BPNN through experiments and demonstrated to have better performance.

2.2 Methods

2.2.1 Data Acquisition

Pilocarpine Treatment

Male Swiss mice weighing 25-30g were used for the study according to the established procedures in [73, 74]. Mice were given a single subcutaneous injection of methyl-scopolamine nitrate (1mg/kg) 30 min before the injection of either saline in the control or pilocarpine in the experimental group. In the latter group, the mice received a single i.p. injection of 300mg/kg pilocarpine and experienced acute status epilepticus (SE). All experiments were approved by the Tan Tock Seng Hospital, National Neuroscience Institute, Institutional

Animal Care and Use Committee. In the handling and care of all animals, the guidelines for animal research of NIH were strictly followed. Efforts were made throughout the study to minimize animal suffering and to use the minimum number of animals.

EEG and Video Recording

For EEG and video monitoring, 14 experimental mice at 2 months after inducing pilocarpine and 2 age-matched control mice were used. EEG data were recorded continuously (24 hrs/day) using TSE EEG Telemetry System (TSE Technical and Scientific Equipment GmbH, Germany) according to the protocols used in our previous study [73]. In brief, two leads of the transmitter were connected to two tiny screws which were fixed on the skull 2.3 mm posterior the bregma and 2mm lateral to the midline, and then consolidated with cyanoacrylate and dental acrylic cement (Boswarth Company, USA) under deep anesthesia with hydrochloride (40mg/kg). The transmitter has a built-in 1000-times amplification capacity with input voltage range of $3\mu V$ to $0.7mV$, and frequency ranges from 0.4 to 60Hz. The signal from transmitter was transmitted wirelessly to the receiver which was then digitized (sampling frequency 50Hz) and stored in a personal computer. EEG and digital video acquisition monitoring (Chateau digital surveillance network system, Chateau Technical Corp, Singapore) were done continuously 24 hrs/day (12 hr light on/ 12 hr light off), and all data were stored in computer for further processing and analysis.

A Traditional Technique of Manual Seizure Detection

All recorded EEG data were first assessed manually which contains 2 steps: the observation of the raw EEG signal; and the careful watching of the subjects appearance on simultaneous

recorded video. Though the manual observation is a crude method, it confirmed all obvious epilepsy on the EEG signal and the time and duration of those epilepsy occurrences. The key points we need to observe in a raw EEG signal are basically on (i) the base line, (ii) the background noise level, (iii) the presence of any artifact, (iv) the change of amplitude and (v) the change of frequency. We observed all these points upon performing the four steps described below:

(i) display (plot) the EEG signal in 1 to 2 hours epoch basis which gives an idea on signal's base line and background noise level. It also helps to locate and mark the artifact on the signal, if any. The artifact signal exhibits extra ordinary high voltage - mostly signal's peak is truncated.

(ii) mark the time point where the appearance of the EEG signal is different from its background noise level, and also mark background noise signal for comparison. This type of signal marking reduces the burden of checking a vast number of data points which mostly shows the background noise signal.

(iii) divide the marked signal points into consecutive 1s epochs to make it easy to observe interictal spike and its rate of presence, and

(iv) display in a view of 10 to 20 second plot, if it shows high rate of spike or signal peak in 1s epoch plot.

According to traditional technique, an epoch of EEG signal is assumed containing seizure signal when the neuron fires repeatedly with a frequency of greater than or equal to 5 Hz, and the appearance of EEG signal changes: the amplitude of peak to peak amplitude

increases or decreases, and the inter-spike interval becomes shorter.

For the video assessment, we watched the entire recorded video and marked the EEG recording time where we found any obvious behavior changes which can be ranked as stages 4 and 5 according to revised criteria of kindling model [75]: rearing (stage 4) and falling or lose of posture (stage 5). Through the manual observation, we confirmed the obvious seizures onset in the EEG signal and the raw EEG data were labeled according to the time and duration of those epilepsy occurrences.

2.2.2 Signal Preprocessing

During a seizures, the repeated spikes are normally observed in EEG signal up to 16 Hz [76–78]. But depending on the subject and activation of seizures, the lower and higher frequency components are also observed in EEG signals [78]. In this work, we concentrate on the EEG signal within the frequency band of 8-16 Hz, which normally contains the most information for detection of seizures. As a result, the raw EEG signal is band-pass filtered between 8-16 Hz using equiripple FIR filter, and sampled at 50 Hz.

Furthermore, to extract most valuable features, it is important to maintain stationarity of the data segment. Statistical tests reveal quasi-stationarity of the EEG signal anywhere from 1 s to several minutes [79]. Since seizures spread so quickly, a displacement as small as possible that does not provide too much variability is desired. The raw data are divided into consecutive 1 s epochs. The epoch-divided sections of each channel of the EEG signal $x(n)$, $n = 1, 2, \cdots, (N-1)O + D$ are arranged as the columns (pattern vectors) of an $D \times N$ matrix X, where D is the dimension (number of samples) of each pattern vector, N is the

number of patterns, and O is the delay between patterns.

$$X = \begin{bmatrix} x(1) & x(O+1) & \cdot & \cdot & x[(N-1)\cdot O+1] \\ x(2) & x(O+2) & \cdot & \cdot & x[(N-1)\cdot O+2] \\ . & . & . & . & . \\ . & . & . & . & . \\ x(D) & x(O+D) & \cdot & \cdot & x[(N-1)\cdot O+D] \end{bmatrix} \tag{2.1}$$

Motivated by analysis on stationarity and redundancy in [79], we divide the EEG signal into 1 s epoches, say, $D = 50$ since the sampling rate is 50 Hz. We choose $O = N/2$ (overlap of half of the samples between consecutive pattern vectors). Such short and overlapped windows ensure that all transient events will be completely represented and dominant in at least one of the patterns, yet they are long enough to characterize the main rhythms of the on-going EEG signal.

2.2.3 Feature Extraction

A number of promising feature extraction methods, each with different theoretical bases, have demonstrated usefulness in seizure prediction. Iasemidis and Sackellares applied nonlinear dynamical techniques, principal Lyapunov exponent (PLE), for prediction the beginning of seizures [80]. Some considered exhaustive search and genetic approach for feature selection [81], however, the optimal results can only be obtained by testing 850 features using genetic algorithm and 4300 features using the exhaustive search, thus the computational complexity is really a problem. Numerous features revealed in the literature are considered from time domain analysis, frequency domain analysis, and nonlinear dynamics [3, 82, 83]. Selected features are chosen to be computationally efficient and have potential for on-line

implementation in low-power, implantable environments. The five selected features derived from the I-EEG for this analysis are described below.

(i) **Mean value**:

$$M(n) = \frac{1}{N} \sum_{i=(n-1)N+1}^{nN} |x(i)| \tag{2.2}$$

(ii) **Curve length**:

This feature was originally introduced by Olsen as the "line length" prior to being described as the "curve length" in [32]. The mathematical representation of the curve length in its discrete form is

$$CL(n) = \frac{1}{N} \sum_{i=1+(n-1)(N-D)}^{n(N-D)+D} |x(i-1) - x(i)| \tag{2.3}$$

where $CL(n)$ is the running curve length of the time series $x(n)$, N is the length of the sliding observation window expressed in number of points, n is the discrete time index, and D is the overlap. The curve length is useful for observing amplitude and frequency changes and dimensionality of the signal.

(iii) **Accumulated energy**:

Let the sequence $x(n)$ be a preprocessed and fused input signal, then the instantaneous energy of $x(n)$ is given by $x^2(n)$. Considering that a sliding window is used, the energy of the signal becomes the average power over the window mathematically defined as

$$E(n) = \frac{1}{N} \sum_{i=(n-1)N+1}^{nN} x^2(i) \tag{2.4}$$

where N is the size of the sliding window expressed in number of points; n is the discrete time index. If an overlap of D points is allowed, then the average energy becomes

$$E_D(n) = \frac{1}{N} \sum_{i=(n-1)(N-D)+1}^{n(N-D)+D} x^2(i) \tag{2.5}$$

where E_D is the average energy or moving average of the power with D points of overlap. An overlap of 100 points (0.5 s overlap) is used in this work.

(iv) **Average nonlinear energy**:

This algorithm was presented by Kaiser who was searching for a measure of energy proportional to both signal amplitude and frequency [84]. For the input signal $x(n)$, in its discrete form, the nonlinear energy (NE) operator is represented by

$$NE(n) = x^2(n) - x(n-1)x(n+1) \tag{2.6}$$

The NE is an instantaneous feature, such that it provides one value for each value of original data. After the NE is obtained, the feature is weighted with a Hanning window; then the mean of the windowed data, $NE_w(n)$, is taken over the desired sliding window. After windowing, the average nonlinear energy is then

$$ANE(n) = \frac{1}{N} \sum_{i=1+(n-1)(N-D)}^{n(N-D)+D} NE_w(i) \tag{2.7}$$

where $ANE(n)$ is the average NE at time n; N is the desired window length; D is overlap in number of point; and i is discrete time index. The algorithm is sensitive to both amplitude and frequency changes, and is computationally efficient and simple to calculate.

(v) **Six Power**:

It is found that sixth power is empirically useful for observing small amplitude differences in the I-EEG. The sixth power is the sixth power of each data point and is expressed as:

$$SP_D(n) = \frac{1}{N} \sum_{i=1+(n-1)(N-D)}^{n(N-D)+D} x^6(i) \tag{2.8}$$

where $SP_D(n)$ is the running sixth power of the time series $x(n)$, N is the length of the sliding observation window, and n is the discrete time index.

2.2.4 Classification

Support Vector Machine

SVM are widely used for learning classifiers and regression models. Its theoretical support is from statistical learning theory. The SVM empirically works very well, at least for some classes of problems, provide a good generalization performance on pattern classification problems despite the fact that it does not incorporate problem-domain knowledge. As an unsupervised approach, SVM has many important advantages. An unsupervised approach allows for uniform treatment of seizure detection and prediction without supervised, patient-specific tuning during training. Also, the assumption that seizures are electrographically homogeneous, which is often needed in classifier training due to very small data sets, is relaxed.

The objective of SVM is to find an optimal hyperplane that correctly classifies points as much as possible and separates the points of two classes as far as possible. Given the training sample $\{x_i, d_i\}_{i=1}^N$, where $x_i \in R^m$ is the i^{th} sample and $d_i \in \{-1, 1\}$ is the corresponding

desired output. Using a discriminant function

$$g(x) = w^T x + b \tag{2.9}$$

and choose a weight vector $w \in R^m$ and bias $b \in R$ such that

$$\begin{cases} g(x_i) = w^T x_i + b \geq 0, for\ d_i = +1 \\ g(x_i) = w^T x_i + b < 0, for\ d_i = -1 \end{cases} \tag{2.10}$$

The equation

$$g(x) = w^T x + b = 0 \tag{2.11}$$

is called the equation of the hyperplane that separate the two class of response. If $p \in R^m$ is an arbitrary point in the hyperspace, the distance of the point p from the hyperplane can be expressed to be $\rho = \frac{w^T p}{|w|} + \frac{b}{|w|} = \frac{g(x)}{|w|}$.

The objective is to find the optimal weight vector $w \in R^m$ and bias $b \in R$ such that for a given sample $\{x_i, d_i\}_{i=1}^N$, we want the nearest sample is at least some desired distance away from the hyperplane,

$$\rho = \frac{1}{|w|} \tag{2.12}$$

Hence, the condition in (2.10) can be rewritten as

$$\begin{cases} g(x_i) &= w^T x_i + b \geq 1,\ for\ d_i = +1 \\ g(x_i) &= w^T x_i + b < -1,\ for\ d_i = -1 \end{cases} \tag{2.13}$$

In this condition, the distance between the margins of the two classes is

$$2\rho = 2/|w| \tag{2.14}$$

The condition can also be written as

$$d_i g(x_i) = d_i(w^T x_i + b) \geq 1, for\ i = 1, 2, \ldots, N \tag{2.15}$$

Fig. 2.1 shows the geometry of SVM in feature space.

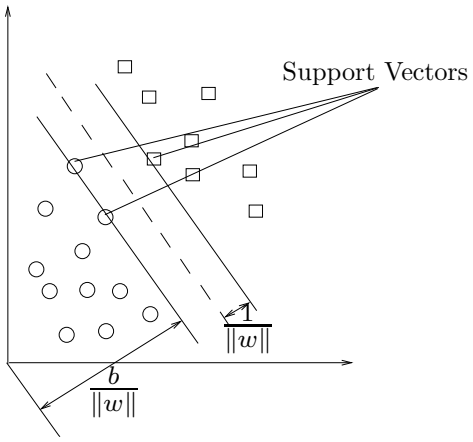

Figure 2.1: Geometry of SVM in feature space with the hyperplane.

The objective is, for a given sample $T = \{x_i, d_i\}_{i=1}^N$, to find an optimal hyperplane such that the condition in (2.15), and the separation margin should be as large as possible. From the define the margin distance in (7.10), we know that maximizing the separation margin can be achieved by minimizing $|w|$.

Therefore, the constrained optimization problem can be defined as follows,

Definition 2.1. *Given the training sample $x_i, d_{i i=1}^N$, find the optimum values of the weight vector w, and bias b such that they satisfy the constrains*

$$d_i g(x_i) = d_i(w^T x_i + b) \geq 1, for\ I = 1, 2, \ldots, N \tag{2.16}$$

and the weight vector w minimizes the cost function

$$\Phi(w) = \frac{1}{2} w^T w \tag{2.17}$$

To solve this, use the method of Lagrange multipliers.

$$J(w,b,\alpha) = \frac{1}{2}w^T w - \sum_{i=1}^{N} \alpha_i [d_i(w^T x_i + b) - 1] \tag{2.18}$$

In this Lagrangian function, we should minimize $J(w,b,\alpha)$ with respect to w and b, while maximize $J(w,b,\alpha)$ with respect to α.

Thus, the constrained condition is

$$\frac{\partial J(w,b,\alpha)}{\partial w} = w - \sum_{i=1}^{N} \alpha_i d_i x_i = 0 \tag{2.19}$$

$$\frac{\partial J(w,b,\alpha)}{\partial b} = \sum_{i=1}^{N} \alpha_i d_i = 0 \tag{2.20}$$

where $\frac{\partial}{\partial w} = \left[\frac{\partial}{\partial w_1} \ \frac{\partial}{\partial w_2} \cdots \frac{\partial}{\partial w_m}\right]$.

With regard to the optimization with respect to the Lagrange multiplier λ_i, we re-formulate $J(w,b,\alpha)$ using the duality theorem. From (2.18), we can re-write the Lagrangian function to

$$J(w,b,\alpha) = \frac{1}{2}w^T w - \sum_{i=1}^{N} \alpha_i [d_i(w^T x_i + b) - 1] \tag{2.21}$$

$$= \frac{1}{2}w^T w - \sum_{i=1}^{N} \alpha_i d_i w^T x_i - b\sum_{i=1}^{N} \alpha_i d_i + \sum_{i=1}^{N} \alpha_i \tag{2.22}$$

From (2.20) we know the third term on the right hand side of (2.22) is zero. And from (2.19), we have

$$\frac{1}{2}w^T w = \frac{1}{2}\sum_{i=1}^{N}\sum_{j=1}^{N} \alpha_i \alpha_j d_i d_j x_i^T x_j \tag{2.23}$$

and

$$\sum_{i=1}^{N} \alpha_i d_i w^T x_i = \sum_{i=1}^{N} \sum_{j=1}^{N} \alpha_i \alpha_j d_i d_j x_i^T x_j \tag{2.24}$$

Hence, (2.22) can be re-written as

$$Q(\alpha) = \sum_{i=1}^{N} \alpha_i - \frac{1}{2} \sum_{i=1}^{N} \sum_{j=1}^{N} \alpha_i \alpha_j d_i d_j x_i^T x_j \tag{2.25}$$

Therefore, the problem can be re-formulated into: Given the training sample $\{x_i, d_i\}_{i=1}^{N}$, find the lagrange multiplier $\{\alpha_i\}_{i=1}^{N}$ that maximize the objective function (2.25). And subject to the constraints $\sum_{i=1}^{N} \alpha_i d_i = 0$ and $\alpha_i \geq 0,\ for\ i = 1, 2, \ldots, N$.

Solving (2.25) will find that most $\alpha_i = 0$, except for the support vectors. Hence the solution for w can be solved by (2.19) to be

$$w = \sum_{i=1}^{N} \alpha_i d_i x_i \tag{2.26}$$

And the bias term can be solved to be $b = d_i - w^T x_i$.

Artificial Back Propagation Neural Network

Artificial neural networks (ANN) are used as a powerful means in engineering area especially after the development in computer technology. The fundamental characteristic of the neural networks is an adaptive, non-algorithmic and parallel-distributed memory [85]. Artificial neural networks are modeled by inspiring from biological neural system and have a more simple structure. Many neural networks were developed for resembling several known characteristics of biological neural networks such as learning and reacting. Some characteristics, however, are realized with an engineering approach instead of neuropsychological one [86].

For the pattern recognition procedure, a three layer feed forward networks (see Fig. 2.2) employing the back propagation learning algorithm, called BPNN will be applied. The features matrix can be directly used as the input to the ANN, each column of this matrix is an input pattern of the neural network. As such, the number of input nodes is equal to the length of feature vector. And there is only one output node to give the classification result. After training, the parameters of the network could be decided and used to classify other data.

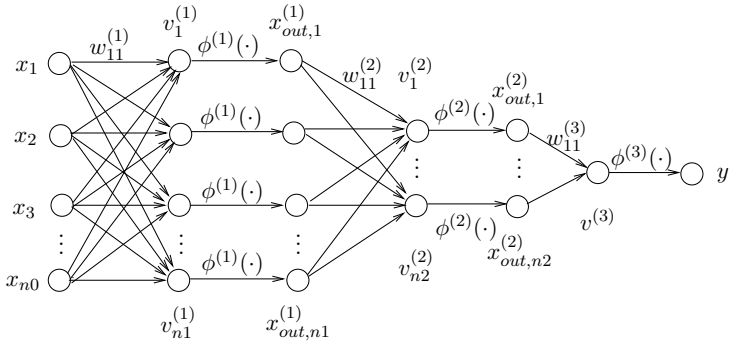

Figure 2.2: Structure of three-layer perceptron neural network.

Consider this multilayer perceptron neural network in Fig. 2.2, the back-propagation algorithm is derived to minimize energy of the instantaneous error

$$E_q = \frac{1}{2}(d_q - x_{out}^{(3)})^T(d_q - x_{out}^{(3)}) = \frac{1}{2}\sum_{j=1}^{n_3} e_{qj}^2 \tag{2.27}$$

Update law of the synaptic weights can be derived as

$$w_{ji}^{(s)}(k+1) = w_{ji}^{(s)}(k) + \eta^{(s)}\delta_j^{(s)}x_{out,i}^{(s-1)} \tag{2.28}$$

where

$$\delta_j^{(s)} \quad = \quad (d_{qj} - x_{out,j}^{(s)})\phi'(v_j^{(s)}) \tag{2.29}$$

for output layer;

$$\delta_j^{(s)} = \left(\sum_{k=1}^{n_{s+1}} \delta_k^{(s+1)} w_{kj}^{(s+1)}\right) \phi'(v_j^{(s)}) \tag{2.30}$$

for hidden layer.

2.3 Experimental Evaluation

2.3.1 Simulation Study

In this section we use five data sets including normal EEG signal and epileptic spike-wave discharge signal to study the classification effect of the SVM algorithm, and compare it with that of BPNN. These five EEG signals to be studied can be downloaded from www.vis.caltech.edu/ rodri. We thank Gilles van Luijtelaar and Joyce Welting for allowing their usage and distribution.

Among the five data, each sample contains 5 s of a two-channel EEG recording at the left and right frontal cortex of male adult WAG/Rij rats (a genetic model for human absence epilepsy). Signals were referenced to an electrode placed at the cerebellum, they were filtered between 1-100 Hz and digitized at 200 Hz. Sample A corresponded to a normal EEG and samples B, C, D and E contained epileptic spike-wave discharges. Details on the recordings as well as on the physiological results can be obtained from [87].

Two samples of the EEG signal are plotted as in Fig. 2.3, while Fig. 2.3(a) is the normal EEG signal and Fig. 2.3(b) is the EEG signal containing epileptic spike waves. From the EEG signal display, we can directly observe some discriminative characteristics of the signal, e.g., amplitude, frequency, etc. The five statistical features described in Section 2.2.3 are used as inputs to SVM and BPNN.

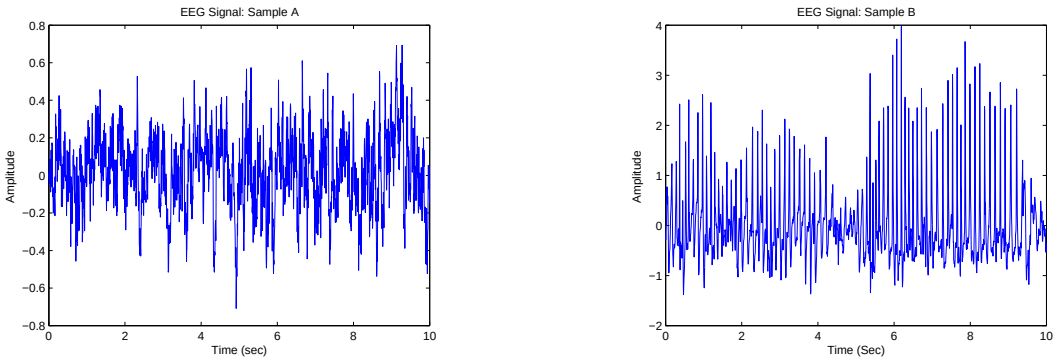

(a) Time series waveform of data set A

(b) Time series waveform of data set B

Figure 2.3: EEG data for simulation study

Table 2.1 provides a summary of the detection results obtained in this simulation study. In this table, every row demonstrates the results of each sample data from sample A to sample E. Columns show number of total epochs of each sample; the number of normal epochs (N_n); the number of seizures epochs (N_{sz}); and accuracy rate of SVM and BPNN classification respectively.

Table 2.1: Statistics and classification results of simulation study

Sample	Epoch	N_n	N_{sz}	Accuracy$_{svm}$	Accuracy$_{bp}$
A	38	38	0	1.0000	0.9737
B	38	0	38	1.0000	0.8947
C	38	0	38	1.0000	0.9737
D	38	0	38	1.0000	0.8684
E	38	0	38	1.0000	0.8684

In the simulation, training is performed using a group of random data sets combine with normal EEG and spike-wave EEG. Testing is performed on sample A to Sample E. According to the simulation result in Table 2.1, it is obvious that SVM classifier has a very good performance of 100% accuracy rate for this simple case with artifact free data. However the BPNN does not have as good performance as SVM with the accuracy rate of

the five sample between 86.8%-97.4%.

2.3.2 Experimental Results

Long term I-EEG signal (24hrs), recorded from both normal mice and pilocarpine treated mise who were freely moving are used to test our seizure detection approach. The sampling rate is 50Hz, and it is a large amount of data in a whole day's record. We choose a couple of epoches containing both normal EEG and epileptic EEG, and label them based on the observation of EEG signal and the video records.

In this experiment, we select two 600 sec (30000 samples) epoches as the train data to verify the effectiveness of our detection algorithm, one is in normal state and another one is in seizure. We also choose another 600 sec (30000 samples) I-EEG data with both epileptic and normal states as test data for validation.

Two epoches of the EEG data are plotted as in Fig. 2.4. Fig. 2.4(a) is the epoch of normal EEG signal and Fig. 2.4(b) is the epoch of EEG signal labeled as seizures onset.

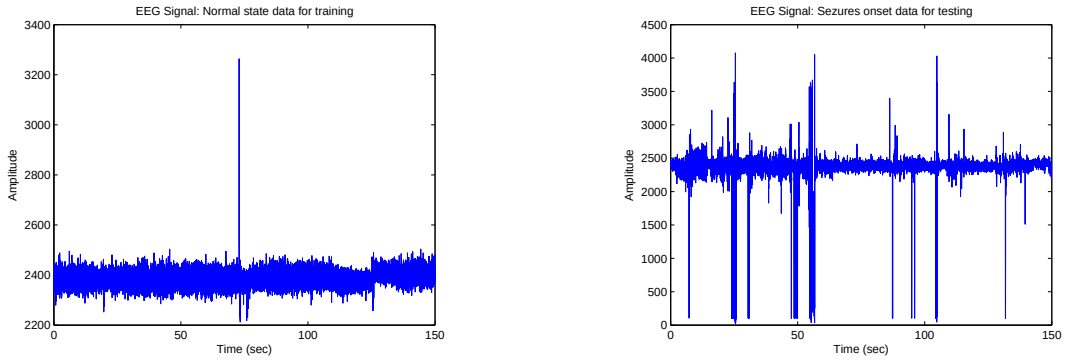

(a) Normal state EEG data

(b) Seizures onset EEG data

Figure 2.4: EEG signal recorded from mice

For all the EEG signals, we first rearrange signals to 1 s windows with 0.5 s overlap. Each

epoch containing 30000 samples is rearranged into 1199 pattern vectors with dimension of 50. The statistical features are extracted for each pattern vector. The feature vector consists of the selected statistical features (as mentioned in Section 2.2.3) are then classified by specific classification method like SVM and BPNN.

Table 2.2 provides a summary of the detection results obtained in this experiment. In this table, columns show number of total epochs of each sample; the number of normal epochs (N_n); the number of seizures epochs (N_{sz}); and accuracy rate of SVM and BPNN classification respectively.

Table 2.2: Statistics and classification results of experiment on mice data

Sample	Epoch	N_n	N_{sz}	Accuracy$_{svm}$	Accuracy$_{bp}$
Training Sample	2398	1199	1199	0.9708	0.9475
Testing Sample	1199	599	600	0.9541	0.8829

According to the experimental result in Table 2.2, we can conclude that SVM classifier outperforms BPNN in both training and testing phases in classification of I-EEG data collected from mice.

2.4 Conclusion

Traditional approaches to seizure detection have many limitations such as the need to collect precise mark of seizure data for training; requirement of patient-specific parameter tuning for detection; and the need that seizures are electrographically homogeneous. In this work, we presented a new, EEG-based, brain-state identification method for detecting epileptic seizures. To automatically classify the EEG signals and diagnose the epileptic seizures, we

firstly used some statistical features to obtain low-dimensional representatives of the raw EEG data. The features which capture the most important features to differentiate epileptic and normal states are linear separable and easy to be classified. SVM and BPNN were used to classify the linear separable features. Through these manipulations, seizures onset states were identified from normal states of the epilepsy patients. Real-time EEG signals recorded from mice were used for experimental evaluation to show the advantages of the proposed algorithms.

Chapter 3

Intelligent Close-loop Control for Epilepsy Prevention

3.1 Introduction

Among the treatment methods for epilepsy, neurosurgery is suitable for patients for whom a defined resectable seizure focus can be identified, and vagal nerve stimulation for a small percentage of patients who are not adequately controlled by existing antiepileptic drugs (AED) [37]. However, for most patients, pharmacotherapy is still considered to be the mainstay of treatment.

Since the introduction of the first antiepileptic drug, bromides, in 1857, many effective antiepileptic drugs have been found,such as Primidone, Carbamazepine, Clonazepam, Ethoxuximide, Valproate, etc. Unfortunately, such systemic drug therapy is not an ideal treatment because systemic side effects prohibit use of very high concentrations of the antiepileptic drug at the seizure focus. This problem, however, can be surmounted by local

injection of an antiepileptic drug directly into a seizure focus. Many previous studies have demonstrated the ability to stop seizures in animal models with injection of antiepileptic medication directly into the seizure focus [88–90]. These novel direct delivery may ensure better drug efficacy and also avoid potential problems of whole-brain and systemic toxicity.

Recently, a variety of new strategies have been employed or proposed to reduce the frequency and severity of neocortical seizures [38, 39, 41, 88, 91]. Among the most promising are implantable devices that deliver local therapy, such as direct electrical stimulation or chemical infusions, to affected regions of the brain [38]. Among these therapies, most are open loop systems that operate based on the amplitude and duration of stimulation set by the medical doctor. It therefore strongly suggests that more intelligent "closed loop" seizure prevention based upon understanding of mechanisms underlying seizure generation and thorough investigation on the dynamic changes in the brain with seizures are urgently needed.

Restoration of disordered states in brain for therapeutic purpose can be viewed as a control problem. Motivated by previous works on both modeling of synaptic plasticity in neuronal network [92, 93] and nonlinear control [94–96], we investigate the dynamics of synaptic plasticity in neural network and design a closed loop drug delivery strategy by model-based feedback control design to obtain maximum efficiency while keeping a low toxicity level. By exploring the dynamic properties of the system, the model of synaptic plasticity is divided into two subsystems. The stability of the first subsystem is thoroughly analyzed and the control law for the second subsystem is designed via backstepping. This study demonstrate that intelligent control can help in fast design of drug delivery schemes for epilepsy once a pertinent model of the involved biological mechanism is available. To

the best of our knowledge, there are few works dealing with epilepsy treatment using such kind of control therapy in the literature.

The contributions in this Chapter lies in

(i) the combination of biomodeling and nonlinear control design in helping fast design of drug delivery schemes achieving therapy of epilepsy;

(ii) the division of the original synaptic plasticity system into two subsystems to make the system become strict feedback form so that the backstepping procedure applicable; and

(iii) the feedback control design by utilizing backstepping method for the case with parameters known; the adaptive control design for the case with parameters unknown.

3.2 Problem Formulation

In this work, we shall investigate the problem of treating seizures by controlling the synaptic plasticity model to restore disordered states in the brain. The simplified mathematical model describing the dynamic interaction between intracellular calcium concentration and synaptic plasticity has been proposed in [93] and drawn from [92].

For the convenience of control design, we can rewrite the model in [93] as follows

$$\dot{x}_1 = f_1(x_3) - g_1(x_3)x_1 \tag{3.1}$$

$$\dot{x}_2 = f_2(x_2) + g_2(x_2)x_3 \tag{3.2}$$

$$\dot{x}_3 = f_3(x_2, x_3) - u \tag{3.3}$$

where

$$f_1(x_3) = \frac{\frac{e^{80(x_3-0.55)}}{1+e^{80(x_3-0.55)}} + 0.25\left(1 - \frac{e^{80(x_3-0.35)}}{1+e^{80(x_3-0.35)}}\right)}{1 + \frac{10}{0.001+x_3^3}} \tag{3.4}$$

$$g_1(x_3) = \frac{1}{1 + \frac{10}{0.001+x_3^3}} \tag{3.5}$$

$$f_2(x_2) = -p_2 x_2 \tag{3.6}$$

$$g_2(x_2) = p_1(1 - x_2) \tag{3.7}$$

$$f_3(x_2, x_3) = p_2 p_3 x_2 - p_1 p_3 x_3(1 - x_2) - p_4 \frac{x_3}{x_3 + p_5} \tag{3.8}$$

x_1, x_2 and x_3 are the state variables, p_i $(i = 1, 2, \cdots, 5)$ are constant parameters, u is the control variable.

Table 3.1: Description of variables and parameters in synaptic plasticity model

Variables/Parameters	Description
x_1	synaptic strength
x_2	fraction of buffer that are occupied by Ca^{2+}
x_3	intracellular calcium concentration
p_1	forward binding rates
p_2	backward binding rates
p_3	total concentration of the buffer
p_4	rate of calcium removal by Ca^{2+} pump
p_5	modifier of calcium removal by Ca^{2+} pump
u	control signal, $u = -\alpha I_{Ca} + I_{NMDA}$

The definitions according to the model in [92], [93] are given in Table 3.1, and their chemical properties and interpretation are described as follows:

(i) In this synaptic plasticity model, synaptic strength x_1 is controlled by the intracellular calcium concentration x_3;

(ii) Intracellular calcium dynamics are described by (3.2) and (3.3), and p_3 is the total concentration of the buffer, x_2 represents the fraction of buffer that are occupied by

Ca^{2+}, p_1 and p_2 are forward and backward binding rates respectively;

(iii) I_{NMDA} and I_{Ca} are currents carried by Ca^{2+} ions through the N-methyl-D-aspartate (NMDA) Receptor channels and by voltage dependent calcium channels (VDCC); and

(iv) p_4 represents rate of calcium removal by Ca^{2+} pump, and p_5 is the modifier in the Ca^{2+} pump expression.

Seizure is a disturbance of the neuronal electrochemical activity whereby a set of neurons suddenly produce a repetitive, synchronous discharge. It has been proved that non-synaptic neural plasticity (i.e. calcium dependent afterhyperpolarization in neurons) can regulate the frequency of the dominant rhythm in EEG, while synaptic potentiation may be responsible for irregular bursting prior to seizure termination [93], [97]. The underlying hypothesis is that synaptic potentiation and afterhyperpolarization (which regulates patterns of neuronal bursting) play significant roles in alteration of neural rhythmic activity during seizures. Therefore, synaptic strength is a critical factor in regulating seizure. By decreasing the synaptic strength, we aim to restore the neural rhythmic activity. Thus further modeling must take into account the way in which the synaptic strength acts on regulate neural rhythmic.

Translated into control terms, the problem here is to act upon a system in order to modify the biological properties (strength, concentration or amplitude etc.) to make it closer to a behavior considered as "normal".

From the models, it is reasonable to think of modifying calcium concentration by NMDA receptor channels current I_{NMDA} and voltage dependent calcium channels current I_{ca}, which

can be chosen as control signals and become negative and positive feedback signal respectively. However, I_{NMDA} and I_{ca} can be acted upon by more conventional means: drugs, such as calcium channel blockers (CCBs) and antiepileptic drugs etc., which are known to have an influence on I_{Ca} and I_{NMDA} [88]. Accordingly, we do not consider the underlying mechanism of the relationship between drugs and these two kinds of currents, and suppose a parameter $u = -\alpha I_{Ca} + I_{NMDA}$ that we are able to vary as a control signal. From a strict automatic control point of view, we are now dealing with a nonlinear system with three state variables x_1, x_2, x_3 and one control variable u.

3.3 Control Design Methods

Let $x_0 = [x_{10}\ x_{20}\ x_{30}]^T \in R^3_{\geq 0}$ denote the health value. Consequently, the control objective is to force x to converge to x_0. We introduce the external control agent u to reduce the strength of synaptic plasticity for preventing the seizures. Before proceeding further, we need to study the properties of the system.

3.3.1 Nonnegativity

For the synaptic plasticity system, it is easy to prove that the states of this system are nonnegative. To show this, the following Lemma is needed:

Lemma 3.1. *For $a, b \in R$, $\frac{ab}{a+b} < a$ and $\frac{ab}{a+b} < b$, if $a + b > 0$.*

From the chemical property, we know the variables $x_1(t) > 0$, $x_2(t) > 0$, $x_3(t) > 0$, $\forall t$, which will also be proved mathematically later. Therefore, we can assume that the initial values $x_i(0) > 0$, $i = 1, 2, 3$.

According to Lemma 3.1, we can see that in (3.4), the term $\frac{e^{80(x_3-0.35)}}{1+e^{80(x_3-0.35)}} < 1$. And it is easy to show that if $x_3 > 0$, we have that

$$f_1(x_3) \;>\; 0 \tag{3.9}$$

$$g_1(x_3) \;>\; 0 \tag{3.10}$$

From (3.1), we know that $\dot{x}_1(t) > 0$ whenever $x_1(t)$ approaches 0. Consequently, if $x_1(0) > 0$, $x_1(t)$, $\forall t$, will never be negative.

Similarly, from (3.2), because the parameters p_1 and p_2 are positive constants, and assume $x_2(0) > 0$, we know that $\dot{x}_2(t) > 0$ whenever $x_2(t)$ approaches 0. From equation (3.3), we know that with a suitable designed u, $\dot{x}_3(t) > 0$ whenever $x_3(t)$ approaches 0. Therefore, if $x_1(0) > 0$, $x_2(0) > 0$ and $x_3(0) > 0$, $x_1(t)$, $x_2(t)$ and $x_3(t)$ will always be positive, $\forall t > 0$. The following properties can be obtained.

Property 3.1. *From system (3.1)-(3.2)-(3.3), it is noted that if $x_i(0) > 0$, then $x_i(t) > 0$ $\forall t > 0$, $i = 1, 2, 3$.*

3.3.2 Stability Analysis for the Synaptic Plasticity Model

From (3.1), it is noted that x_1 depends only on x_3, and thus the stabilization of x_1 relies on the proof of the stability of x_3. This is because the synaptic strength x_1 is controlled by the intracellular calcium concentration x_3. For stability analysis, let us present the following technical lemma on bounded input and bounded output property for stable dynamic inequalities.

Lemma 3.2. *Consider the continuous functions $y(t) \geq 0$, $\forall t \in R_+$ with $y(0)$ bounded. If*

the function $y(t)$ satisfies the following inequality:

$$\dot{y}(t) \leq -\lambda(t)y(t) + v(t) \tag{3.11}$$

where $\lambda(t)$ is a positive continuous function with a lower bound ($\lambda(t) \geq \lambda_{min} > 0$), and $v(t)$ is a nonnegative continuous function with a upper bound, we can conclude that $y(t)$ is bounded.

Proof: Define λ_{min} to be the greatest lower bound of $\lambda(t)$, and v_{max} to be the smallest upper bound of $v(t)$. According to (3.11), we can obtain

$$\dot{y}(t) \leq -\lambda(t)y(t) + v(t) \leq -\lambda_{min}y(t) + v(t) \tag{3.12}$$

Multiplying both sides by $e^{\lambda_{min}t}$ [98], (3.12) becomes

$$\frac{d}{dt}(y(t)e^{\lambda_{min}t}) \leq v(t)e^{\lambda_{min}t} \tag{3.13}$$

Integrating it over [0, t], we have

$$\begin{aligned} y(t) &\leq y(0)e^{-\lambda_{min}t} + e^{-\lambda_{min}t}\int_0^t v(t)e^{\lambda_{min}\tau}d\tau \\ &\leq y(0)e^{-\lambda_{min}t} + e^{-\lambda_{min}t}v_{max}\int_0^t e^{\lambda_{min}\tau}d\tau \\ &= y(0)e^{-\lambda_{min}t} + \frac{v_{max}}{\lambda_{min}}(1 - e^{-\lambda_{min}t}) \\ &\leq y(0)e^{-\lambda_{min}t} + \frac{v_{max}}{\lambda_{min}} \\ &\leq y(0) + \frac{v_{max}}{\lambda_{min}} \end{aligned} \tag{3.14}$$

Therefore, we can conclude that $y(t)$ is bounded. □

Since $f_1(x_3)$ and $g_1(x_3)$ are monotonic nondecreasing continuous function, and as discussed in (3.9) and (3.10), $f_1(x_3) > 0$, $g_1(x_3) > 0$ and $g_1(0) = \frac{1}{10001}$, together with

$$\lim_{x_3 \to \infty} f_1(x_3) = 1 \tag{3.15}$$

$$\lim_{x_3 \to \infty} g_1(x_3) = 1 \tag{3.16}$$

we know that $f_1(x_3)$ and $g_1(x_3)$ are upper and lower bounded by

$$0 < f_1(x_3) < 1 \tag{3.17}$$

$$\frac{1}{10001} < g_1(x_3) < 1 \tag{3.18}$$

From Property 3.1, $x_1 > 0$, $\forall t > 0$. According to Lemma 3.2, and from (3.1), we can conclude that $x_1(t)$ is bounded.

3.3.3 Non-adaptive Control Design for Intracellular Calcium Dynamic

Examining the synaptic plasticity system, it can be seen that (3.2) and (3.3) are in the strict feedback form, and backstepping design can be directly applied.

To show it clearly, equations (3.2) and (3.3) are written as:

$$\dot{y}_1 = f_3(y_1) + p_1 g_3(y_1) y_2 \tag{3.19}$$

$$\dot{y}_2 = f_4(y_1, y_2) - u \tag{3.20}$$

where

$$f_3(y_1) = -p_2 y_1 \tag{3.21}$$

$$g_3(y_1) = (1 - y_1) \tag{3.22}$$

$$f_4(y_1, y_2) = p_2 p_3 y_1 - p_1 p_3 y_2 (1 - y_1) - \frac{p_4 y_2}{y_2 + p_5} \tag{3.23}$$

In this section, the controller design is developed based on backstepping. Backstepping is a standard design procedure for handling systems in strict feedback form, which use intermediate control to handle unmatched uncertainties and final control to be designed at the last step.

Step 1

Consider Subsystem (3.19)-(3.20). Define $z_1 = y_1 - y_{10}$. Its derivative is given by

$$\dot{z}_1 = \dot{y}_1 = -p_2(z_1 + y_{10}) + p_1(1 - z_1 - y_{10})(z_2 + y_{20} + \alpha) \tag{3.24}$$

where $z_2 = y_2 - y_{20} - \alpha$, and α is the virtual control to be defined later.

Choose the Lyapunov function candidate

$$V_1 = \frac{1}{2}z_1^2 \tag{3.25}$$

Its derivative is given by

$$\begin{aligned} \dot{V}_1 &= z_1\dot{z}_1 \\ &= -c_1 z_1^2 + c_2 z_1 + (p_1 - p_1 y_{10})z_1 z_2 - p_1 z_1^2 z_2 + p_1 z_1(1 - y_1)\alpha \end{aligned} \tag{3.26}$$

where $c_1 = p_2 + p_1 y_{20}$, and $c_2 = p_1 y_{20} - p_2 y_{10} - p_1 y_{10} y_{20}$.

Theorem 3.1 (Young's inequality)**.** *Let f be a real-valued, continuous, and strictly increasing function on $[0, c]$, with $c > 0$. If $f(0) = 0$, $a \in [0, c]$, and $b \in [0, f(c)]$, then*

$$\int_0^a f(x)dx + \int_0^b f^{-1}(x)dx \leq ab \tag{3.27}$$

where $f^{-1}(\cdot)$ is the inverse function of $f(\cdot)$. Equality holds iff $b = f(a)$. Taking the particular function $f(x) = x^{p-1}$ gives the special case

$$\frac{a^p}{p} + \left(\frac{p-1}{p}\right) b^{\frac{p}{p-1}} \leq ab \tag{3.28}$$

which is often written in the symmetric form

$$\frac{a^p}{p} + \frac{b^q}{q} \leq ab \tag{3.29}$$

where $a, b > 0$, $p > 1$ *and*

$$\frac{1}{p} + \frac{1}{q} = 1 \tag{3.30}$$

Using Young's inequality presented above [99–101] , we have

$$\dot{V}_1 \quad \leq \quad -c_1 z_1^2 + \frac{c_2^2 \epsilon}{2} + \frac{z_1^2}{2\epsilon} + (p_1 - p_1 y_{10}) z_1 z_2 - p_1 z_1^2 z_2 + p_1 z_1 (1 - y_1)\alpha \tag{3.31}$$

where ϵ is an arbitrary small constant.

In reality, y_1 is small. If we can guarantee $y_1 \ll 1$, which will be proved later, then we can choose the well defined virtual control,

$$\alpha = \frac{-z_1}{2\epsilon p_1 (1 - y_1)} \tag{3.32}$$

Accordingly, equation (3.31) becomes

$$\dot{V}_1 \leq -c_1 z_1^2 + \frac{c_2^2 \epsilon}{2} + (p_1 - p_1 y_{10}) z_1 z_2 - p_1 z_1^2 z_2 \tag{3.33}$$

The first term is stabilizing because $c_1 = p_2 + p_1 y_{20} > 0$, and the rest terms $\frac{c_2^2 \epsilon}{2} + (p_1 - p_1 y_{10}) z_1 z_2 - p_1 z_1^2 z_2$ will be handled in the next step.

Remark 3.1. *For the original $\dot{V}_1$ function (3.26), a virtual control $\alpha = \frac{1}{p_1(1-y)}(-c_2 - kz_1)$, where $k > 0$, can be easily found to eliminate the $c_2 z_1$ term and obtain a stable term $-(c_1 + k)z_1^2$. However, if α contains the term $\frac{-c_2}{p_1(1-y)}$, it can never converge to zero. Since $z_2 = y_2 - y_{20} - \alpha$, our objective of y_2 converge to y_{20} cannot be obtained even when $z_2 = 0$. By utilizing Young's inequality, the $\frac{z_1^2}{2\epsilon}$ term is formed, the virtual control can be chosen as $\alpha = \frac{-z_1}{2\epsilon p_1(1-y_1)}$, therefore it can converge to zero when z_1 converges to zero. In that case, y_2 will converge to y_{20} if z_2 converge to zero.*

Step 2

Since $z_2 = y_2 - y_{20} - \alpha$, the derivative of z_2 is expressed as

$$\begin{aligned} \dot{z}_2 &= \dot{y}_2 - \dot{\alpha} \\ &= p_2 p_3 y_1 - p_1 p_3 y_2 (1 - y_1) - \frac{p_4 y_2}{y_2 + p_5} - u + \frac{-2p_1(1 - y_1) - 2p_1 z_1}{4\epsilon p_1^2 (1 - y_1)^2} \dot{y}_1 \end{aligned} \tag{3.34}$$

For (3.24) and (3.34), we shall now design the control law u to render the time derivative of a Lyapunov function negative definite. Consider the Lyapunov function candidate

$$V_2 = V_1 + \frac{1}{2} z_2^2 \tag{3.35}$$

According to (3.33) and (3.34), its derivative is

$$\begin{aligned} \dot{V}_2 &= \dot{V}_1 + z_2 \dot{z}_2 \\ &\leq -c_1 z_1^2 + \frac{c_2^2 \epsilon}{2} + z_2 [(p_1 - p_1 y_{10}) z_1 - p_1 z_1^2 + \\ &\quad p_2 p_3 y_1 - p_1 p_3 y_2 (1 - y_1) - p_4 \frac{y_2}{y_2 + p_5} \\ &\quad + \frac{-2p_1(1 - y_1) - 2p_1 z_1}{4\epsilon p_1^2 (1 - y_1)^2} \dot{y}_1 - u] \end{aligned} \tag{3.36}$$

It is easy to see that the well defined control

$$\begin{aligned} u &= (p_1 - p_1 y_{10}) z_1 - p_1 z_1^2 + p_2 p_3 y_1 - p_1 p_3 y_2 (1 - y_1) \\ &- p_4 \frac{y_2}{y_2 + p_5} + \frac{-2p_1(1 - y_1) - 2p_1 z_1}{4\epsilon p_1^2 (1 - y_1)^2} \dot{y}_1 + c_3 z_2 \end{aligned} \tag{3.37}$$

leads to

$$\dot{V}_2 \leq -c_1 z_1^2 - c_3 z_2^2 + \frac{c_2^2 \epsilon}{2} \tag{3.38}$$

Consequently, by choosing a suitable small ϵ, it follows from LaSalle-Yoshizawa Theorem [102, 103] that (z_1, z_2) approach the set $\Omega : \{(z_1, z_2) \in R \times R \mid \dot{V}_2 = 0\}$ [104]. In view of $z_1 = y_1 - y_{10}$, $z_2 = y_2 - y_{20} - \alpha$ and $\alpha = \frac{-z_1}{2\epsilon p_1 (1 - y_1)}$, we can conclude that for bounded initial conditions, all signals in the closed-loop system remain bounded, and the output tracking error $y(t) - y_0$ converges to a neighborhood around zero by appropriately choosing design parameters [105]. The previous assumption that $y_1 \ll 1$ is also guaranteed to assure the well defined virtual control.

Remark 3.2. *We proved in Remark 3.1 that $\alpha \to 0$ when z_1 converges to zero. However, z_1 and z_2 only converge to a neighborhood around zero actually, such α does not converge to zero but a neighborhood around zero, too. Without using the method discussed in Remark 3.1, z_1 and z_2 may converge to zero, but since $y_2 - y_{20} = z_2 + \alpha$, y_2 will be more different from the healthy value y_{20}. Since we pay more attention to the state of Calcium concentration y_2, we choose this trade-off between convergency of y_1 and y_2.*

3.3.4 Adaptive Control Design for Intracellular Calcium Dynamic

For complex biological systems, the values of parameters are usually difficult to be precise. As a consequence, the model must have a fairly general structure and the control strategy

must be robust with respect to uncertainties of model parameters. Therefore, finding a robust adaptive control for the unknown parameters case is necessary for the implementation in real therapy procedure.

Assume that p_i, $(i = 1, \ldots, 5)$, are unknown, considering the plant (3.19)-(3.20), we find that it is difficult to obtain an adaptive control for plant (3.19)-(3.20) because of the nonlinear element $\frac{y_2}{y_2+p_5}$, which is not in linear-in-the-parameters (LIP) form. This unknown function can be approximated by function approximation.

The radial-basis function neural network (RBFNN) is usually used as a tool for modeling nonlinear functions because of its good capabilities in function approximation [106]. In this work, the following RBFNN [107] is used to approximate the continuous function $h(Z)$: $R^q \rightarrow R$

$$h_{nn}(Z) = W^T S(Z) \tag{3.39}$$

where the input vector $Z \in \Omega \subset R^q$, weight vector $W = [w_1, w_2, \ldots, w_l]^T \in R^l$, the NN node number $l > 1$; and $S(Z) = [s_1(Z), \ldots, s_l(Z)]^T$, with $s_i(Z)$ being chosen as the commonly used Gaussian functions, which have the form

$$S(Z) = exp\left[\frac{-(Z-\mu_i)^T(Z-\mu_i)}{\eta_i^2}\right] \tag{3.40}$$

where $\mu_i = [\mu_{i1}, \mu_{i2}, \ldots, \mu_{iq}]^T$ is the center of the receptive field and η_i is the width of the Gaussian function.

It has been proven that network (3.39) can approximate any continuous function over a compact set $\Omega_Z \subset R_q$ to arbitrary any accuracy as

$$h(Z) = W^{*T} S(Z) + \epsilon, \forall Z \in \Omega_Z \tag{3.41}$$

where W^* is ideal constant weights, and ϵ is the approximation error.

Assumption 3.1. *There exists ideal constant weights W^* such that $|\epsilon| \leq \epsilon^*$ with constant $\epsilon^* > 0$ for all $Z \in \Omega_z$.*

The ideal weight vector W^* is an artificial quantity required for analytical purposes. W^* is defined as the value of W that minimizes $|\epsilon|$ for all $Z \in \Omega_Z \subset R_q$. In general, the ideal NN weight, W^*, is unknown though constant, its estimate, $\hat{W}$, is used for controller design as will be shown later.

Once the function approximation problem is solved, control design can proceed. At first, we make the following assumptions for the uncertainties in system (3.19)-(3.20), which will be used throughout the chapter.

Assumption 3.2. *Considering that $g_3(y_1)$ is strictly positive since $y_1 \ll 1$, we suppose that there exist constant $g_{31} \geq g_{30} > 0$ such that $g_{31} \geq g_3(y_1) \geq g_{30} > 0$, $\forall y_1 \in \Omega \subset R$.*

Assumption 3.3. *There exist constant $g_{3d} > 0$ such that $|\dot{g}_3(y_1)| \leq g_{3d}$, $\forall y_1 \in \Omega \subset R$*

In this section, we present robust adaptive neural control design for system (3.19)-(3.20) in strict-feedback form. By combining backstepping methodology with adaptive neural design, we propose a smooth adaptive neural control for system (3.19)-(3.20). The detailed design procedure is described in the following steps.

Step 1

Define $z_1 = y_1 - y_{10}$. Its derivative is given by

$$\dot{z}_1 = \dot{y}_1 = f_3(y_1) + p_1 g_3(y_1) y_2 \tag{3.42}$$

By viewing y_2 as a virtual control input, there exists a desired feedback control

$$\alpha_1^* = -c_1 z_1 - \frac{f_3(y_1)}{p_1 g_3(y_1)} \tag{3.43}$$

where $c_1 > 0$ is a design constant.

Since $f_3(y_1)$ and $p_1 g_3(y_1)$ are unknown, the desired feedback control α_1^* cannot be implemented in practice. The unknown nonlinearity $h_1(Z_1) = \frac{f_3}{p_1 g_3}$, which is a continuous function of y_1, can be approximated by an RBF neural network $W_1^T S_1(Z_1)$, i.e.

$$h_1(Z_1) = W_1^{*T} S_1(Z_1) + \epsilon_1 \tag{3.44}$$

where $Z_1 = y_1 \in R$, W_1^* denotes the ideal constant weights, and $|\epsilon_1| \leq \epsilon_1^*$ is the approximation error with constant $\epsilon_1^* > 0$.

Since y_2 is only taken as a virtual control, not as the real control input for the z_1 subsystem, by introducing the error variable $z_2 = y_2 - y_{20} - \alpha_1$, the practical virtual control α_1 is chosen as

$$\alpha_1 = -c_1 z_1 - \hat{W}_1^T S_1(Z_1) \tag{3.45}$$

where $\hat{W}_1$ is the estimate of the neural network to be tuned online. The $\dot{z}_1$ equation becomes

$$\begin{aligned} \dot{z}_1 &= p_1 g_3(y_1)(z_2 + y_{20} + \alpha_1 + \frac{f_3(y_1)}{p_1 g_3(y_1)}) \\ &= p_1 g_3(y_1)(z_2 + y_{20} - c_1 z_1 - \tilde{W}_1^T S_1(Z_1) + \epsilon_1) \end{aligned} \tag{3.46}$$

where $\tilde{W}_1 = \hat{W}_1 - W_1^*$.

Choose the Lyapunov function candidate

$$V_1 = \frac{1}{2 p_1 g_3(y_1)} z_1^2 + \frac{1}{2} \tilde{W}_1^T \Gamma_1^{-1} \tilde{W}_1 \tag{3.47}$$

where $\Gamma_1 = \Gamma_1^T > 0$ is an adaptation gain matrix.

The derivative of V_1 is given by

$$\begin{aligned}\dot{V}_1 &= \frac{z_1\dot{z}_1}{p_1 g_3} - \frac{\dot{g}_3 z_1^2}{2p_1 g_3^2} + \tilde{W}_1^T\Gamma_1^{-1}\dot{\tilde{W}}_1 \\ &= z_1 z_2 - c_1 z_1^2 + z_1(\epsilon_1 + y_{20}) - \frac{\dot{g}_3 z_1^2}{2p_1 g_3^2} + \tilde{W}_1^T\Gamma_1^{-1}[\dot{\tilde{W}}_1 - \Gamma_1 S_1(Z_1) z_1] \qquad (3.48)\end{aligned}$$

Let $c_1 = c_{10} + c_{11}$, with c_{10} and $c_{11} > 0$. According to Assumptions 3.2 and 3.3, we obtain the following inequalities

$$-c_{11}z_1^2 + z_1(\epsilon_1 + y_{20}) \leq \frac{(\epsilon_1 + y_{20})^2}{4c_{11}} \qquad (3.49)$$

$$-(c_{10} + \frac{\dot{g}_3}{2p_1 g_3^2})z_1^2 \leq -(c_{10} - \frac{g_{3d}}{2p_1 g_{30}^2})z_1^2 \qquad (3.50)$$

We can obtain

$$\dot{V}_1 \leq z_1 z_2 + \frac{\epsilon_1^{*2}}{4c_{11}} - c_{10}^* z_1^2 + \tilde{W}_1^T\Gamma_1^{-1}[\dot{\tilde{W}}_1 - \Gamma_1 S_1(Z_1) z_1] \qquad (3.51)$$

where $\epsilon_1^* = \epsilon_1 + y_{20}$, and c_{10} is chosen such that $c_{10}^* = c_{10} - \frac{g_{3d}}{2p_1 g_{30}^2} > 0$, therefore this term is stabilizing, and the rest terms will be handled in the next step.

Step 2

The derivative of $z_2 = y_2 - y_{20} - \alpha_1$ is expressed as

$$\begin{aligned}\dot{z}_2 &= \dot{y}_2 - \dot{\alpha}_1 \\ &= f_4(y_1, y_2) - u - \dot{\alpha}_1 \qquad (3.52)\end{aligned}$$

From equation (3.45), it can be seen that α_1 is a function of y_1 and $\hat{W}_1$. Thus, $\dot{\alpha}_1$ is given by

$$\begin{aligned}\dot{\alpha}_1 &= \frac{\partial \alpha_1}{\partial y_1}\dot{y}_1 + \frac{\partial \alpha_1}{\partial \hat{W}_1}\dot{\hat{W}}_1 \\ &= \frac{\partial \alpha_1}{\partial y_1}[f_3(y_1) + p_1 g_3(y_1) y_2] + \psi \qquad (3.53)\end{aligned}$$

Note that $\dot{\alpha}_1$ is unknown because it contains unknown nonlinear functions in $\dot{y}_1$, however, it does not matter as the unknown terms can be elegantly handled in the next step.

By noting u is the control input to stabilize the system, there exists a desired feedback control

$$u^* = z_1 + c_2 z_2 + f_4(y_1, y_2) - \dot{\alpha}_1 \tag{3.54}$$

where $f_4(y_1, y_2)$ is an unknown function. Utilizing an RBF neural network $W_2^T S_2(Z_2)$ to approximate the unknown nonlinearity denoted as $h_2(Z_2)$, i.e.

$$\begin{aligned} h_2(Z_2) &= f_4(y_1, y_2) - \dot{\alpha}_1 \\ &= W_2^{*T} S_2(Z_2) + \epsilon_2 \end{aligned} \tag{3.55}$$

where $Z_2 = [y_1, y_2, \frac{\partial \alpha_1}{\partial y_1}, \psi]^T \in R^4$, W_2^* is the ideal constant weights, and $|\epsilon_2| \leq \epsilon_2^*$ is the approximation error with constant $\epsilon_2^* > 0$.

The actual control input u is chosen as

$$u = z_1 + c_2 z_2 + \hat{W}_2^T S_2(Z_2) \tag{3.56}$$

Thus, the $\dot{z}_2$ equation becomes

$$\begin{aligned} \dot{z}_2 &= f_4(y_1, y_2) - \dot{\alpha_1} - u \\ &= -z_1 - c_2 z_2 - \tilde{W}_2^T S_2(Z_2) + \epsilon_2 \end{aligned} \tag{3.57}$$

Consider the Lyapunov function candidate

$$V_2 = V_1 + \frac{1}{2} z_2^2 + \frac{1}{2} \tilde{W}_2^T \Gamma_2^{-1} \tilde{W}_2 \tag{3.58}$$

where $\Gamma_2 = \Gamma_2^T > 0$ is an adaptation gain matrix. The derivative of V_2 is

$$\begin{aligned}\dot{V}_2 &= \dot{V}_1 + z_2\dot{z}_2 + \tilde{W}_2^T\Gamma_2^{-1}\dot{\hat{W}}_2 \\ &\leq \frac{\epsilon_1^{*2}}{4c_{11}} - c_{10}^* z_1^2 + \tilde{W}_1^T\Gamma_1^{-1}[\dot{\hat{W}}_1 - \Gamma_1 S_1(Z_1)z_1] - \\ &\quad c_2 z_2^2 + z_2\epsilon_2 + \tilde{W}_2^T\Gamma_2^{-1}[\dot{\hat{W}}_2 - \Gamma_2 S_2(Z_2)z_2] \end{aligned} \tag{3.59}$$

let $c_2 = c_{20} + c_{21}$, with c_{20} and $c_{21} > 0$.

Consider the following adaptation law

$$\dot{\hat{W}}_1 = \Gamma_1[S_1(Z_1)z_1 - \sigma_1\hat{W}_1] \tag{3.60}$$

$$\dot{\hat{W}}_2 = \Gamma_2[S_2(Z_2)z_2 - \sigma_2\hat{W}_2] \tag{3.61}$$

and the following inequalities

$$-c_{21}z_2^2 + z_2\epsilon_2 \leq \frac{\epsilon_2^2}{4c_{21}} \tag{3.62}$$

$$-\sigma_1\tilde{W}_1^T\hat{W}_1 \leq -\frac{\sigma_1\|\tilde{W}_1\|^2}{2} + \frac{\sigma_1\|W_1^*\|^2}{2} \tag{3.63}$$

$$-\sigma_2\tilde{W}_2^T\hat{W}_2 \leq -\frac{\sigma_2\|\tilde{W}_2\|^2}{2} + \frac{\sigma_2\|W_2^*\|^2}{2} \tag{3.64}$$

the derivative of V_2 becomes

$$\begin{aligned}\dot{V}_2 \leq\ & -c_{10}^* z_1^2 - c_{20}z_2^2 + \frac{\epsilon_1^{*2}}{4c_{11}} + \frac{\epsilon_2^2}{4c_{21}} - \frac{\sigma_1\|\tilde{W}_1\|^2}{2} + \\ & \frac{\sigma_1\|W_1^*\|^2}{2} - \frac{\sigma_2\|\tilde{W}_2\|^2}{2} + \frac{\sigma_2\|W_2^*\|^2}{2}\end{aligned} \tag{3.65}$$

Theorem 3.2. *Consider the closed-loop system containing the plant (3.19)-(3.20), the controller (3.56), and the NN weight updating laws (3.60) and (3.61). Assume there exist sufficiently large compact sets $\Omega_1 \in R^1$, $\Omega_2 \in R^4$, such that $Z_1 \in \Omega_1$ and $Z_2 \in \Omega_2$ for all $t \geq 0$, for bounded initial conditions, all signals in the closed-loop system remain bounded, and the*

output tracking error $y(t) - y_0$ converges to a neighborhood around zero by appropriately choosing design parameter [105].

Proof: Let $\delta = \frac{\epsilon_1^{*2}}{4c_{11}} + \frac{\epsilon_2^2}{4c_{21}} + \frac{\sigma_1\|W_1^*\|^2}{2} + \frac{\sigma_2\|W_2^*\|^2}{2}$. If we choose $c_{10}^* > \frac{\gamma}{2p_1g_{30}}$, $c_{20} > \frac{\gamma}{2}$ and choose σ_i and Γ_i such that $\sigma_i \geq \gamma\lambda_{max}\{\Gamma_i^{-1}\}$, $i = 1, 2$, then from (3.65) we have the following

$$\begin{aligned}
\dot{V}_2 &\leq -\frac{\gamma}{2p_1g_{30}}z_1^2 - \frac{\gamma}{2}z_2^2 - \frac{\gamma\tilde{W}_1^T\Gamma_1^{-1}\tilde{W}_1}{2} - \frac{\gamma\tilde{W}_2^T\Gamma_2^{-1}\tilde{W}_2}{2} + \delta \\
&\leq -\gamma\left[\frac{1}{2p_1g_3}z_1^2 + \frac{1}{2}z_2^2 + \frac{\tilde{W}_1^T\Gamma_1^{-1}\tilde{W}_1}{2} + \frac{\tilde{W}_2^T\Gamma_2^{-1}\tilde{W}_2}{2}\right] + \delta \\
&\leq -\gamma V_2 + \delta
\end{aligned} \tag{3.66}$$

Thus, z_1, z_2, $\hat{W}_1$ and $\hat{W}_2$ are uniformly ultimately bounded. Since $z_1 = y_1 - y_{10}$ and y_{10} is a constant, we can conclude that y_1 is bounded. From $z_2 = y_2 - y_{20} - \alpha_1$, and the definition of virtual control α_1 in (3.45), we also can conclude that y_2 remains bounded. Using (3.56), we conclude that control u is also bounded. Thus, all the signals in the closed-loop system remain bounded.

Let $\rho = \frac{\delta}{\gamma} > 0$, then (3.66) satisfies

$$0 \leq V_2(t) < \rho + (V_2(0) - \rho)e^{-\gamma t} \tag{3.67}$$

From (3.67), we have

$$\frac{1}{2p_1g_3}z_1^2 + \frac{1}{2}z_2^2 < \rho + (V_2(0) - \rho)e^{-\gamma t} < \rho + V_2(0)e^{-\gamma t} \tag{3.68}$$

Define $g^* = max\{1, \bar{g}_{12}\}$, where $\bar{g}_{12}$ is the upper bound of p_1g_3, we have

$$\frac{1}{2g^*}\sum_{i=1}^{2} z_i^2 \leq \frac{1}{2p_1g_3}z_1^2 + \frac{1}{2}z_2^2 < \rho + V_2(0)e^{-\gamma t} \tag{3.69}$$

leads to

$$\sum_{i=1}^{2} z_i^2 < 2g^*\rho + 2g^*V_2(0)e^{-\gamma t} \tag{3.70}$$

which implies that given $\mu > \sqrt{2g^*\rho}$, there exists T such that for all $t \geq T$, the tracking error satisfies

$$|z_i(t)| < \mu \tag{3.71}$$

where μ is the size of a residual set which depends on the NN approximation error ϵ_i and controller parameters c_i, σ_i and Γ_i. □

As proved in [105], in this adaptive neural network control, we only need bounded initial conditions and bounded states (all states of the control system are proved to be bounded in [105]) to ensure the convergency of the outputs. In other words, the initialization and persistence excitation are not a problem.

3.3.5 Complete Control

For the whole system, the stability of subsystem (3.19)-(3.20) assures that $x_2 \to x_{20}$, $x_3 \to x_{30}$ as $t \to \infty$. Therefore, the convergence of x_3 makes x_1 converge to a healthy value, such that the disordered states are restored and the whole system is stable. Consequently, the disordered states in brain are restored to a normal rhythm and the bursting activity in epileptic seizures is constrained.

3.4 Simulation Study

3.4.1 Known Parameters Case

To simulate the calcium dynamics, buffer dynamics and synaptic plasticity strength, the values of the parameters used are: $y_{10} = 1 \times 10^{-5}$ mol/L, $y_{20} = 10^{-7}$ mol/L, $p_1 = 10^8$, $p_2 = 100$, $p_3 = 3 \times 10^{-5}$, $p_4 = 1.8 \times 10^{-5}$, and $p_5 = 5 \times 10^{-8}$ [92], and $Healthy(y_1) = y_{10}$, $Healthy(y_2) = y_{20}$. The initial conditions are $y_1(0) = 2 \times 10^{-5}$, $y_2(0) = 2 \times 10^{-5}$.

To verify the effectiveness of the proposed approach, we add the control algorithm designed in section 3.3.3 to form the closed loop system. Dynamics of buffer and calcium are shown in Fig. 3.1(a). As shown in Fig. 3.1(a), the states y_1, y_2 asymptotically regulate to $y_1 = y_{10}$ and $y_2 = y_{20}$ respectively, all the states remain bounded and the control action u is bounded as shown in Fig. 3.1(b), too.

The overall strength of a connection between neurons is represented by a single synaptic weight parameter. According to the state of calcium, the state of synaptic strength can also be calculated using equation (3.1). The dynamic of synaptic strength is shown in Fig. 3.1(c). From Fig. 3.1(c) we can see that with the controller we design, the synaptic strength decreases to a low level, which means synaptic depression between neurons.

3.4.2 Unknown Parameters Case

In this case, p_i $(i = 1, 2, \ldots, 5)$ are assumed to be unknown. The simulation parameters are: $y_{10} = 1 \times 10^{-5}$ mol/L, $y_{20} = 10^{-7}$ mol/L, and the initial conditions are $y_1(0) = 2 \times 10^{-5}$, $y_2(0) = 2 \times 10^{-5}$.

With the control and adaptive algorithm designed in section 3.3.4, the simulation results

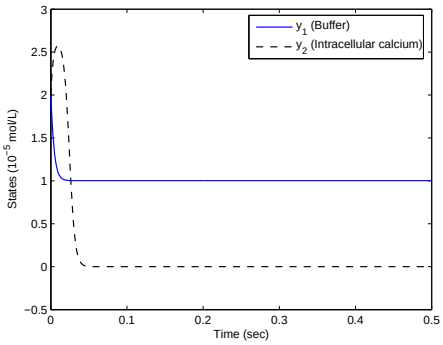

(a) States of known-parameters closed loop system

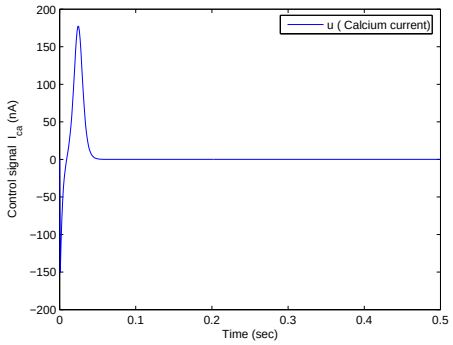

(b) Control signal of known-parameters closed loop system

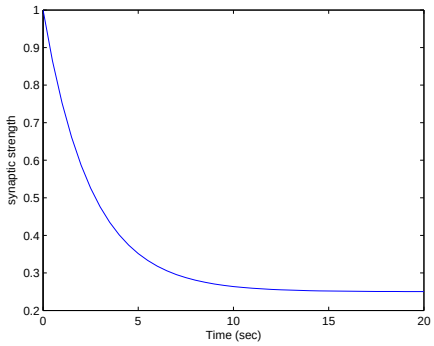

(c) Synaptic strength x_1 in known-parameters case

Figure 3.1: Simulation results of the known-parameters case

of the adaptive control system are shown in Figs. 3.2(a), 3.2(c) and 3.2(b). Dynamics of buffer and calcium concentration are shown in Fig. 3.2(a). According to the state of calcium concentration, the state of synaptic strength is calculated and shown in Fig. 3.2(c).

As shown in Fig. 3.2(a), states y_1 and y_2 converge to the healthy values y_{10} and y_{20}, respectively, while the control signal remains bounded as shown in Fig. 3.2(b). The synaptic strength, x_1, shown in Fig. 3.2(c), decreases to a low level.

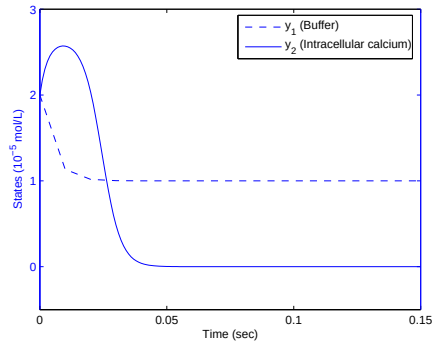

(a) States of the unknown-parameters closed loop system

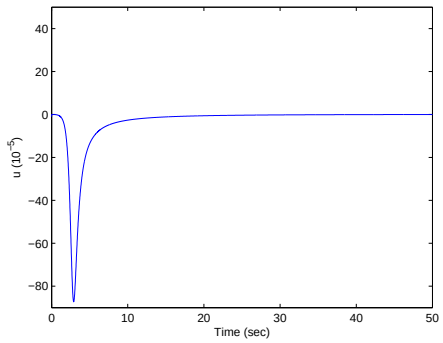

(b) Control signal of the unknown-parameters closed loop system

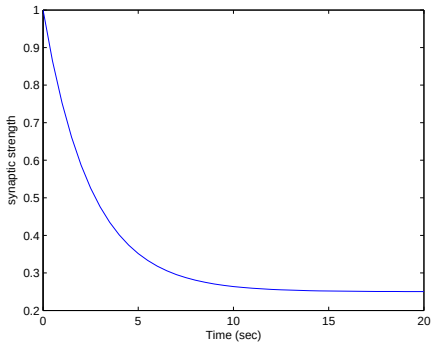

(c) Synaptic strength x_1 in unknown-parameters case

Figure 3.2: Simulation results of the unknown-parameters case

3.4.3 Simulation of Synchronized Bursting Activity

To show the synchronized bursting pattern of seizures and its constraint, we use spatially distributed single compartment neurons neural networks model. The detailed method has been described in [108]. The network consists of an array of up to 250 $\times$ 250 neurons connected locally. Each neuron is connected with two neurons randomly chosen from eight neighbors. The single neurons model is drawn from [92]. The results of Section 3.4.1 and Section 3.4.2 are used as the value of synaptic strength in this simulation.

In [108], the simulation results in the full array of neurons suggest that the spread of

firing activity and the velocity of spread are dependent on the strength of the connection, i.e., the synaptic strength. For that reason, decrease of synaptic strength might have effects on constraint of the bursting activity in seizures. This is also demonstrated in our simulation results.

The simulated local field potential is shown in Figs. 3.3(a) and 3.3(b). The former used synaptic strength which resulted from non-adaptive method, and the latter used the result of adaptive control. From Figs. 3.3(a) and 3.3(b), we can see that the seizure is constrained corresponding to the decrease of synaptic strength.

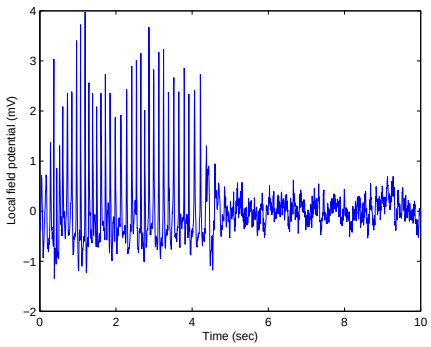

(a) Simulated local field potential in known-parameters case

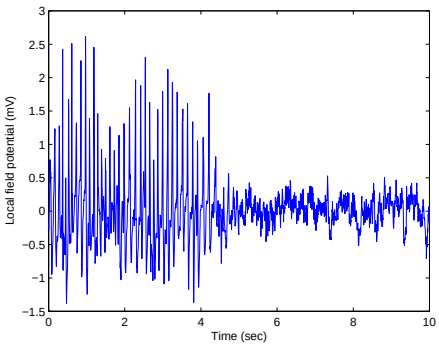

(b) Simulated local field potential in unknown-parameters case

Figure 3.3: Simulated local field potentials

3.5 Discussion

Based on the developed control strategy, a closed loop drug deliver system is designed to obtain maximum efficiency while keeping a low toxicity level. Since the direct drug injection technology bypasses the systemic circulation, it may allow higher local concentrations without systemic side effects, and do not require penetration of the blood-brain barrier,

nor systemic safety. Due to these reasons, the closed-loop, automatic direct drug injection system is promising for the treatment of focal epilepsy.

The significant progresses in measurement of cell signals and concentrations make it reasonable to think that the state variables in our study, intracellular calcium concentration, and fraction of calcium buffer, are measurable. In the past years, many genetically targetable fluorescent indicators are developed [109–111], for example, fluorescent proteins that change color upon binding Ca^{2+} [112,113], which is one of the most important dynamic signals in many types of cells, especially neurons. Although there are several measurement techniques to evaluate experimentally these concentrations, it may have a high cost or not applicable for real time measurement. Consequently, an important problem is that to estimate the states by using the output and control signal based on the information of the synaptic plastic dynamical model, in other words, design an observer. We will address the observer design problem in our next study to make the closed-loop automated drug delivery scheme more implementable in real epilepsy patients.

In this chapter, we transpose the control problem of antiepileptic drugs' dose to the value of I_{NMDA} and I_{ca}, but do not consider the underlying mechanism of the relationship between drugs and these two kinds of currents. This means further modeling should take into account the way in which the injected drug acts on control parameter u. This is in itself quite an involved problem, and we do not consider it in the present work. We suppose we can directly change the value of u, and because $u = -\alpha I_{Ca} + I_{NMDA}$, we can allow it to vary between positive and negative value. In simulation, the values of u depends on calculation of the control algorithm designed in section 3.3.

It seems that current rapid progress in biology and medicine, especially the biosensor,

drug design and biomodeling etc., will make it possible in an everyday closer perspective to complete models such as the one under study here, and open a new and very exciting field for control theory application.

3.6 Conclusion

In this chapter, the dynamic properties of the synaptic plasticity model were studied. By exploiting the system properties, the system was regrouped into two subsystems and one was in strict feedback form. The control strategy was designed via backstepping. For the unknown-parameters case, an adaptive neural control was designed. The proposed control was able to drive all the positive states asymptotically to the normal values, therefore restored the brain activities to a normal behavior. Simulation results illustrated the stability of the closed-loop system and the constraining of bursting activity in epileptic seizures. Through this study, we conclude that nonlinear control and adaptive control can be applied to biological system models to bring about a fast and systematic way to help designing therapeutics schemes.

Part II

Mind Robotic Rehabilitation of Stroke

Chapter 4

Motor Imagery BCI-based Mind Robotic Rehabilitation

4.1 Introduction

Stroke is a neurological disorder that causes severe disabilities or death [42]. Fortunately, stroke patients could partially regain their functional impairment and continue with their activities of daily living with effective rehabilitation. Traditionally, physical therapy is the de facto motor rehabilitation for stroke patients [49]. It involves human therapists for assisting stroke patients to recover their motor ability. However, physiotherapies are currently labor intensive and expensive [50]. Furthermore, hospitals and medical specialists become insufficient to support these patients suffering from stroke with rehabilitation treatment. A recent innovation in rehabilitation is robot-assisted rehabilitation. Several research studies have reported significant improvements on robotic rehabilitation outcome based on clinical measures [51, 114–117]. However, most of the designs still remain at the laboratory

prototype stage, and the appearance of these rehabilitation robots is not human-friendly. Thus there is increasing demand to develop human-friendly rehabilitation robots for stroke patient to have regular rehabilitation training at home. In this study, we aim to develop a human-friendly and interactive rehabilitation robot based on BCI technology, which is called mind rehabilitation robot.

BCI technology enables the translation of thoughts and intents of humans to actions by machines. Recently, motivated by the advances of BCI technology, BCI-based robotic rehabilitation is introduced [53], which can be called mind robotic rehabilitation. The mind robotic rehabilitation directly translates brain signals that involve motor or mental imagery into commands for controlling the robot and bypasses the normal motor output neural pathways. Hence this mind robot rehabilitation approach provides a means for stroke patients to use motor imagery to help them recover limb movement.

Studies have shown that distinct brain signals such as event-related desynchronization (ERD) or event-related synchronization (ERS) [118] are detectable from EEG for both real and imagined motor movements in healthy subjects [118–121]; as well as from NIRS [122]. Hence motor imagery brain-computer interface (MI-BCI) [123–125] which translates the imagination of movements into commands, provides a promising neural communication system for stroke patients who suffer from motor disabilities [126, 127].

In this study, based on background of motor rehabilitation and robotic rehabilitation, a recently developed mind robot rehabilitation is presented based on a non-invasive motor imagery-based BCI. We propose a way to analyze EEG data using feature fusion of CSP algorithm and AR spectral analysis, and classification algorithm, QDA, for classifying the combined features. The EEG analysis algorithms are evaluated by both off-line experiment

using some well-known open source data and a real-time experiment on the human-friendly interactive rehabilitation robot we developed.

The contributions in this Chapter lies in

(i) A human-friendly rehabilitation robot called mind rehabilitation robot is developed for training stroke patients at home as an assistive treatment instead of labor intensive and expensive hospital treatment.

(ii) Feature fusion of features derived from both CSP algorithm and AR spectral analysis is proposed, which outperforms each of the single-feature extraction methods and significantly improves BCI performance.

(iii) Both off-line experiment using some well-known data set and a real-time experiment on the mind rehabilitation robot we developed are performed. Experimental results are evaluated to demonstrate the performance of proposed EEG analysis algorithms.

4.2 Training Scenario with Human-friendly Interactive Rehabilitate Robot

The mind robotic rehabilitation system, which consists of a BCI system, a human friendly bear robot, and the subject, is shown in Fig. 4.1.

The framework and major function of the robotic rehabilitation system as well as the main modules of the BCI system are briefly shown in Fig. 4.2.

There are mainly two phases in the implementation of mind robotic rehabilitation. The first stage is the model training phase. This phase aims to obtain the best discriminative

Figure 4.1: Mind robotic rehabilitation system

parameters, including power band of bandwidth filter, the order of AR model, and projection matrix in CSP algorithm that give the best classification accuracy. The second stage is to perform the real-time experiment based on the model derived from the training phase.

The human-friendly bear robot can interactively act corresponding to the control signal obtained from the BCI system. There are three simple actions - head shaking, left arm shaking and right arm shaking, which correspond to wrong detection of motor imagery, correct detection of left hand movement imagination and right hand movement imagination, respectively.

Based on this characteristic, there are two ways of using the mind robotic rehabilitation. The first is training the motor imagery with the visual feedback from the bear robot. The cute appearance of the robot can make the training less boring and help the patient to be more cognitively engaged. The second is the motor training with physical action. Under this scenario, the patient makes a handclasp with the bear. In this way, when the bear takes

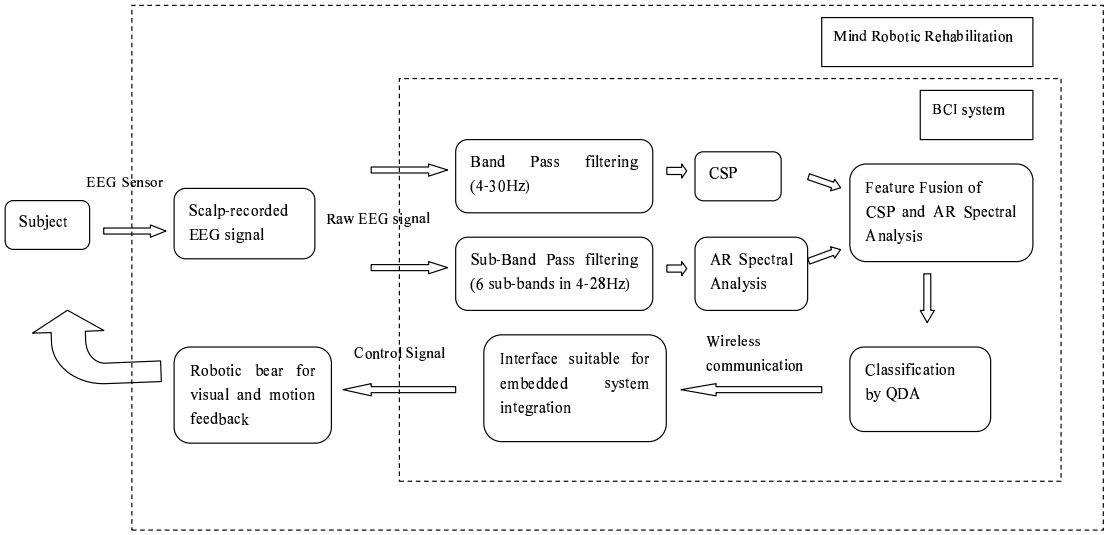

Figure 4.2: Framework of mind robotic rehabilitation system

the action of hand shaking, the physical training of patient's upper limb is also performed at the same time. As such, the patient has extensive exercises of the brain as well as the muscles during the rehabilitation training.

In conventional BCIs using EEG technology, the lengthy training periods involved for proficient usage can often lead to frustration and anxiety on the part of the user. The proposed interactive robot may solve this problem. We argue that this human-friendly robotic rehabilitation, which is relatively low cost, can make the user more engaged in rehabilitative training during the human robot interaction. This system has the potential to offer an assistive home program as aid to labor intensive and expensive hospital treatment for stroke patients.

4.3 Data Preprocessing by Band-Pass Filtering

The first stage of in the EEG analysis is to decompose the EEG data into frequency bands by band-pass filtering.

In this work, we adopt several sub-band filters as the data preprocessing for CSP algorithm, which ranges from 4 Hz to 28 Hz [128] with bandwidth of 4 Hz using optimal equiripple FIR filter. The filter which has 1 Hz transition width, 0.1 pass-band ripple and 0.0001 stop-band ripple, is designed using Parks-McClellan algorithm. The raw EEG signal is then convolved with the filter to obtain desired time-series data that contain information in the specified frequency band for further analysis in CSP algorithm.

For the AR modeling, raw EEG data is filtered using optimal equiripple FIR filter with the band width of 4-30 Hz, 0.1 passband ripple, 0.0001 stopband ripple and 1 Hz transition width. The band width 4-30 Hz is selected because it encompasses the alpha and beta frequency bands, which contain rich information on motor activity [129].

4.4 Feature Extraction and Feature Fusion

In motor imagery-based BCI, numerous methods have been proposed as filters to extract feature patterns from EEG signal. One of the promising and commonly used methods is CSP analysis which uses covariance to design common spatial patterns based on the simultaneous diagonalization of two covariance matrices. Since CSP algorithm is optimal for the discrimination of two populations, it is well suited for discrimination mental states that are characterized by motor imagery. In other words, it utilizes spatial pattern classification to determine spatial filters that maximize the variance of signals of left trials and at the

same time minimize the variance of signals of right trials.

But because the CSP method is very sensitive to artifacts, the motor imagery based BCI system using CSP method will have a high false alarm rate, that's to say, during the on-line operation of the BCI, even when the subject is not responding, the system may give a right or left command. Some preliminary work has solved this problem by performing a weighted spatial averaging of the EEG to reduce the influence of artifacts [130].

In this study, we try to solve this problem in another way by combining two different feature extraction algorithms, the spatial filter CSP and a temporal filtering algorithm AR spectral analysis. The feature fusion of both CSP derived features and AR derived features is utilized for later classification of motor imagery EEG signal in both model training and real time implementation.

4.4.1 Common Spatial Patterns Analysis

The CSP technique [131] is able to determine spatial filters that maximize the variance of signals of one condition and at the same time minimize the variance of signals of another condition. In other words, the CSP algorithm gives spatial filters based on a discriminative criterion. The decomposition (or filtering) of the EEG leads to new time series, which are optimal for the two population. The patterns are designed such that the signal results from the EEG filtering with the CSP has maximum variance for left trials and minimum variance for right trials or vice versa.

In this way, the difference between left and right populations is maximized, and the only information contained in these patterns is where the variance of the EEG varies most when comparing two conditions. As such, CSP filters are well suited to discriminate mental

states that are characterized by motor imagery [53,128,130]. The CSP filters are commonly utilized in BCI systems, most of which are calculated individually for each subject on the data of a calibration measurement. In [130], subject-specific spatial patterns are derived by common spatial patterns to be weighted for each electrode according to its importance to the discrimination task and suppress noise in individual channels by using correlations between neighboring electrodes. In [124], subject independent features by CSP are utilized to develop a non-invasive BCI system with fast acquisition of effective performance in untrained subjects.

The goal of CSP algorithm is to design spatial filters that lead to new time series whose variances are optimal for the discrimination of two classes of EEG [132]. From technical point of view, the CSP algorithm gives a projection matrix $W^T \in R^{N\times N}$ (N denotes the number of channels), that projects the signal $x(t) \in R^N$ from original sensor space to $y(t) \in R^N$ in a surrogate sensor space, as:

$$y(t) = Wx(t) \tag{4.1}$$

Usually, we call each row vector $w_j \in R^N$, $j = 1, 2, \ldots, N$ of W a spatial filter and each column vector $a_j \in R^N$, $j = 1, 2, \ldots, N$ of the matrix $A = W^{-1} \in R^{N\times N}$ a spatial pattern. In [131], the authors showed that two pairs of vectors (w, a) that correspond to the largest and the smallest eigenvalues for one subject topographically mapped onto a scalp and demonstrated that the interpolation of the value of the components of vectors w_j, and a_j at electrode positions can be somehow related to the neurophysiological understanding of ERD/ERS for motor imagination.

Through a optimized spatial filter, the filtered signal $y(t)$ in (4.1) have maximized differences in the variance of the two classes of EEG measurements. Let X^1 and X^2 be the data matrices of a short segment of the band-pass filtered EEG signals under two different conditions, i.e., left hand or right hand imagination, respectively. X^1 and $X^2 \in R^{N\times D}$, where N denotes the number of channels, and D denotes the number of samples in a trial in each channel. In training phase, given Q^i trials of EEG signal X^i, $i = 1, 2$ for left hand movement imagination and right hand movement imagination, the corresponding estimates of the average normalized covariance matrices $\Sigma^i \in R^{N\times N}$ can be obtained by

$$\Sigma^i = \frac{1}{Q^i}\sum_{Q^i}\frac{X^i(X^i)^T}{\text{trace}[X^i(X^i)^T]}, i \in \{1, 2\} \tag{4.2}$$

Then the CSP analysis is given by the simultaneous diagonalization of two covariance matrices.

$$W\Sigma^i W^T \quad = \quad \Lambda^i \tag{4.3}$$

where Λ^i $(i = 1, 2)$, is a diagonal matrix and $\Lambda^1+\Lambda^2 = I$. Note that $\lambda^i_j = w^i_j\Sigma^i(w^i_j)^T$ $(i = 1, 2$ and $j = 1, 2, \ldots N)$ is the corresponding j-th diagonal elements of Λ^i, and $\lambda^1_j+\lambda^2_j = 1$, since λ^i_j is in fact the variance of y_j in condition i in the corresponding surrogate space of x_j, a large value of λ^1_j close to one indicates that the corresponding spatial filter w_j yields high variance in condition 1 and a low variance in condition 2, and vice versa.

Technically, the simultaneous diagonalization can simply be achieved by solving the generalized eigenvalue problem

$$\Sigma^1 W^T = \Lambda\Sigma^2 W^T \tag{4.4}$$

using the command $[W^T, \Lambda] = \text{eig}(\Sigma^1, \Sigma^2)$ in MATLAB, where Λ is a diagonal matrix of generalized eigenvalues λ_j, and W^T is a full matrix whose columns are the corresponding

eigenvectors to fulfill (4.4). Since $\lambda_j = \lambda_j^1/\lambda_j^2$, based on the former analysis, the largest and smallest diagonal elements in Λ are corresponding to the spatial filters which keep most discriminative information.

Mathematically, the problem can be solved by singular value decomposition, as for the composite spatial covariance is given by

$$\Sigma^c = \Sigma^1 + \Sigma^2 = U^c \psi (U^c)^T \tag{4.5}$$

where U^c is a matrix of normalized eigenvectors with corresponding matrix of eigenvalues, ψ. We then define a whitening transformation as

$$P = \sqrt{\psi^{-1}}(U^c)^T \tag{4.6}$$

This transformation equalizes the variances in the space spanned by U^c, so that the CSP can be extracted based on the simultaneous diagonalization of whitened covariance matrices for Σ^1 and Σ^2

$$\begin{aligned} \hat{\Sigma}^1 &= P\Sigma^1 P^T \\ \hat{\Sigma}^2 &= P\Sigma^2 P^T \end{aligned}$$

and the decomposition maximizes the differentiation between two groups of data can be done by calculating orthogonal matrix B and diagonal matrix f,

$$\begin{aligned} \hat{\Sigma}^1 &= BfB^T \\ \hat{\Sigma}^2 &= B(1-f)B^T \end{aligned}$$

With this, we have the CSP projection matrix

$$W = B^T P \tag{4.7}$$

and the spatial mapping of t-th trial of EEG signal as

$$y(t) = Wx(t) \tag{4.8}$$

For classification, the features of each single-trials are calculated as the log-variance in CSP projected signals. Since the largest and smallest diagonal elements in Λ are corresponding to the spatial filters which keep most discriminative information, in other words, the first r and the last r rows of W would contain the most discriminative information, only $2r$ (r is usually chosen as 2) patterns are used. The variance features are approximately chi-square distributed, and taking logarithm makes them similar to Gaussian distributions so that a linear classifier can be used for classifying the features. Therefore, feature vector of t-th trial EEG signal is generated as follows:

$$F_t = \log \frac{\text{var}[y_j(t)]}{\sum_j \text{var}[y_j(t)]}, j = 1, \ldots, r, N - r + 1, \ldots, N \tag{4.9}$$

There are $2r$ features for each sub-band. As there are 6 sub-bands after the band pass filtering as mentioned above in Section 4.3, $6 \times 2r$ features can be derived each single trail of EEG.

4.4.2 Autoregressive Spectral Analysis

Besides CSP algorithm, attenuation or increase of localized neural rhythmic due to actual and imagined motor activity can also be detected by observing the change in band power [133, 134]. Before the band power spectral analysis, the raw EEG time series is convolved with the band-pass filter mentioned in Section 4.3. The estimate Power Spectral Density (PSD) of the filtered signal is then calculated through autoregressive (AR) spectral analysis.

Filtering before estimating its PSD is important because noisy data (contains high frequency component, i.e., more than 30 Hz) will affect the AR modeling accuracy.

A proper order of the AR model should be examined to ensure good modeling quality. In this study, AR model of 8 is selected and it is consistent with other works [135, 135, 136].

Yule-Walker method [137] is used to estimate the AR parameters. The estimated AR parameters are then used to calculate estimated PSD of the EEG signal. The power spectrum is given by

$$P_{xx}(f) = \frac{\sigma^2}{\|1 + \sum_{k=1}^{p} a_p(k) e^{-j2\pi fk}\|^2} \tag{4.10}$$

where $a_p(k)$ denotes the estimates of the AR parameters obtained using Yule-Walker method, σ^2 is the variance of the white noise, and p denotes the order of AR model.

The discriminative band normally lies within 8 to 25 Hz [120]. Since the most important brain activities during motor imagery are within the α and β range, the power spectral density is calculated in 4 frequency ranges: $8-10$ Hz, $10-12$ Hz for α; and $20-24$ Hz, $24-28$ Hz forβ. Let d_0 represents the beginning of band power, bw represents the selected bandwidth, P_{xx} represents the power spectral density estimation obtained using Yule-walker's method. The selected range of band power P_b for one channel EEG can be calculated as

$$P_b = \sum_{d_0}^{d_0+bw} P_{xx} \tag{4.11}$$

The band power P_b is used as feature for classification, and the feature vector consists of P_b of four different frequency band range in two channel of EEG signal, C3 and C4. As such, 8 features in total are extracted from one trial of EEG signal. This 8-elements feature

vector is then appended to the $6 \times 2r$-element feature vector F_i derived from CSP algorithm to form a fused feature, which can be denoted as $F_{combined}$.

4.5 Classification by Quadratic Discriminant Analysis

Using the combined feature vector, $F_{combined}$, QDA [138] is used for classification. Quadratic discriminant analysis (QDA) is closely related to linear discriminant analysis (LDA), the difference is in QDA there is no assumption that the covariance of each of the classes is identical.

The classifier works by estimating the probability that an observation, x, belongs to each class, k, and then selects the class with the highest probability. The posterior probability of each class k is given as

$$Pr(k) = \frac{f_k(x)\pi_k}{\sum_{j=1}^{k} f_j(x)\pi_j} \tag{4.12}$$

where $f_k(x)$ is the probability density function of data in class k, and π_k is the prior probability of class k.

Assume all the classes have multivariate normal distribution, the probability density function of data in class k is given as,

$$f_k(x) = \frac{1}{(2\pi)^{p/2}\|\Sigma_k\|^{1/2}} e^{-\frac{1}{2}(x-\mu_k)^T \Sigma_k^{-1}(x-\mu_k)} \tag{4.13}$$

where p is the dimension of x, $\mu_k = \sum_{x_i \in k} \frac{x_i}{N_k}$ is the Gaussian mean of data in class k, and covariance matrix $\Sigma_k = \sum_{x_i \in k}(x_i - \mu_k)(x_i - \mu_k)^T$.

The prior probability of class k can be estimated as

$$\pi_k = \frac{N_k}{N} \tag{4.14}$$

Ignore the same denominator of posterior probability for each class, if we take the log of the numerator and ignore the constant $(2\pi)^{p/2}$ in the density function, we can get the quadratic discriminant function:

$$\delta_k(x) = -\frac{1}{2}\log|\Sigma_k| - \frac{1}{2}(x-\mu_k)^T\Sigma_k^{-1}(x-\mu_k) + \log\pi_k \tag{4.15}$$

Then, the class for a observation x can be selected as the class with the highest score according the the discriminant function.

4.6 Experimental Evaluation

This section reports an empirical evaluation of the proposed EEG analysis algorithms for BCI-based mind robotic rehabilitation. The EEG analysis algorithms are evaluated by both off-line experiment using some well-known open source data and a real-time experiment on the human-friendly interactive rehabilitation robot developed.

4.6.1 Data Acquisition

To evaluate our method, we first use dataset III from BCI competition II 2002 [139] for off-line training experiment. The experiment consisted of 7 runs with 40 trials each. Each trial was 9 s in length. The first 2 s was quiet, followed by an acoustic stimulus indicating the beginning of the trial at $t = 2$ s. A cross "+" was displayed for 1s followed by an arrow (left or right) at $t = 3$ s. The subject was asked to move a bar into the direction of the cue. The recording was made using a G.tec amplifier and a Ag/AgCl electrodes. Three bipolar EEG channels (anterior '+', posterior '-') were measured over $C3$, C_Z and $C4$. The EEG signal was sampled at 128 Hz and it was filtered between 0.5 and 30 Hz.

In the real-time implementation, the EEG signal was acquired at sampling frequency 128 Hz by a wireless EEG acquisition system, Bioradio150 Kit by Clevemed. Three electrodes were positioned at C3, C4 and CZ according to the international 10-20 standard electrode placement. There were 200 trials for training and each trial lasted for 9 seconds with a cue of left or right arrow to remind the subject. After training, real-time testing was performed based on the data analysis model obtained from the training phase. For each trial, a 1 second windowing was used. These time segments are well-chosen so that each segment contains most of the useful information. It should neither be too long to be unstationary nor too short to have incomplete information.

4.6.2 Off-line Training Experimental Results

Although in Chapter 2, SVM gives good results for epilepsy detection, for this study, the SVM cannot perform well to classify the motor imagery signals. The classification results are shown in Table 4.1.

Table 4.1: The classification accuracy obtained by SVM classifier

Subject (number of training trials)	Accuracy Rate (CSP+AR)
subject 1 (200)	0.5182
subject 2 (200)	0.4
subject 3 (200)	0.5556
BCI competition 2, dataset III	0.6124

To improve the experimental results, in this experiment, QDA classifier is used instead of SVM. We compare the classification accuracy in the training phase between CSP method, AR spectral analysis method, and the feature fusion with both CSP features and AR feature. A 10×10 fold cross validation is used to obtain the classification accuracy, as shown in Fig. 4.3 and Table 4.2.

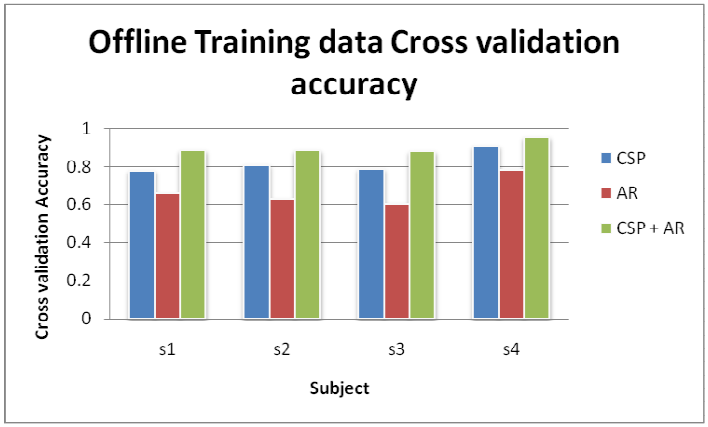

Figure 4.3: Classification accuracy for off-line training

Table 4.2: The classification accuracy (mean ± standard deviation) in off-line training

Subject (number of training trials)	CSP only	AR only	CSP+AR
subject 1 (200)	0.7758 ± 0.0172	0.656 ± 0.0168	0.8814 ± 0.0122
subject 2 (200)	0.8063 ± 0.0188	0.6281 ± 0.0219	0.8809 ± 0.0146
subject 3 (200)	0.7859 ± 0.0194	0.6016 ± 0.0184	0.8762 ± 0.0149
BCI competition 2, dataset III	0.9054 ± 0.0139	0.7819 ± 0.0233	0.9513 ± 0.0109

As a reference information, the maximum accuracy rate obtained by the winners of BCI competition 2, dataset III is 89.29%. The cross validation results suggest that the fusion method does provide an improvement in classification accuracy as shown in Fig. 4.3 and Table 4.2.

4.6.3 Real-time Testing Experimental Results

A comparison of the classification accuracy in the real-time testing phase between CSP method, AR spectral analysis method and the feature fusion with both CSP features and AR feature is also performed. The testing data directly use the data analysis model derived from the training phase to obtain the label of left/right hand movement imagination. The results are shown in Fig. 4.4 and Table 4.3.

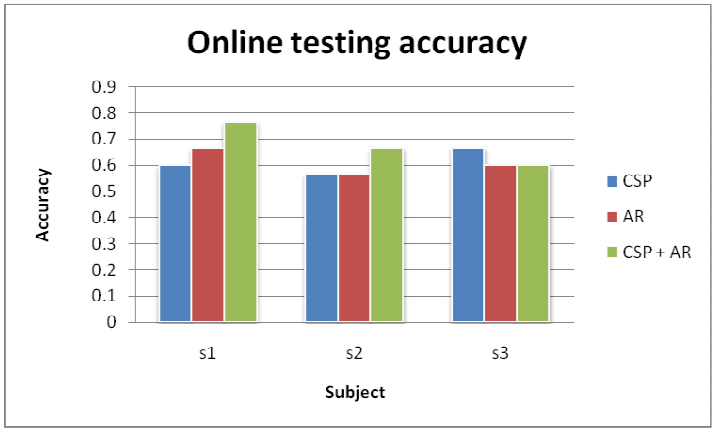

Figure 4.4: Classification accuracy for real-time testing

Table 4.3: The real-time testing accuracy

Subject (Number of test trials)	CSP only	AR only	CSP+AR
subject 1 (30)	0.6	0.6667	0.7667
subject 2 (30)	0.5667	0.5667	0.6667
subject 3 (30)	0.6667	0.6	0.6

The results suggest that the fusion method also outperforms single feature extraction algorithm in real-time testing phase as shown in Fig. 4.4 and Table 4.3.

4.7 Discussion

The fusion method aims to provide as many features as possible for the classifier in order to improve the accuracy. CSP method contains information on spatial distribution while AR method captures changes in band power due to brain activities. Thus, the combination of the two may offer more useful discriminative information for classification of the EEG data.

Evidence suggests that BCI robotic rehabilitation resulted in greater motor improvements than standard robotic rehabilitation. However, the results are currently inconclusive due to the large variations in motor improvements in both groups and the limited number

of stroke patients recruited for the study. A final conclusive result could be drawn from a larger scale study. Nevertheless, the outcome of this preliminary study is promising as it demonstrated the role of the mind robot approach in neurological rehabilitation.

4.8 Conclusion

In this chapter, a human robot interface called mind robotic rehabilitation was developed based on BCI technology for regular training of neurological rehabilitation for stroke patients. A human-friendly interactive robot was used as a visual and motion feedback for BCI to make the user better engaged into rehabilitative training during the human robot interaction. Feature fusion of CSP algorithm and AR spectral analysis was proposed. QDA was used as classifier to classify the combined feature vectors. Off-line experiment and real-time implementation were performed using some well-known open source data and real-time recording data. The experimental results demonstrated that feature fusion significantly improved BCI performance.

Part III

Social Therapy of Autism

Chapter 5

RoBear with Multimodal HRI for Social Therapy of Autism

5.1 Introduction

According to some earlier research [140], the social-emotional disorder of autistic children may be caused by badly developed connections between brain cells in the social brain region. Prevention and rehabilitation of this disorder may rely on social training, which is effective for development of neuron connections in the social brain region. In this chapter, social training scenarios are designed based on well-known hypotheses of cognitive science and social psychology, in the form of interactive games between robot and patient. During the social rehabilitation process, robot will automatically identify patient and elicit certain information of that patient, followed by therapy of management according to societal norms.

In view of the growing problem of autism among children today, the proposed interactive robot for social therapy is primarily envisioned as a valuable tool that will better the lives

of children with autism, by facilitating the learning of social norms and preparing them for future integration into society. Apart from autism, it can also be further developed for other forms of social-emotional disorders, for example, depression, anxiety, or utilized as an educational tool for training normal children during their social-emotional development period and as a social companion to enhance social skills.

The contributions in this Chapter lies in

(i) An interactive robot pet, RoBear, is developed based on a good understanding of autism-related hypotheses of neuroscience and cognitive science to help autistic children. The robotic social therapy can reduce the cost for hospital training while helping reinforced learning of the social skill.

(ii) A multimodal HRI framework is proposed, and several important modules of the multimodal HRI is presented. With the multimodal HRI, RoBear has potential to act as a social companion of autistic children.

(iii) A social training schemes for social-emotional development of autistic children is proposed as the form of child robot interaction.

5.2 Hypotheses of Human Social-Emotional Development

Knowledge of what social and emotional activities have to do with the brain could has a great impact on improving human social development. Only by understanding how the brain acquires and lays down information and skills will we be able to help people make good use of and adapt to social communication.

Autism is a life-long developmental disorder that affects 0.2-0.6% of the population. Autism is a social-emotional developmental disorder that impairs the ability to communicate and socialize. Autistic children experience social impediments of varying degrees, including fear of social interaction, lack of empathy for other individuals, and difficulties in managing emotional response to stimuli from environment. To be concise, the core feature of autistic disorders is the failure of perfectly ordinary social communication at all ages and all levels of ability [140].

In [141], the authors explored a phenomenon showing that an extensive vocabulary, and self-taught reading skills are common in autistic children who usually got a low score in IQ test though. This phenomenon suggests that the brain is specialized into different modules, and only some but not all brain systems are disrupted in autism.

One controversial and still speculative idea is that the brain of the newborn infant comes equipped with various star-up mechanisms. These enable fast-track learning in particularly important domains. In autism, one or more of these modules may be faulty [140]. However, some researchers prefer to think that specialization is an outcome of development and not its staring point. In [142, 143], the authors suggest that brain development is not explained well by start-up kits and modules, but that instead, experience itself will lead to the gradual development of modules in the adult brain. This hypothesis can be explained by development of human brain modules.

Before discussing the development of human brain, some assumptions derived from neuroscience need to be presented.

Assumption 5.1. *In normal brain development, connections between brain cells (synapses) at first multiply, and are then pruned away according to how much they are used. [67, 140,*

144]

Assumption 5.2. *Appropriate synaptic pruning does not occur in brain of those with social-emotional disorder.*

Assumption 5.3. *As soon as a baby is born, its brain connections start growing and changing. Which connections survive and grow and which fade away and die is determined partly by the genes the baby inherits from its parents and partly by the baby's early experiences [140].*

Based on these assumptions, children should be exposed to all kinds of experiences to build the related ability. In [145], it is claimed that the synaptic of the brain region in charge of the social ability will lead to gradual development by related experience. The production of synapses in the brain is strongly linked to the ability to learn. The studies on development of auditory cortex, primary visual cortex, and middle frontal gyrus [146, 147] may implicate similar developing pattern of brain region related to social ability.

Children, especially those in the first year of life, develop the capability for social communication through physical and social interactions with their caregivers and toys [67,148,149]. The three stages of social development in a supportive environment during the first year of life are as follows:

(i) In the first three months, the child establishes eye contact with the caregiver, as shown in Fig. 5.1.

(ii) From three to nine months, the caregiver can observe active response of the child, and the child gradually learns to predict the caregiver's behavior, which makes the interaction more sociable. This is simply demonstrated in Fig. 5.2.

(iii) Over nine months, the child and caregiver will successfully form a joint attention. This is usually initiated by the caregiver sharing the awareness and perception of the target through vocalization or facial expressions, as shown in Fig. 5.3

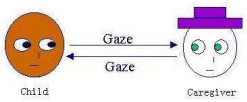

Figure 5.1: Eye contact

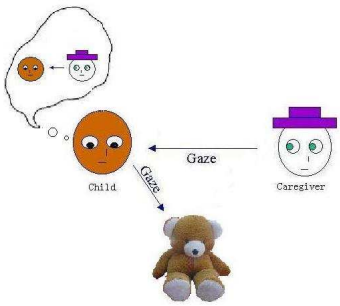

Figure 5.2: Actively responds

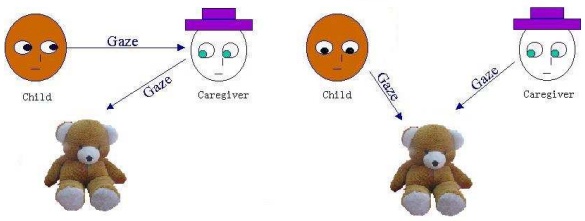

Figure 5.3: Joint attention

In summary, touch, eye contact, and joint attention are fundamental behaviors that maintain child-caregiver interactions and establish a basis for empathetic understanding of

each other's mental states [148, 150]. A Child and a caregiver spatially and temporally correlate their attention and emotions, referring to each other's subjective feelings of pleasure, surprise, or frustration [151–153]. All such successful social-emotional communications are helpful for children to learn social skills [152–154], since experience itself will lead to the gradual development of modules in the brain [142, 143]. Connections between brain cells increase and decrease according to how much they are used. In [155–158], it is suggested that there are specific brain regions which are active when individuals engage in social activity, called the *social brain*. The target of this study can be simply presented as "training the social brain".

5.3 Interactive Social Robot for Training the Social Brain

5.3.1 Child-Robot Interaction

Studies showed that individuals with social-cognitive disabilities, including autistic children, tend to be more receptive to robots than human beings [67]. Several mobile and interactive robots were utilized to build interaction between autistic children and robots for the study of children's social development [68–70]. Studies showed that autistic children interacting with robots exhibited positive proto-social behaviors such as touching, vocalizing, smiling, which were rare in their daily life. A possible explanation for these facts lies in the simple and cute appearances of the social robots, which make the social robots commonly seem more harmless and acceptable to children. Also, by discarding traditional complex physical structure of robot like humanoid robot and android robot, social robots convey less information so that even the children with autism will not be confused by overwhelming

information.

Assumption 5.4. *People normally have a social filter that extracts the basic information such as "attention" and "emotion" from the large quantities of raw information produced by other's behavior, as shown in Fig. 5.4. It is also assumed that this kind of social brain function in autistic children is possibly disabled, which result in an information overload so that the autistic children cannot handle it and get confused, as shown in Fig. 5.5. [67]*

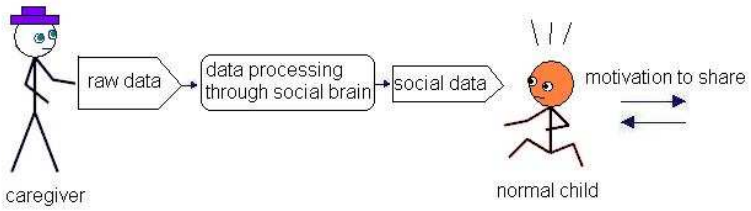

Figure 5.4: The social filter in typically developing children

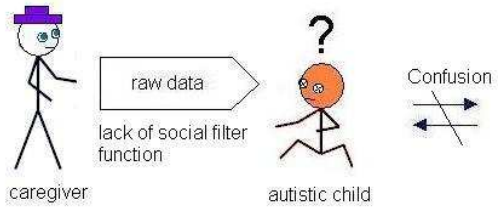

Figure 5.5: Dysfunction of social filter in autistic children

The possibly simple and modular function and emotion expression of social robot may open a bypass channel directly transmit robots' attention, emotion, touch, eye contact, which is simple and comprehensible information for the autistic children so that their confusions caused by overwhelming information are avoided, as shown in Fig. 5.6.

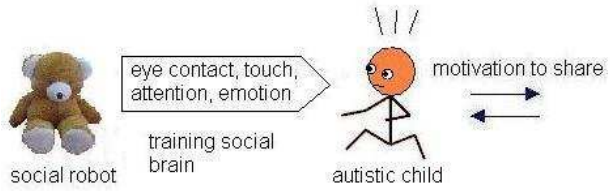

Figure 5.6: Bypass channel for social brain training by social robot

It has been demonstrated that early behavioral or cognitive intervention can help autistic children gain self-care, social, and communication skills. As such, it is promising to develop effective child-robot interaction that helps autistic children to acquire key social skills that allow them to integrate better with society.

5.3.2 Development of the Interactive Bear Robot

In neurological therapy for autism, an individualized treatment plan should be established for each patient after an in-depth evaluation of the patient's needs and goals. To maximize progress, patients receive individualized treatment by the same therapist. However, the hospital treatment of autism is expensive. In [159], a study estimated an average lifetime cost of $3.66 million. In [160], a study found a 14% average loss of annual income in families of children with autism. As an alternative way, home programs are also helpful for reinforced learning of the social skill. As such, there is increasing need of more effective and low cost autism therapy to help the autistic children to be better engaged in society to increase quality of life and to lessen the associated deficits and distress of family.

A possible solution is the interactive robot. In [67], the author claimed that a humanoid

robot *Infanoid*, with an anthropomorphic but highly mechanistic appearance, conveyed an overwhelming amount of information to children under three years of age. It was also found that children's attention is often attracted by moving parts, especially the hands, fingers, eyes, and eyebrows. Effort is required to integrate the qualitative movements into some holistic recognition of a social agent.

To encourage children to engage robots naturally, the aesthetic appearances of robots should be designed. Additionally, the robot should be designed for safe and compliant interactions with humans. Inspired by these observations, appearance of social robot for children should be simple and cute, without complicated physical and mechanistic structure. The popular humanoid and android robot is not suitable here. In our study, an interactive social robot with a cute and attractive bear appearance is designed as illustrated in Fig. 5.7. This robot is named "RoBear".

Figure 5.7: Appearance of RoBear

With the rapid developments in the fields of sensing technologies and robotics, there is an increasing need for interactive social robots to employ a multimodal HRI to obtain natural,

human like communication capabilities [161, 162]. There are several core and indispensable modules in the making of multimodal HRI, including human identification, flexible dialog and speech understanding, human like facial expressions, and emotional interaction, etc. The multimodal HRI can enable robots to interact and communicate between themselves, with humans, and with the environment, so that it can work as an ideal alternative caregiver of autitic children.

Fig. 5.8 shows an overview of the modules employed for multimodal HRI. In this work, several moduls would be integrated on RoBear for real-time multimodal HRI which can help to train the social ability of autistic children.

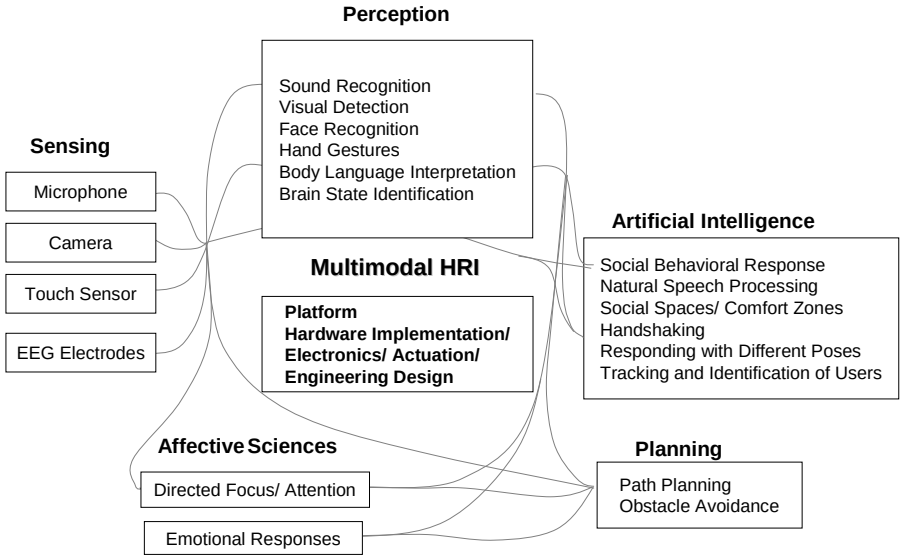

Figure 5.8: Overview of the core technologies involved in multimodal HRI

The most important modules of RoBear are presented as follows.

Touch Reaction

A low cost touch sensing system is developed to enable RoBear to sense and react to a human's touch. A recognition system is designed to accurately interpret the human's intention to offer a handshake and respond to the offer, mimicking the socially accepted behavior associated with the initiation handshaking. Additional considerations include the decision to continue or terminate the handshaking process. A pressure sensor in the abdomen of the bear will sense the hit, then the bear will react mimicking human.

Sound Localization

Effective sound localization allows robots to focus their attention on pertinent objects within their environment much like how humans act. Sound localization is a listener's ability to identify the location or origin of a detected sound or, the methods in acoustical engineering that simulate the placement of an auditory cue in a virtual 3D space. In this study, sound localization serves as an enabling technology to realize a human-like behavior in RoBear. During conversations, it is natural and polite for the listener to face the speaker. Through research on sound localization techniques, this behavior is replicated in RoBear. The detailed algorithms and implementations for sound localization were presented in [163, 164].

Voice Recognition and Conversation

Speech is the most common and natural form of communication between humans. However, natural speech is difficult for robots to understand during human-robot communications. To develop a natural and human-centric robot, we seek to empower RoBear with speech capabilities, whereby RoBear is able to understand simple phrases and commands and respond

accordingly either through speech or actions. Through the integration of a limited speech recognition module and speech synthesis module, RoBear is equipped with a vocabulary of up to 40 phrases to be able to maintain simple conversations with its user.

On the other hand, because autistic children with different neurological problems will have different kinds and levels of difficulties during social activity, each of then should be treated differently. As such, a very important aspect in developing RoBear for autistic children is the ability to identify people. The ability to identify people allows the robot to authenticate user and provide separate services for each user. An intelligent robot auditory perception system is developed to robustly detect and identify human's voice from a variety of background sounds by sound resource recognition algorithms. The objective of sound source recognition for audio human detection is to identify human's voice among a group of sound sources for robot to communicate and cooperate with people. The detailed methods of sound recognition for intelligent robot auditory perception system are presented in Chapter 6.

Vision System for Human Face Detection and Recognition

Besides the sound recognition for human identification, a real-time robot vision is developed for detecting and recognizing human face. The vision system consists of a normal camera that is placed in the RoBear. The human face is detected using Adaboost-based Haar-Cascade classifier, and then Extreme learning machine (ELM) is used to improve the real human face detection. Feature extraction algorithm, Weighted locally linear embedding (WLLE) are utilized for finding compact and distinctive descriptors for face images to recognize human face. The detailed algorithms and implementations are presented in

Chapter 7.

Human Facial Expression Recognition

Due to the important roles facial expressions play in human expression of emotions and non-verbal communications, it is not sufficient for RoBear to just display its own emotions. To make RoBear truly interactive, it is necessary to build a facial expression recognition system for RoBear to understand subtle changes in its user's facial expression and react accordingly. The detailed facial expression recognition framework was illustrated in [165].

Robotic intelligence and control

To provide interactive responses to users in real time, feedback control is required for various actuators in the robot. Control and decision-making issues that need to be addressed include stability and safety, robustness to uncertainties, as well as additional difficulties due to the inclusion of human users in the loop, abrupt changes in human intentions, and time delays in interactions from computational and signal processing. The system needs to respond with minimal delay in computational processing so as not to disrupt the natural flow of communication between user and robot.

5.4 Training Scheme for Social-Emotional Development

For the social rehabilitation process, training scenarios designed based on well-known knowledge of cognitive science and social psychology, in the form of games between the robot and children, are carried out. During the social rehabilitation training, the robot elicits certain physical and psychological states in the subject, followed by specific therapy of management

according to societal norms.

The training scenarios are designed according to some basic stages of social development adopted from cognitive science and social science.

5.4.1 Eye Contact

The vision system of the bear can detect and recognize human face and act responsively by tracking the face through controlled slow movement of the bear's head for centering the face in the camera view. As such, the bear will turn its head to face child, once he gazes at the bear. This response of bear works like eye contact apparently. To encourage children for the eye contact, the bear will say "hello" to children once their gaze is on it for more than 5 seconds, which is also a natural response in human social environment. The eye contact action between child and bear is shown in Fig. 5.9

Figure 5.9: Eye contact between child and RoBear

5.4.2 Touch Reaction

Touch is an important aspect of human social interactions and communications. A social behavior related to touch is handshaking. Although not a universal form of greeting, hand shaking is still recognized as one of the most commonly used greeting in the world today and it is commonly associated with the demonstration of good will between the two parties. The bear robot is designed to have the ability to react to handshaking and touching on its abdomen. During this training, the caregiver can demonstrate the touch reaction of the bear to children and then let them try it themselves. The touch reaction and handshaking with interactive social robot are shown in Fig. 5.10.

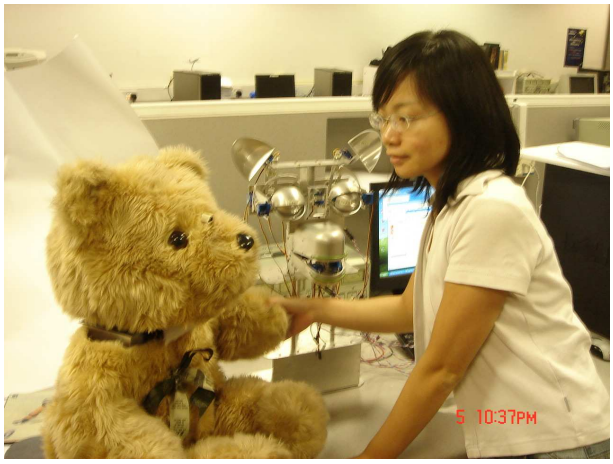

Figure 5.10: Touch reaction and handshaking with RoBear

5.4.3 Vocal Communication

Speech is the most common and natural form of communication between humans. To build an effective conversation skill is important for children's social-emotional development, thus it is natural and important to contain the vocal communication in the social-emotional

training for children. In this study, the bear is empowered with speech capabilities, whereby the bear is able to understand simple phrases and commands and respond accordingly either through speech or actions. According to Assumption 5.4, children with autism cannot handle the massive information brought by other's complex behavior, so the conversation between children and bear should be really simple and fixed without confusion. Based on this observation, a simple conversation scenario is built for training autistic children.

In the human robot interaction through conversation, the bear can make some dialogue as follows:

(i) Introduction:

- Bear: Hello! My name is Teddy. What's your name?
- Child: My name is John.
- Bear: Nice to meet you, John! Let me sing a song for you.
- Child: Thank you!
- Bear: (Singing)

In this conversation, the bear will only start singing if the child gives some vocal reaction. If the child keeps silence, the bear will repeat the question.

(ii) Requisition:

- Bear: Can you pass me a banana?
- Child: (pass the banana)
- Bear: This is a banana. Thank you!

or

- Child: (pass the apple)
- Bear: No, this is an apple.

This process is illustrated in Fig. 5.11.

Figure 5.11: Conversation interaction with RoBear

All these conversations should be demonstrated by the caregiver at the beginning of the training, and then done by children. Through repeated exercise of listening and speaking, the child may gradually become more conformable in vocal communication.

5.5 Conclusion

In this chapter, the development of an interactive robot pet, RoBear, for social therapy of autism was presented. The RoBear was developed based on knowledge of cognitive and social science, by combining multimodal HRI and pattern recognition algorithms. Through implementation of a variety of social-emotional training for children, we found RoBear is an ideal robot companion for children, and even has potential for helping autistic children. The ongoing research is aimed at testing the interactive robot pet, RoBear, on autistic children

to evaluate the effectiveness of the proposed methods and training scheme. We should also test our underlying assumptions about social interaction and development, and broadening our understanding of human social behavior on the neuroscience, cognitive science and social science level. Another future research may be building user-friendly hardware for EEG-based BCI system and developing empathetic social robot. This empathetic robot should rely primarily on EEG-based BCI technology to extract information of the mental and emotional state of the subject.

Chapter 6

Sound Source Recognition for Human Robot Interaction

6.1 Introduction

In last chapter, the development of an interactive pet robot is proposed based on multimodal HRI. The ability to identify people is essential for robot to communicate and cooperate with people in HRI. This ability allows the robot to authenticate user and provide separate services for each user. In this chapter, we focus on one of the important human identification technologies, the intelligent auditory perception system to robustly detect and identify human's voice from a variety of background sounds.

The intelligent audio system for sound source recognition is implemented on RoBear proposed in last chapter. In order to obtain a similar model as a human-human interaction model, we designed a human-like perception system with two cameras and two microphones, to imitate human perceptual capabilities.

Auditory system analysis is experiencing a surge of research activities in the literatures [166–169]. The objective of sound source recognition for audio human detection is to identify human's voice among a group of sound sources. However, one of the difficulties for sound source processing is that sound is a kind of high dimensional signal. Therefore, dimension reduction is critical for convenience of subsequent operations such as classification and clustering of the sound data. Thus, it is helpful to find a way to reduce its dimension while extracting most of its feature. For robot to identify individuals, we propose a machine learning algorithm, SINLE to do dimension reduction as well as feature extraction.

Using the proposed algorithm, we construct the interesting sound source recognition system for identifying human, and apply it to a multimodal HRI platform, the RoBear. By utilizing the two microphones in RoBear, we can implement the proposed algorithm for real-time sound source processing and provide the robot with the ability to distinguish users.

The contributions in this Chapter lies in

(i) A novel voice recognition method is presented for developing robust auditory system for human robot interaction.

(ii) Unsupervised learning algorithm, neighborhood linear embedding (NLE), is proposed to discover the intrinsic relationship among a set of voice data.

(iii) Motivated by scale adaptation of human's perception, scale-invariant metrics are designed and used to greatly improve the clustering property of the NLE.

6.2 Methods

6.2.1 Neighborhood Linear Embedding for Feature Extraction

Locally linear embedding (LLE) [170] is an unsupervised manifold learning algorithms which can be used for internal feature extraction and dimension reduction. The unsupervised property of LLE makes it especially suitable for sound source recognition without prior knowledge of the number and nature of sound sources. LLE algorithm contains three major steps: (i) constructing nearest neighborhood for expressing a data point as linear combination of its neighbors; (ii) obtaining the optimal reconstruction weight matrix by minimizing the difference between the data point and the linear combination of its neighbors; and (iii) mapping the original high-dimensional data to low-dimensional embedding using the reconstruction weights. The detailed algorithm is presented in Appendix A.

Based on the observation that neighbor selection is a critical process in the manifold learning algorithm such as LLE, we have proposed a modified algorithm named NLE [171]. It is an adaptive scheme that selects neighbors according to the inherent properties of the input data substructures to solve the problem of redundancy presented in the structure and isolated nodes that result from unsuitable neighbor selection.

The key idea of NLE is to use a criterion for neighborhood selection that avoids redundancy. In the LLE algorithm, each data point is expressed as a linear combination of its neighbors. If a neighbor is quite similar to another neighbor, it may be redundant in this combination. We define a similarity measure for two samples, x_i and x_j ($x_i, x_j \in R^D$), by

$$\zeta_{i\sim j} = \frac{1}{e^{\varrho(x_i,x_j)}}, \tag{6.1}$$

where $\varrho(x_i, x_j)$ is a function (possibly a metric) measuring the distance between x_i and x_j.

Some properties of this similarity measure are:

(i) $\zeta_{i\sim j}$ is maximized, i.e., 1, if $\varrho(x_i, x_j) = 0$. It indicates that x_i and x_j are identical, and x_i can be fully represented or approximated by x_j.

(ii) $\zeta_{i\sim j}$ is minimized, i.e., 0, if $\varrho(x_i, x_j) \to +\infty$, which means that x_j is totally different from x_i. Thus, point x_j has no contribution to the presentation of x_i.

(iii) $\zeta_{i\sim j}$ decreases monotonically with respect to $\varrho(x_i, x_j)$. It means that the further x_j is from x_i, the less contribution of x_j to the representation of x_i.

These properties provide an evaluation about how much x_j can be used to approximate x_i. If x_j is the nearest point to x_i, $\zeta_{i\sim j}$ is of the maximum value as compared to those of other points. Therefore, we should always include the nearest point to x_i as one of its neighbors. If a new point, say x_k, is considered to be a neighbor of x_i, we need to evaluate the additional information provided by x_k to avoid any redundancy in the overall representation of x_i. This evaluation is obtained based on the following assumptions:

A1: If x_k coincides with x_j, x_k can be fully represented by x_j. It has no contribution to the approximation of x_i and should be discarded to avoid redundancy of x_i representation.

A2: Point x_k is a new neighbor of x_i if it is more similar to x_i than x_j. Mathematically, this condition can be expressed by $\zeta_{i\sim k} \geq \gamma\zeta_{j\sim k}$, where γ is a constant.

A3: Point x_k has the same similarity to both x_i and x_j if $\varrho(x_i, x_k)$ and $\varrho(x_j, x_k)$ is large compared to $\varrho(x_i, x_j)$.

From these assumptions, an algorithm for the neighborhood phase of manifold learning can be summarized as,

(i) If x_j is the closest point to x_i, it is assumed to be a neighbor of x_i. Thus $\Omega_i = j$ initially.

(ii) For x_k and non-empty neighborhood Ω_i we update Ω_i according to

$$\Omega_i = \begin{cases} \Omega_i \cup x_k, & \text{if } \varrho(x_j, x_k) \geq \varrho(x_i, x_k) + \ln\gamma,\ \forall x_j \in \Omega_i \\ \Omega_i, & \text{otherwise.} \end{cases} \tag{6.2}$$

When this algorithm is used to construct the Ω_i in the LLE algorithm we call the resulting compound algorithm NLE. The constant γ must be fed to the algorithm. Moreover, it is reasonable to simply set $\gamma = 1$, which means that x_i is more similar to x_j than to x_k if $\varrho(x_i, x_j) < \varrho(x_i, x_k)$.

The performance of the LLE and NLE algorithms can be greatly affected by the distance metric used. To improve the performance of LLE and NLE for sound source recognition, we propose scale invariant distance measures motivated by the human's perceptional capability of adapting to scale changes. The scale invariant distance measures, which are robust to scale changes, have potential for developing computer perception dealing with signal scaling.

6.2.2 Scale Invariant Distance Measures

Many early works on metric optimization were presented, such as optimal metric for k-nearest neighbor density estimation [172], optimal local metric [173] and optimal global metric [174]. Based on the idea that a robust similarity measures should recognize an object with scaling, we propose scale invariant distance measures which are robust to scale changes. In most of the literature, researchers focus on rotation invariant analysis, but are less concerned about scale invariance. However, scale invariance is quite important since all natural signals are subject to scale transformations, due to distance from the sensor, as

well as optical or acoustical zooming. This means that we can automatically adapt to the scale changes of items viewed by our visual systems. It provides further motivation for the development of computer perception dealing with signal scaling.

Given two high dimensional data points, say, x and y, the distance $d(x, y)$ between these two should preferably represent their qualitative similarity. The simplest distance measure that can be used is the standard Euclidean metric given by

$$d_2(x, y) = \sqrt{\sum_{i=1}^{D}(x[i] - y[i])^2}, \tag{6.3}$$

where D is the dimension of input data. It is a special case of the more general Minkowski metric

$$d_k(x, y) = (\sum_{i=1}^{D}(x[i] - y[i])^k)^{\frac{1}{k}}, \tag{6.4}$$

where k is a natural number or possibly infinity. For the Euclidean and Minkowski metrics, the distance may be much larger between two similar but high amplitude signals than between two weak but less similar signals. This may cause wrong interpretation of the data's qualitative similarity. To combat this kind of problem, we propose scale-invariant distance measures for the LLE and NLE algorithms. In this section, we will look at several distance measures which are scale-invariant in the sense that they obey the condition

$$d(x, y) = d(ax, ay), \tag{6.5}$$

where a is a constant.

The motivation of the scale-invariant distance measure is demonstrated in Fig. 6.1. It is known that the human visual system can utilize scale information in the perception of visual expansion without estimation of optic flow [175]. This means that we can automatically

adapt to the scale changes of items viewed by our visual systems. Motivated by this scale adaptation of human's perception, the distance measures which are robust to scale changes are proposed.

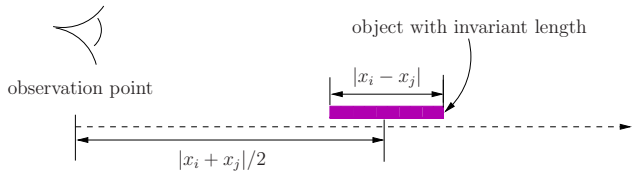

Figure 6.1: Illustration of invariant distance measure

A distance measure is said to be a metric if it obeys the following three requirements ,

(i) $d(x, y) \geq 0$ and $= 0$ only if $x = y$;

(ii) $d(x, y) = d(y, x)$;

(iii) $d(x, z) \leq d(x, y) + d(y, z)$.

The third requirement is known as the triangle inequality, and it is what distinguishes a metric from an arbitrary distance measure. Indeed, many distance measures employed in pattern recognition do not obey it. An example is the cosine similarity measure,

$$d_{\cos}(x, y) = \arccos(\frac{\mathrm{x}^{\mathrm{T}}\mathrm{y}}{\|\mathrm{x}\|\|\mathrm{y}\|}). \tag{6.6}$$

It is easy to choose x and y so that the triangle inequality is violated.

Another scale-invariant distance measure that actually is a metric is given by

$$d_{\mathrm{y}}(x, y) = \frac{\|x - y\|}{\|x\| + \|y\|}. \tag{6.7}$$

The proof that $d_{\mathrm{y}}(\cdot, \cdot)$ does indeed satisfy all three requirements can be found in [176].

In addition to not being a metric, the cosine similarity measure (6.6) has another undesirable property. Changing a single coordinate in the vector x may have a high impact on $d_{\cos}(x, y)$ since the angle may be changed with as much as 180 degrees. This problem is not entirely avoided with the metric $d_{\mathrm{Y}}(x, y)$ since it is also essentially angular, although the normalization is different.

As an alternative to these cross-bin distance measures one may use single-bin distance measures which do not encounter the mentioned problems. One such distance measure is given by

$$d_{abs}(x, y) = \sum_{i=1}^{D} |\frac{x[i] - y[i]}{x[i] + y[i]}|. \tag{6.8}$$

Lemma 6.1. *$d_{abs}(x, y)$ is a metric in R^+.*

Proof: The first two requirements to be a metric are obviously fulfilled. For the third requirement, we first introduce an R^1 metric. It is straightforward that $d(x, y) = \left|\frac{x-y}{x+y}\right|$ is a metric in R^+. An easy proof exists and a very similar R^1 metric is employed in [177]. As such, we have

$$\frac{|x[i] - y[i]|}{x[i] + y[i]} + \frac{|y[i] - z[i]|}{y[i] + z[i]} \geq \frac{|x[i] - z[i]|}{x[i] + z[i]}. \tag{6.9}$$

Based on this inequality (6.9), we can obtain the following straightforwardly.

$$\begin{aligned} & \sum_{i=1}^{D} \left|\frac{x[i] - y[i]}{x[i] + y[i]}\right| + \sum_{i=1}^{D} \left|\frac{y[i] - z[i]}{y[i] + z[i]}\right| \\ \geq & \sum_{i=1}^{D} \left|\frac{x[i] - z[i]}{x[i] + z[i]}\right|. \end{aligned} \tag{6.10}$$

□

Another quite similar distance measure is

$$d_{\mathrm{sqrt}}(x, y) = \sqrt{\sum_{i=1}^{D} (\frac{x[i] - y[i]}{x[i] + y[i]})^2}. \tag{6.11}$$

Lemma 6.2. *$d_{sqrt}(x, y)$ is a metric in R^+.*

Proof: The first two requirements to be a metric are obviously fulfilled. For the third requirement, we have the mathematic proof as follows:

$$\begin{aligned}
& [d_{sqrt}(x,y) + d_{sqrt}(y,z)]^2 \\
= & \sum_{i=1}^{D} \left(\frac{x[i]-y[i]}{x[i]+y[i]} \right)^2 + \sum_{i=1}^{D} \left(\frac{y[i]-z[i]}{y[i]+z[i]} \right)^2 \\
& +2\sqrt{\sum_{i=1}^{D} \left(\frac{x[i]-y[i]}{x[i]+y[i]} \right)^2 \sum_{i=1}^{D} \left(\frac{y[i]-z[i]}{y[i]+z[i]} \right)^2}. \qquad (6.12)
\end{aligned}$$

Based on Holder's inequality,

$$\left| \sum_{1}^{i} a_i b_i \right| \leq \left(\sum_{1}^{i} |a_i|^p \right)^{1/p} \left(\sum_{1}^{i} |b_i|^q \right)^{1/q} \qquad (6.13)$$

where $\frac{1}{p} + \frac{1}{q} = 1$, $p > 1$, $q > 1$, we can obtain that

$$\begin{aligned}
& [d_{sqrt}(x,y) + d_{sqrt}(y,z)]^2 \\
\geq & \sum_{i=1}^{D} \left(\frac{x[i]-y[i]}{x[i]+y[i]} \right)^2 + \sum_{i=1}^{D} \left(\frac{y[i]-z[i]}{y[i]+z[i]} \right)^2 \\
& +2\sum_{i=1}^{D} \left| \frac{x[i]-y[i]}{x[i]+y[i]} \frac{y[i]-z[i]}{y[i]+z[i]} \right| \\
= & \sum_{i=1}^{D} \left(\frac{x[i]-y[i]}{x[i]+y[i]} + \frac{y[i]-z[i]}{y[i]+z[i]} \right)^2 \\
\geq & \sum_{i=1}^{D} \left(\frac{x[i]-z[i]}{x[i]+z[i]} \right)^2 \\
= & [d_{sqrt}(x,z)]^2. \qquad (6.14)
\end{aligned}$$

□

6.3 Experimental Results

In order to test the clustering properties of the NLE algorithm with scale invariant distance measures we have tried it on a set of sound data that are distinguished easily by human ear and a set of artificial voice data.

The set of sound data contains three totally different data that can be easily distinguished by human ear: music, noise, and human speech. We aim to investigate whether the NLE algorithm can distinguish them. As shown in Figs 6.2(a) and 6.2(b), the result using scale invariant metric $d_{\text{abs}}(\cdot,\cdot)$ in both neighborhood and reconstruction phase of the NLE algorithm is much more superior than the result of Euclidian Metric $d_2(\cdot,\cdot)$.

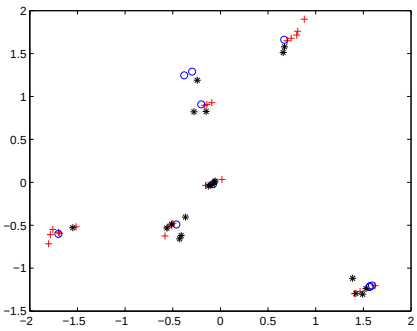

(a) NLE applied to sound data using $d_2(\cdot,\cdot)$ in both neighborhood and reconstruction phase

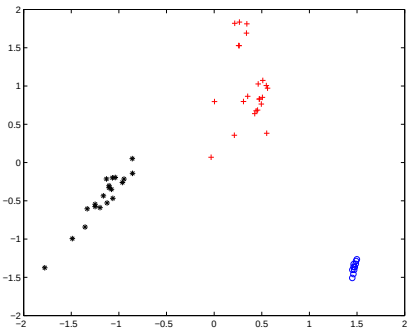

(b) NLE applied to sound data using $d_{\text{abs}}(\cdot,\cdot)$ in both neighborhood and reconstruction phase

Figure 6.2: Experimental results of sound data

The set of artificial voice data contains Microsoft Sam, Microsoft Mary and Microsoft Mike, which are built in Microsoft Windows system. We let each artificial voice read the same 8 words: hello, good, happy, beautiful, knowledge, property, attractive and information. Then we use the NLE algorithm with Euclidian metric $d_2(\cdot,\cdot)$ and NLE algorithm with scale invariant metric $d_{\cos}(\cdot,\cdot)$ to extract 2D features the three different voices, respectively.

The simulation results for the artificial voice data are shown in Figs. 6.3 and 6.4, where the shape of points represents the voice of different speaker, and the color of points represents different words. For this simple data set, each algorithm can give satisfactory result as in Figs. 6.3 and 6.4. However it is obvious that the NLE algorithm with scale invariant distance measure $d_{\cos}(\cdot,\cdot)$ gives better result. From Fig. 6.4, we see that the 2D embeddings of the artificial voice data using $d_{\cos}(\cdot,\cdot)$ preserve clusters features quite clearly and the voices of different speakers are linear separable for classification. However, the one using $d_2(\cdot,\cdot)$, shown in Fig. 6.3, has some overlaps among the three clusters in the 2D embeddings, which cause difficulty for accurately classifying the three different artificial voices.

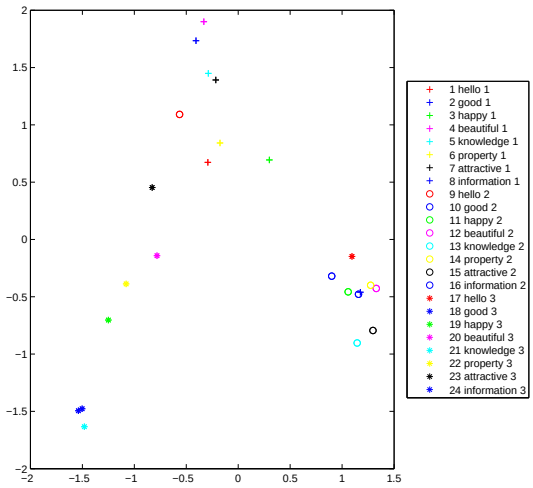

Figure 6.3: NLE applied to artificial voice data using $d_2(\cdot,\cdot)$ in both neighborhood and reconstruction phase

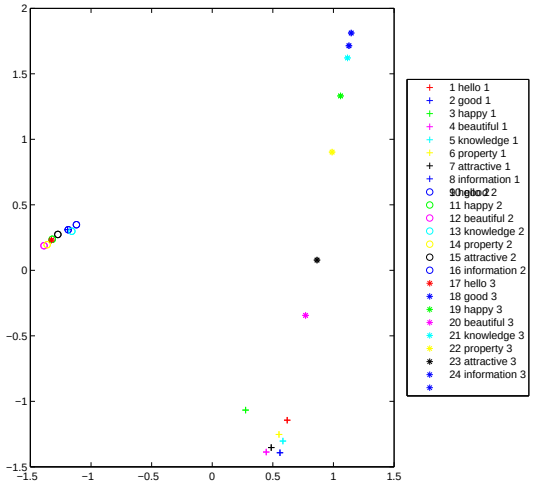

Figure 6.4: NLE applied to artificial voice data using $d_{\cos}(\cdot,\cdot)$ in reconstruction phase

6.4 Conclusion

In this chapter, we proposed an unsupervised learning algorithm which can be used as a novel voice recognition method for detecting human's voice in human robot interaction. The algorithm, named NLE, is able to discover the intrinsic relationship among a set of voice data. To improve the clustering property of NLE, scale-invariant distance measures, which were motivated by the scale adaptation of human's perceptual functions, were proposed and utilized. Through the simulation study, we concluded that the performance of clustering strongly depends on how distance between neighbor points is measured. The scale invariant neighborhood linear embedding (SINLE) can be applied to robots for improving auditory system of HRI because of its potentials for robust sound recognition and identification.

Chapter 7

Human Face Detection and Recognition for Human Robot Interaction

7.1 Introduction

One of the most important human robot interactions is the human identification technology. Many technologies such as face recognition, iris recognition, voice recognition are helpful to distinguish people. This chapter focuses on one of the important human identification technologies, the intelligent facial vision system to robustly detect and recognize human face from a variety of real environment.

Facial vision system has attracted considerable attention in many practical applications [178, 179] because they are critical parts in the whole robot system and directly lead to

whether robots are interactive communication in the social environment. A facial vision system is normally divided into two main modules: face detection and face recognition. Face detection as the first module in a facial vision system is the problem of determining whether or not a sub-window of an image belongs to the set of face images. Face recognition focuses on classifying the set of face images of different people to identify them.

Among a variety of face detection methods, one of the most impressive studies is AdaBoost algorithm [180, 181], which uses the concept of an "integral image", along with a rectangular feature representation and an AdaBoost algorithm as its learning method, to detect faces at 15 frames per second. This represents an improvement in the computation time of an order of magnitude over previous implementations of face detection algorithms. One disadvantage of the AdaBoost algorithm is that it cannot distinguish face-like images from the real face images because those face-like images may pass every stage. To conquer this problem, we consider applying neural networks to face detection due to their approximation capability. However, drawback of neural network is that the network architecture has to be extensively tuned (number of layers, number of nodes, learning rates, etc) to reach satisfactory performance. Due to the random character of hidden neurons, ELM breaks through the drawback of conventional neural network algorithms, and has been proven to be an effective method to make neural networks achieve a better generalization performance at a fast learning speed. Thus, it is natural to combine ELM algorithm and Viola and Jones's work to exclude those false face images. The ELM not only improves the face detection accuracy, but also retains the real-time learning speed at the same time.

The second module of the facial vision system is face recognition. In recent decades, a variety of pattern recognition methods have been applied to this field [178, 179, 182–187].

Among these methods, manifold learning algorithm like LLE has its own advantages because it is an unsupervised learning algorithm. On one hand, it do not need training samples, which is especially helpful for small sample size of the face pattern's distribution. On the other hand, it only has one simple parameter, K number of neighbors selected, to be chosen, which makes it easy for application. However, the performance of LLE declines when the data are not well and uniformly distributed. Another problem is that the algorithm is not robust to parameter changes. To combat these problems, we proposed WLLE [187] which may have better performance for complicated data set such as face images.

In summary, the facial vision system is designed to detect human faces and extract those faces from the background environment, then recognize the detected faces based on an existing face data set, with a high accuracy and feasible learning speed.

The contributions in this Chapter lies in

(i) Utilization of active vision to make robot better understand the environment and increasing target resolution for higher level tasks such as recognition and classification;

(ii) Combination of two precise filters, corner detection filter and ELM, with the Adaboost algorithm to improve the accuracy of the Haar-Cascade Classifier for face detection;

(iii) WLLE is proposed for face recognition and compared with several well-known algorithms. An improvement of classification rate is shown in experimental results, which indicates the better performance of WLLE algorithm in face recognition.

7.2 System Description

The proposed facial vision system consists of a normal camera that is placed in the RoBear, which serves as a sensor to capture the images, as shown in Fig. 7.1.

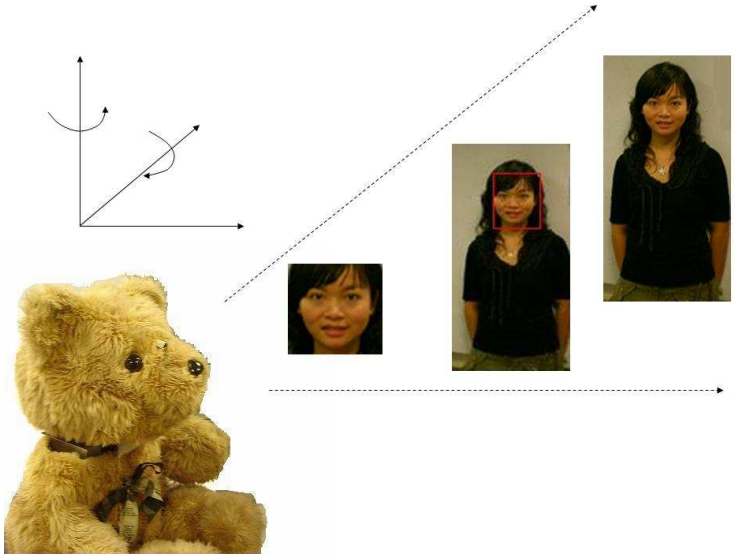

Figure 7.1: Robot facial vision system based on robot mounted cameras

The camera in the bear robot is able to interact with the environment to optimize the face recognition procedure by zooming in and focusing on the face region to obtain a higher resolution picture after a face is detected; and tracking the specific person after the face is recognized. Without an expensive 3D stereo triangulation for person tracking, the zooming-in and tracking operation are simply and efficiently achieved through mechanical control algorithm. Once human's face is detected precisely by face detection module, the mechanical control of robot mounted camera is triggered to zoom in around the face region. Before the zoom-in operation takes action, the bear's head needs to turn left and right and move up and down until the subject's face is in its center. By accurately tracking the selected region while continuously updating the position of camera's current center view,

the center of camera will effectively converge to selected region, i.e., the human face. Then, the zooming in function of the camera is triggered to obtain high resolution picture of the detected face, which is used as input of the face recognition module.

The real-time facial vision system contains two main modules: face detection module and face recognition module. The major process is briefly demonstrated in Fig. 7.2.

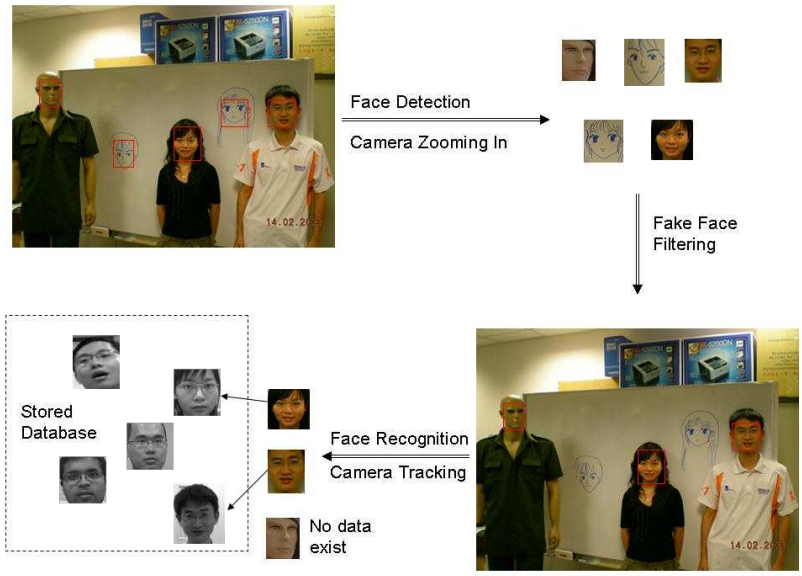

Figure 7.2: Main process of the facial vision system

7.3 Face Detection Module

Face detection as a computer vision task has many applications [188, 189]. It is directly relevant to the face recognition problem and human-computer interfaces. The face detection problem can be defined as follows: given any image input, which could be a digitized video signal or a scanned photograph, the system determines whether or not there are human faces in the image, and if there are, the system returns their locations. Since face

locations in the image are random and unpredictable, a well designed face detection system normally requires a high frame rate, a low false detection accuracy, a wide range of working environment, and the ability to cope with different scale, location, orientation, occlusion and lighting conditions.

In this work, AdaBoost-based face detector which employs Haar-like classifiers in a cascade structure is used to cope with the accuracy and robustness problem against observations with varying environments and illumination conditions [180, 181, 190–195]. The cascade classifier is a binary classification function based on the statistical technique, which can effectively extract faces from background images at a very rapid speed. The cascade classifier is trained to reject the non-face images, while allowing all the faces to pass to the next stage of cascade.

7.3.1 Haar-Cascade Classifier

The face detector firstly determines the initial location of the faces based on the Haar-like features, available in OpenCV [196]. The statistical model consisting of a cascade of boosted classifiers is trained using face and non-face examples with fixed size. For any new image input, a small sliding window scans the whole image and obtains the fixed-sized gray-scale patches and then each image patch is classified by the Cascade Classifier as either face or non-face. To deal with varying facial size, the coordinates of all rectangles of Haar-like features are repeatedly scaled. A large number of features are applied to different positions in the same rectangular sub-image. The detailed implementation of Haar-Cascade classifier is described as follows.

Firstly, a set of features are computed very rapidly at many scales by the integral image

representation for images. The integral image can be computed from an image using a few operations per pixel. Once computed, these Haar-like features can be rapidly computed at any scale or location in constant time. In this work, the 4 Haar-like features used are shown in Fig 7.3.

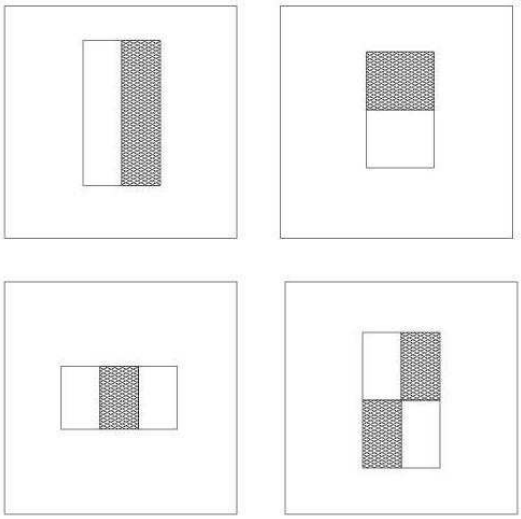

Figure 7.3: Four rectangle Haar-like features.

Secondly, a simple and efficient classifier is constructed by selecting a small number of important features using AdaBoost [197]. A simple AdaBoost is modified to select features: the number of Haar-like features is very large in any image sub-window, thus the learning process must exclude a large majority of the features to ensure fast classification. In the AdaBoost algorithm, it is constrained that each weak classifier can only depend on a single feature. As a result, each stage of the boosting process, which selects a new weak classifier, can be viewed as a feature selection process.

Finally, the weak classifiers are boosted into a stronger classifier in a cascade structure which dramatically increases the speed of the detector by focusing attention on promising regions of the image. By adopting simple-to-complex strategy, most non-face candidates

are rejected in earlier layer of cascade with little computation costs.

A given feature value is the weighted sum of pixels over the whole area added to the weighted sum over the dark regions of the Haar feature. A simple decision tree classifier, which refers to a weak classifier, processes the feature value. A complex classifier is iteratively built as a weighted sum of weak classifiers using the Adaboost, an adaptive boosting procedure. The boosting algorithm for training a strong classifier is a weighted linear combination of N weak classifier. For given sample image dataset, $(x_i, y_i)_{i=1}^{N}$, where $y_i = 0, 1$ is the label for negative and positive samples, the algorithm can be described as follows:

(i) Initialize the weights $w_{1,i} = \frac{1}{2m}, \frac{1}{2l}$ for $y_i = 0, 1$, where m and l are the number of the negative and positive samples, respectively.

(ii) Normalize the weights w_t for $t = 1, \cdots, T$, to make it a probability distribution.

$$w_{t,i} = \frac{w_{t,i}}{\sum_{j=1}^{t} w_{t,j}} \tag{7.1}$$

Then select the best weak classifier with respect to the weighted error

$$\varepsilon_t = \min_{f,p,\theta} \sum_i w_i |h(x_i, f, p, \theta) - y_i| \tag{7.2}$$

where a weak classifier $h(x, f, p, \theta)$ consists of a feature f, a threshold θ and a polarity p indicate the direction of the inequality:

$$h(x, f, p, \theta) = \begin{cases} 1, & pf(x) < p\theta \\ 0, & \text{other} \end{cases} \tag{7.3}$$

Here x is a 24×24 pixel sub-window of an image. After that, choose the classifier $h_t(x) = h(x, f_t, p_t, \theta_t)$ where f_t, p_t and θ_t are the minimizers of ε_t.

Defining $\beta_t = \frac{\varepsilon_t}{1-\varepsilon_t}$, and update the weights:

$$w_{t+1,i} = w_{t,i}\beta_t^{1-e_i} \tag{7.4}$$

where $e_i = 0$, if sample x_i is classified correctly; otherwise, $e_i = 1$.

(iii) By defining $\alpha_t = \log\frac{1}{\beta_t}$, the final strong classifier is:

$$C(x) = \begin{cases} 1, & \sum_{t=1}^{T}\alpha_n h_t(x) \geq \frac{1}{2}\sum_{t=1}^{T}\alpha_t \\ 0, & \text{other} \end{cases} \tag{7.5}$$

7.3.2 Precise Face Detector

In the last section, a Haar-Cascade classifier with AdaBoost for detecting human face is described. However, one disadvantage of the cascade structure is that the cascade structure cannot distinguish face-like images from the real face images. The lack of non-face image database can result in a wrong classification since a non-face but face-like image may satisfy all the criteria of real face in each single stage of the cascade structure so that it can be misclassified as a real face image. In order to improve the face detection accuracy, corner-finding method and neural network method are applied to remove face-like images from the real face images.

Corner Detection

Corner detection or the more general terminology interest point detection is an approach used in computer vision systems to extract certain kinds of features and infer the contents of an image. A corner can be defined as the intersection of two edges or as a point where there are two dominant and different edge directions in a local neighborhood of the point.

The corners with big eigenvalues in the image can be found by calculating the first-order derivative of every pixel of the image to compare with the derivative of its 3×3 pixel neighborhood. Consider that a real face image normally includes more corners due to facial complexity, the number of all the corners counted in the image is compared to the predefined threshold to make decision of whether or not it is a real face image. If the number of corner is smaller than the predefined threshold, the image is assumed to be a false face image; otherwise, the image is real face image.

However, it is noted that many face-like images normally include a large number of corners, thus only corner finding filter cannot totally remove face-like images from the real face images. To further improve the face detection accuracy, false face images can be removed using neural network filter.

Extreme Learning Machine for Fake Face Removal

Neural networks have been applied successfully in many pattern recognition problems due to their approximation capability [198–201]. Since face detection can be treated as a two class pattern recognition problem, various neural network architectures have been proposed. The advantage of using neural networks for face detection is the feasibility of training a system to automatically capture the complex class relationship of face patterns.

Among all the face detection methods that used neural networks, one of the most significant works is presented in [202, 203]. A multilayer neural network is used to learn the face and nonface patterns from face/nonface images. There are two major components: neural networks to detect face patterns and a decision making module to render the final decision. The first component is a neural network that receives a 20×20 pixel region of an image and

outputs a score ranging from -1 to 1. Given a test pattern, the output of the trained neural network indicates a nonface or face pattern. To detect faces anywhere in an image, the neural network is applied at all image locations. To detect faces larger than 20×20 pixels, the input image is repeatedly subsampled, and the network is applied at each scale. In each training image, the eyes, tip of the nose, corners, and center of the mouth are labeled manually and used to normalize the face to the same scale, orientation, and position. The second component is to merge overlapping detection and arbitrate between the outputs of multiple networks. Simple arbitration schemes such as logic operators are used to improve performance.

However, one drawback of this method is that the network architecture has to be extensively tuned (number of layers, number of nodes, learning rates, etc) to reach an exceptional performance. Thus the computation is both time and memory intensive.

Recently, random thinking is successfully applied to neural networks, i.e., ELM [204,205]. Different from common understanding on neural networks, such neural networks not only provide a better generalization performance at a fast learning speed, but still retain universal approximation capability despite the fact that hidden neurons are randomly generated. Without calculating the parameters of hidden neurons, neural networks with random hidden neurons can achieve good generalization performance at a fast speed. A large number of simulation results also demonstrate that ELM can outperform many popular algorithms like BP, SVM and etc [204, 205]. Therefore, it is natural to consider applying the random neural network to the active facial vision system for replacing traditional neural network methods.

For easy and clear presenting, the symbol of neural networks and the ELM algorithm

will be briefly introduced.

The output of an standard single hidden layer feedforward network (SLFN) with L hidden nodes can be represented by $f_L = \sum_{i=1}^{L} \beta_i g(\mathbf{a}_i, b_i, \mathbf{x})$, where $\mathbf{a}_i$ and b_i are the learning parameters of hidden neurons and β_i is the weight connecting the i-th hidden neuron to the output neurons; $g(\mathbf{a}_i, b_i, \mathbf{x})$ is the output of the i-th hidden neuron with respect to the input $\mathbf{x}$. From a network architecture point of view, two main SLFN network architectures, additive neurons and kernel neurons, have been investigated. For the additive neurons, the activation function $g(x) : R \rightarrow R$ takes the form $g(\mathbf{a}_i, b_i, \mathbf{x}) = g(\mathbf{a}_i \mathbf{x} + b_i)$, where $\mathbf{a}_i \in R^n$ is the weight vector connecting the input layer to the i-th hidden neuron, and $b_i \in R$ is the bias of the i-th hidden neuron; $\mathbf{a}_i \mathbf{x}$ denotes the inner product of vectors $\mathbf{a}_i$ and $\mathbf{x}$ in R^n. For the kernel neurons, the activation function $g(x) : R \rightarrow R$ takes the form $g(\mathbf{a}_i, b_i, \mathbf{x}) = g(b_i \|\mathbf{x} - \mathbf{a}_i\|)$, where $\mathbf{a}_i \in R^n$ is the center of the i-th RBF neuron and $b_i \in R^+$ is the impact of the i-th RBF neuron. R^+ indicates the set of all positive real value.

For a series of N arbitrary distinct training samples $(\mathbf{x}_i, \mathbf{t}_i)$, $i = 1, \cdots, N$, where $\mathbf{x}_i = [x_{i1}, x_{i2}, \cdots, x_{in}]^T \in \mathbf{R}^n$ is an input vector and $\mathbf{t}_i = [t_{i1}, t_{i2}, \cdots, t_{im}]^T \in \mathbf{R}^m$ is a target vector. A standard SLFN with L hidden neurons with activation function $g(x)$ can be expressed as

$$\sum_{i=1}^{L} \beta_i g(\mathbf{a}_i, b_i, \mathbf{x}_j) = \mathbf{o}_j, \quad j = 1, \cdots, N,$$

where $\mathbf{o}_j$ is the actual output of SLFN. As mentioned before, $g(\mathbf{a}_i, b_i, \mathbf{x}_j)$ may be additive model or RBF model.

A standard SLFN with L hidden neurons can learn N arbitrary distinct samples $(\mathbf{x}_i, \mathbf{t}_i)$, $i = 1, \cdots, N$, with **zero error** means that there exist parameters $\mathbf{a}_i$ and b_i, for $i = 1, \cdots, L$,

such that

$$\sum_{i=1}^{N} \|\mathbf{o}_i - \mathbf{t}_i\| = 0.$$

Therefore our ideal objective is to find proper parameters $\mathbf{a}_i$ and b_i such that

$$\sum_{i=1}^{L} \beta_i g(\mathbf{a}_i, b_i, \mathbf{x}_j) = \mathbf{t}_j, \;\; j = 1, \cdots, N,$$

The above N equations can be expressed as

$$\mathbf{H}\beta = \mathbf{T} \tag{7.6}$$

where $\beta = [\beta_1, \cdots, \beta_L]^T$, $\mathbf{T} = [t_1, \cdots, t_N]^T$ and

$$\mathbf{H} = \begin{bmatrix} g(\mathbf{a}_1, b_1, \mathbf{x}_1) & \cdots & g(\mathbf{a}_L, b_L, \mathbf{x}_1) \\ \vdots & \ddots & \vdots \\ g(\mathbf{a}_1, b_1, \mathbf{x}_N) & \cdots & g(\mathbf{a}_L, b_L, \mathbf{x}_N) \end{bmatrix}_{N \times L} \tag{7.7}$$

where the matrix $\mathbf{H}$ is called as the hidden layer matrix of the SLFN.

When the number of neurons L is equal to the number of samples N, neural networks can precisely express observed samples. However, the number of hidden nodes is normally much less than the number of distinct training samples, i.e., $L \ll N$. It means that $\mathbf{H}$ is a nonsquare matrix. It is noted that neural networks with randomly generating $\{\mathbf{a}_i, b_i\}$ and determining β_i by Moore-Penrose generalized inverse $\beta = \mathbf{H}^{\dagger}\mathbf{T}$ [206, 207] can approach training target with small errors [204, 205]. This fast learning algorithm is so called ELM. The learning procedures of ELM can be summarized in the following steps:

ELM Algorithm:

Given a training set $\aleph = \{(\mathbf{x}_i, \mathbf{t}_i) | \mathbf{x}_i \in \mathbf{R}^n, \mathbf{t}_i \in \mathbf{R}^m, i = 1, \cdots, N\}$ and L hidden neurons

(i) Assign random parameters $\mathbf{a}_i$ and b_i, for $i = 1, \cdots, L$.

(ii) Calculate hidden layer matrix $\mathbf{H}$.

(iii) Calculate the hidden-to-output weights by $\beta = \mathbf{H}^{\dagger}\mathbf{T}$, where $\mathbf{H}^{\dagger}$ denotes Moore-Penrose generalized inverse of $\mathbf{H}$.

As mentioned above, ELM will be applied to the active facial vision system for detecting human faces in grey level images. The system works by scanning an image for face-like patterns at many possible scales and uses ELM as its classification algorithms to determine the appropriate class (face or non-face). It handles faces over a wide range of scales and works under varying lighting conditions, even with moderately strong shadows. Face detection is a natural and challenging problem for demonstrating and testing the potentials of ELM. There are many other object classes and phenomena in the real world that share similar characteristics with face images. A successful and general methodology for finding faces using ELM should generalize well for other spatially well-defined pattern and feature detection problems. The detailed process is that: we treat each image as a vector in a high-dimensional space, and then ELM is applied to the set of training images to produce a hidden matrix $\mathbf{H}$. Lastly, the hidden-to-output weights by $\beta = \mathbf{H}^{\dagger}\mathbf{T}$, where the elements of $\mathbf{T}$ belong to -1 or +1.

In Fig. 7.4, images are represented as points in a two-dimensional space. ELM is used to approximate the boundary function to separate real face patterns from fake face patterns. After this process, the system removes all the non-face patterns. Then, the face detection module finishes its work and passes face patterns into the face recognition module.

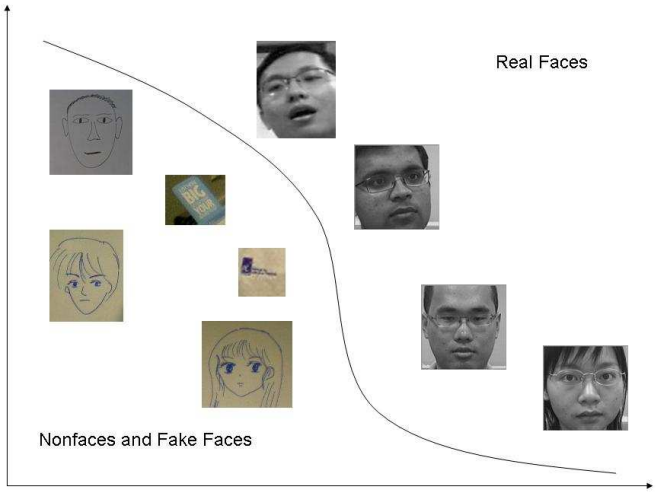

Figure 7.4: Real faces and fake faces are separated by neural networks

7.3.3 Experimental Results

In this experiment, ELM and AdaBoost are combined to improve the face detection accuracy, and the real-time speed are maintained at the same time.

First, AdaBoost of Viola-Jones is implemented using training examples, where positive face images are coming from the UMIST face database [208] and negative background from http://face.urtho.net/. Then profile face-images set is used to test the algorithm. Fig. 7.5(a) shows the face detection result of AdaBoost of Viola-Jones, from which we can find that the detection result using only AdaBoost includes many fake face or face-like objects. To overcome this problem, ELM is used as a filter to exclude those face-like objects. Fig. 7.5(b) illustrates the detection result of combining AdaBoost and ELM. From the comparison of Fig. 7.5(a) and Fig. 7.5(b), it can be concluded that through the ELM filter, those face-like objects are removed and the face detection accuracy is improved. However, as shown in Fig. 7.5(b), the face of the mannequin cannot be filtered out by ELM

filter because of its similar 3D features as human's face. This kind of problem can be solved by using a stereo camera as presented in [209].

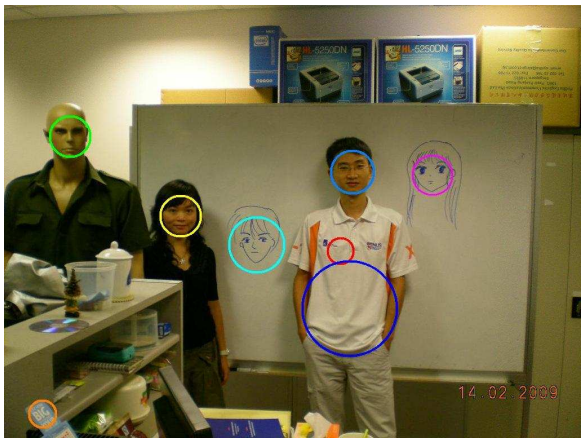

(a) AdaBoost without ELM

(b) AdaBoost with ELM

Figure 7.5: Experimental results of face detection module

7.4 Face Recognition Module

Face recognition is one of the most popular research topics in pattern recognition during this decade [182–184,210,211]. It can be widely used in entertainment, information security, intelligent robotics and so on. Recently, great development has been done by researchers

on both algorithm and system.

7.4.1 Dimension Reduction Algorithm for Feature Extraction

A critical part in face recognition is the dimension reduction algorithm for feature extraction. In this area, global feature extraction algorithm such as principal components analysis (PCA), linear discriminant analysis (LDA) and all the methods based on combination of these two gave many good results in applications on facial recognition [210,211]. Later, as a nonlinear extension of PCA, kernel principal components analysis (KPCA) [212] has shown significant advantages on data representation for clustering and classification of complicated facial data set. Based on the very observation that null subspace contains useful information for clustering, in [213], Lu et. al proposed kernel direct discriminant analysis (KDDA), which is combination of KPCA and direct linear discriminant analysis (DLDA). Another combination of LDA and KPCA, called complete kernel fisher discriminant (CKFD), has been proposed in [214]. All these kernel based methods have a major disadvantage that the selection of kernel function and their parameters are usually obtained by trial and error or based on experience, which greatly weakens the practical value of these methods. Moreover, the final projection is related to all the training samples, so that the requirement for training samples is usually strict.

Compared to these kernel based methods, LLE has its own advantages. Because of its unsupervised property, it do not need training samples. This property makes LLE especially suitable for face recognition with small sample size. Furthermore, it only has one parameter to be chosen, K, number of neighbors selected. The detailed LLE algorithm is presented in Appendix A.

To combat the problem that the performance of LLE declines when the data distribution is deformed, WLLE is proposed [187] which may have better performance for complicated data set such as face images.

7.4.2 Weighted Locally Linear Embedding

The neighbor finding process of LLE is usually carried out using a grouping technique such as K nearest neighbors (KNN) or choosing neighbors within a ball of fixed radius (ϵ-neighborhoods) based on Euclidean distance for each data point in the given data set. After carefully considering the LLE and NLE's neighbor selection criterion, we propose a new algorithm by using weighted distance measurement in neighbor searching. The new algorithm can solve the problem of redundancy in LLE and avoid NLE's problem that no enough data are chosen as neighbors at the same time.

In the data manipulation like nearest neighbor searching, each datum can be regarded as the center of a probability distribution and the similarity of its neighbors to the datum can be measured by Euclidean distance with the assumption that samples are well-distributed. However, because of the attraction, repulsion, strengthening effect and weakening effect between data, the standard normal distributions will be greatly deformed. Obviously, neglecting such a deformation and still using the standard Euclidean distance to measure the similarity will lead to performance decline. As mentioned in [215], the data set should be sufficient and well-sampled, otherwise the performance of LLE algorithm will not be good enough. For example, as illustrated in Fig. 7.6, the samples are not well-distributed, data density changes sharply within a small area, the query point is marked by a cross, and its neighbors marked by circles. We use ϵ-neighborhoods algorithm to finding nearest

neighbors of the query point from its neighbors. For this deformed distribution data set, ϵ-neighborhoods method based on standard Euclidean distance measurement selects neighbors from a single direction, and these neighbors are closely gathered. Obviously, if we use these chosen neighbors to reconstruct the query point, the information captured in this direction will have serous redundancy; at the same time, no information from other directions are reserved for query point reconstruction. These chosen neighbors cannot represent and reconstruct the query point well, most internal features and intrinsic structure will be lost after dimension reduction by LLE.

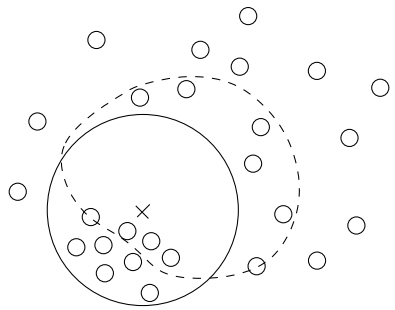

Figure 7.6: Select nearest neighbors using ϵ-neighborhoods algorithm by Euclidean distance (solid line) and weighted distance (dash line).

To solve this problem, we introduce the weighted distance measurement motivated by [216]. The main idea of the weighted distance measurement is giving a different but appropriate distance scale to each prototype to make the distance measure more reasonable for representing the global distribution of the data set. Fig. 7.6 shows the advantages of this scaled adaptive distance measurement. The modified ϵ-neighborhoods method based on weighted distance measurement select neighbors more reasonable than the one based on

standard Euclidean distance by giving the distance measurement from neighbor point with high density a larger weight scaling, while those with low density a smaller weight scaling. Thus, the previous redundancy and deficiency problem can be solved.

To find the suitable adaptive weight scaling, we first construct a simple yet effective transformation to simulate the possible deformation of data distribution.

Definition 7.1. *(Deformed Distribution) Consider a d-dimensional random vector* $Y = (Y_1, Y_2, \ldots, Y_d)^T$ *that takes a standard D dimensional normal distribution* $N(0, I)$*, that is, it has a probability density function*

$$f(y) = \frac{1}{(2\pi)^{d/2}} e^{-1/2 y^T y} \tag{7.8}$$

Let a random vector X *be defined by the transformation*

$$X = (a + b\frac{Y^T \tau}{\|Y\|})Y \tag{7.9}$$

where Y *denotes the original well-distributed data set,* $a > b \geq 0$ *are the parameters that reflect overall scale and orientation of distribution,* τ *is a normalized vector denoting the deformation orientation,* $\|Y\| = \sqrt{Y^T Y}$*, and* X *represent the deformed distribution with parameters* a *and* b *in the direction* τ*, denoted as* $X = D_d(a, b, \tau)$ *[216].*

According to the definition, a deformed distribution biases towards a specific direction, which makes it an eccentric distribution. In this case, the Euclidean distance is not suitable to describe the similarity between two data directly, since the assumption those data are well-distributed is dissatisfied. Instead, we firstly restore the deformation by an inverse transformation $Y = X/(a + b\cos\theta)$, and then measure the distance. We call this weighted distance measurement. This weighted distance redresses the deformation and should be more suitable to describe the similarity for data set that are not well-distributed.

Definition 7.2. *(Weighted Distance) Assume that $x_0 \in R^d$ is the center of a deformed distribution $D_d(a, b, \tau)$. The weighted distance from a point $x \in R^d$ to x_0 is defined to be*

$$\mathrm{Dist}(x_0, x) = \frac{\|x - x_0\|}{a + b\frac{(x-x_0)^T\tau}{\|x-x_0\|}} \tag{7.10}$$

or

$$\mathrm{Dist}(x_0, x) = \|x - x_0\|/(a + b\cos\theta) \tag{7.11}$$

where θ is the angle between vectors $x - x_0$ and τ, and $\frac{1}{a+b\cos\theta}$ is the weight of the distance from x to x_0 [216].

One disadvantage of the weighted distance measurement is just a weighted distance, but not a metric, since $\mathrm{Dist}(x_0, x)$ may not equal to $\mathrm{Dist}(x, x_0)$ under the definition of weighted distance. In fact, it has been discussed in [217] that non-Euclidean or non-metric measures can be informative in statistical learning algorithms.

To facilitate parameter estimation for weighted distance, we first present some properties.

Theorem 7.1. *If a random vector $X = D_d(a, b, \tau)$, then $E(X) = c_1 b\tau$ and $E(\|x\|) = c_2 a$, where c_1 and c_2 are constants.*

$$c_1 = 2^{1/2}\frac{\Gamma((d+1)/2)}{\Gamma(d/2)d} \tag{7.12}$$

$$c_2 = 2^{1/2}\frac{\Gamma((d+1)/2)}{\Gamma(d/2)} \tag{7.13}$$

where Γ is the Gamma function $\Gamma(k) = \int_0^\infty t^{k-1}e^{-t}dt$, $(k > 0)$ [216].

For an arbitrary sample $x_i \in D$, we assume that it represents a deformed distribution and is the origin of this deformed distribution. Then, we use its k-nearest neighbors $X_i =$

$\{x_{i1}, x_{i2}, \ldots, x_{ik}\}$ to estimate the parameters of the deformed distribution, that is, a_i, b_i and τ_i.

First, we calculate the difference between a sample and all its k-nearest neighbors, $V_i = \{v_{i1}, v_{i2}, \ldots, v_{ik}\}$, where $v_{ij} = x_{ij} - x_i$, $j = 1, 2, \ldots, k$. Then, we use $\hat{G}_i$ and $\hat{L}_i$, which are the center of mass and the averaged vector length of V_i:

$$\hat{G}_i = \sum_{j=1}^{k} v_{ij}/k \tag{7.14}$$

$$\hat{L}_i = \sum_{j=1}^{k} \|v_{ij}\|/k \tag{7.15}$$

to estimate $E(X)$ and $E(\|X\|)$, respectively. According to Theorem 7.1, we obtain an estimation to a_i, b_i and τ_i:

$$\hat{a}_i = \frac{\hat{L}_i}{c_2} \tag{7.16}$$

$$\hat{b}_i = \frac{\|\hat{G}_i\|}{c_1} \tag{7.17}$$

$$\hat{\tau}_i = \frac{\hat{G}_i}{\|\hat{G}_i\|} \tag{7.18}$$

The weighted distance can measure similarity more reasonably for the deformed-distributed data set than standard Euclidean distance and is suitable for many distance based methods. Accordingly, we propose a novel dimension reduction algorithm, WLLE which use weighted distance measurement instead of standard Euclidean distance measurement in LLE algorithm so that it can improve the dimension reduction and internal feature extraction performance especially for the deformed distributed data.

The whole procedure of dimension reduction as well as the construction of weighted distance measurement in WLLE algorithm are detailed in Algorithm 1.

Algorithm 1 Weighted Locally Linear Embedding Procedure

Phase 1: Construct Weighted Distance

Given a raw high dimensional data set $D = \{x_i\}, i = 1, 2, \ldots, N$, $x_i \in R^D$, and a parameter k_w, for an arbitrary datum $x_i \in D$,

1: Find k_w-nearest neighbors $X_i = \{x_{i1}, x_{i2}, \ldots, x_{ik_w}\}$, $X_i \subset D$.
2: Obtain V_i, $v_{ij} = x_{ij} - x_i$, $j = 1, \ldots, k_w$.
3: Calculate $\hat{G}_i$ and $\hat{L}_i$, according to equations (7.14) and (7.15).
4: Estimate a_i, b_i, τ_i by using $\hat{G}_i$ and $\hat{L}_i$, according to equations (7.16), (7.17) and (7.18).

Phase 2: Search Neighborhood

For an arbitrary datum $x_i \in D, i = 1, 2, \ldots, N$, find k-nearest neighbors based on the weighted distance

1: Calculate the weighted distance from x_i to $\forall x_j \in D, j \neq i$ according to equation (7.10).
2: Find the k-nearest neighbor $X_j = \{x_{j1}, x_{j2}, \ldots, x_{jk}\}$, $X_j \subset D$, which satisfy

$$\text{Dist}(x_j, x_i) < \text{Dist}(x_k, x_i) \tag{7.19}$$

for $\forall x_j \in X_j$, $\forall x_i \in D$ and $\forall x_k \in D \notin X_j$

Phase 3: Calculate Optimal Reconstruction Weights

1: Compute local covariance matrix as (A.6).
2: Regulate the local covariance matrix according to equation (A.10).
3: Compute the reconstruction weights according to equation (A.9).

Phase 4: Compute Low Dimensional Embedding

1: Construct a symmetric $N \times N$ matrix according to equation (A.15).
2: Calculate eigenvalues and eigenvectors of the symmetric matrix (A.15).
3: Obtain low dimensional embedding using bottom $d+1$ eigenvectors (according to smallest $d + 1$ eigenvalues) of matrix (A.15).

7.4.3 Experimental Results

Classification of Different Faces

To demonstrate the face recognition performance of WLLE and compared to other well-known methods for face recognition, in this section, we utilize the UMIST face database [208, 218] for experiment, which consists of 564 images of 20 people in PGM format, approximately 220 x 220 pixels in 256 shades of grey, covering a range of poses from profile to frontal views. Subjects cover a range of race/sex/appearance. The original 220×220 PGM format face images were cropped to 112×92 images, a standardized image size commonly used in face recognition experiment. In our experiment, we extract a typical subset of the

UMIST face database, which contains face images of 5 different individuals, each individual has 20 face images covering range from profile to frontal views. As such, the subset we used in this experiment are 100 samples with dimensionality of 10304 in 5 classes (different individuals). Six types of low dimensional representations are produced from the face images subset by using different feature extraction algorithms, PCA, KPCA, KDDA, WLLE, LLE and NLE. For PCA, KPCA and KDDA, all of the face images in subset are used in both the training procedure to generate subspaces and the testing procedure to project them onto the generated subspaces. For each image, its projections in the first two most important features bases are visualized in the first row of Fig. 7.7. For WLLE, LLE, and NLE, the high dimensional face image data are mapped into 2D embeddings, which are shown in the second row of Fig. 7.7.

The low-dimensional representations produced by the algorithms are quite different. Among them, the KDDA-based result and WLLE-based result showed better clustering property, but the other four algorithms result in some overlapping between different classes of the face data, which may make them nonseparable. In particular, the result of KDDA is fairly linear separable, which may result from its separability criteria based algorithm. Unlike the diffuse shape of the five classes in result by KDDA, the result by WLLE gives a parallel shape of the five classes. Although there is no overlapping between different classes, the short distance between clusters indicates that the WLLE-based feature representation is less linear separable than the KDDA-based result. Overall, simple inspection of Fig. 7.7 indicates that the feature representations produced by KDDA and WLLE outperform, in view of separability, the ones produced by PCA, KPCA, LLE and NLE. This will be later proved by feeding these 2D features obtained by six algorithms into a simple SVM classifier.

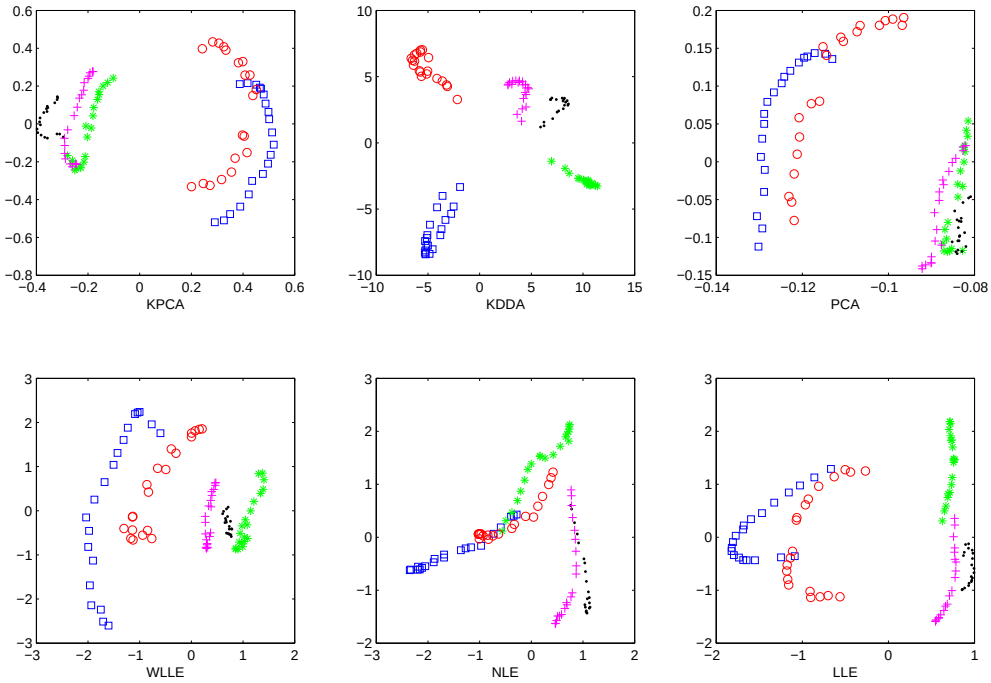

Figure 7.7: Dimension reduction result of UMIST face data by six different methods

Since the objective of this experiment is to compare the performance of different feature extraction algorithms, we keep the parameters of SVM unchanged during all the experiments. The performance is evaluated using average error rate obtained by dividing total number of misclassifications by product of number of samples and number of runs. Eight runs for each algorithm is conducted and 10×10 fold cross validation is used to obtain the generalized error rate.

Noting that the performance of kernel based methods is greatly affected by the kernel function chosen and the parameter changes of the function, we use a RBF kernel function for both KPCA and KDDA, and record the error rate with different kernel parameter, the scale value σ^2 for RBF kernel. Fig. 7.8 shows the error rates and computational cost as

functions of σ^2 within the rage from 1e2 to 1e7 for algorithms KPCA and KDDA. Either error rate or computational cost indicate that the KDDA algorithm outperforms KPCA.

The only parameter for LLE based methods is the number of neighbors, K. As such, we record the error rate with different K for LLE and WLLE algorithm. The NLE algorithm does not need to choose parameter K. Fig. 7.9 shows the error rates and computational cost as functions of K within the rage from 8 to 88 for algorithms WLLE and LLE. Although the computational cost of WLLE is higher than LLE, the error rate shows that the classification performance of WLLE outperforms that of LLE.

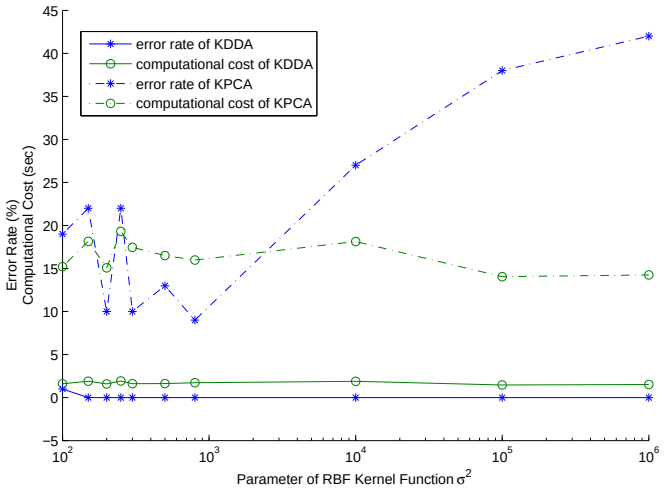

Figure 7.8: Comparison of error rates and computational cost as functions of σ^2 for KPCA and KDDA

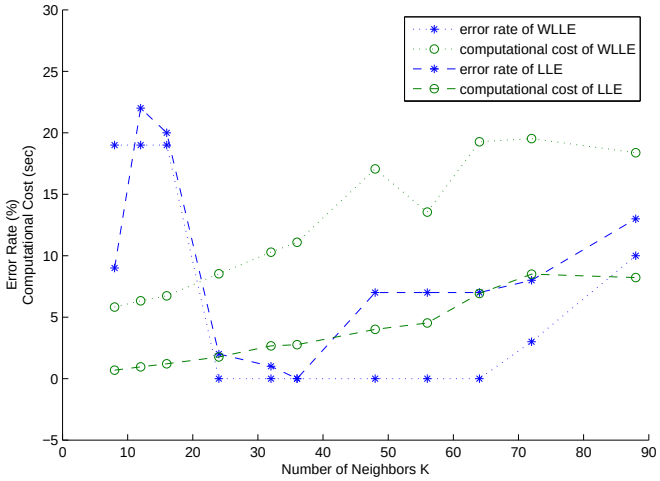

Figure 7.9: Comparison of error rates and computational cost as functions of K for WLLE and LLE

Table 7.1 shows the optimal parameter ranges, average computational cost and average error rate. From Table 7.1, it can be easily observed that PCA is the most simple algorithm but the classification performance is not satisfactory. KDDA has low computational cost and excellent classification performance, and is the best algorithm for this face recognition problem. KPCA and NLE have high computational costs and average classification error rates. WLLE shows good performance for classification, but the computational cost is relatively high compared to KDDA and LLE. Although the smallest error rates for WLLE and LLE are almost the same, we can see from Fig. 7.9 that WLLE gives the optimal performance for a much larger range of parameter than LLE, which means WLLE is more robust to parameter changes than LLE.

Table 7.1: Comparisons of classification error rates and computational time

Algorithm	Parameter	Computational Time (S)	Error Rate
PCA	N.A.	0.5	47%
KPCA	$\sigma^2 : 2e2 \sim 8e2$	16.5	10%
KDDA	$\sigma^2 \geq 2e2$	1.7	0%
LLE	$K : 24 \sim 36$	2.4	1%
WLLE	$K : 24 \sim 72$	13.3	0%
NLE	N.A.	11.5	8%

Manifold Learning of Different Poses of A Face

In next simulation study, the feature extraction algorithms are used to find the coherent relationship among a set of face images [219]. This data set contains $N = 698$ gray images at a resolution of 64×64 with different poses from left side view through front view to right side view of the same face. The input datum x_i of X is constructed by formatting the image pixel column by column from left to right and concatenate them to form a column vector.

The computed 2-Dimensional embeddings by WLLE are shown in Fig. 7.10, several face images are shown next to the corresponding embedding point. These embeddings form an arch-bridge shape. To a certain extent, it is identical to the motion trajectory of the faces. From the left end of the arch, through middle peak till the right end of the arch, the embeddings are corresponding to the left pose face, front face and right pose face. Although the face images are high dimensional data, the 2D embeddings of the face images are related

to meaningful attributes of the motion of the subject head in the images. Thus, if a new face image is given, we can compute its corresponding embedding and identify the face direction by finding its position in Fig. 7.10.

For comparison, the same data are also processed by PCA, KPCA and KDDA, which are shown in Figs. 7.11, 7.12, 7.13, respectively. All of them show some patterns according to the different poses of face images. The PCA and KPCA map the left and right views of the face to the top and bottom part of the embedding, respectively. KDDA maps the left and right views of the face to the top right and bottom left part of the embedding, respectively. Simple inspection of Figs. 7.10-7.13 indicates that WLLE extracts a smoother and meaningful string of manifold for the images of different poses.

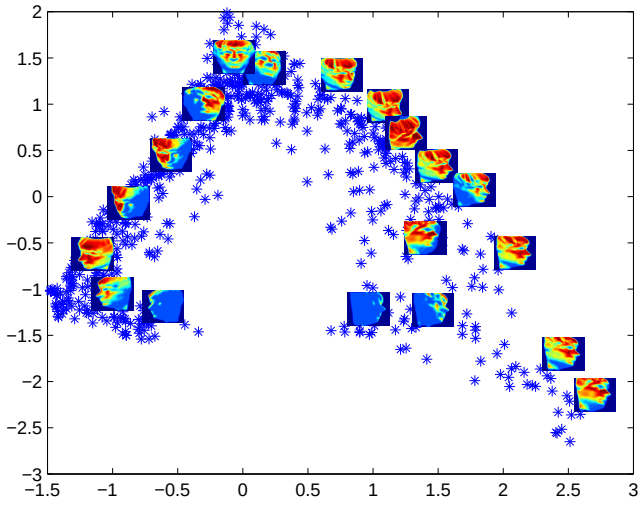

Figure 7.10: 2D embeddings of different pose face images by WLLE

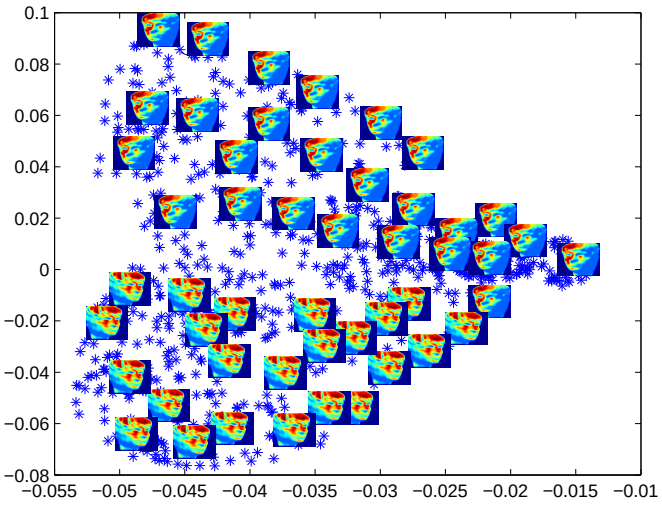

Figure 7.11: 2D embeddings of different pose face images by PCA

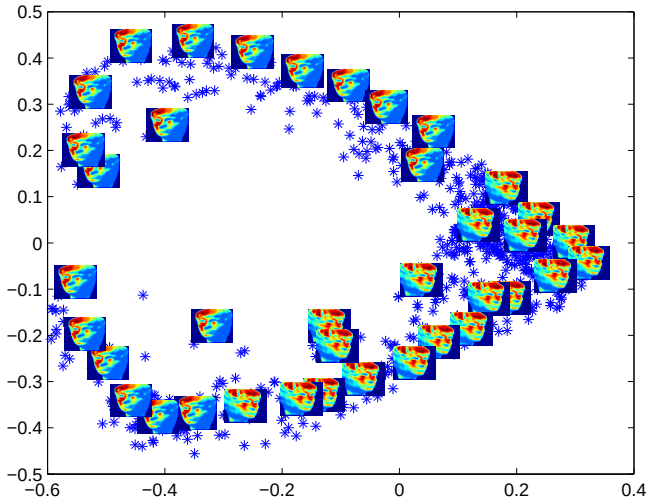

Figure 7.12: 2D embeddings of different pose face images by KPCA

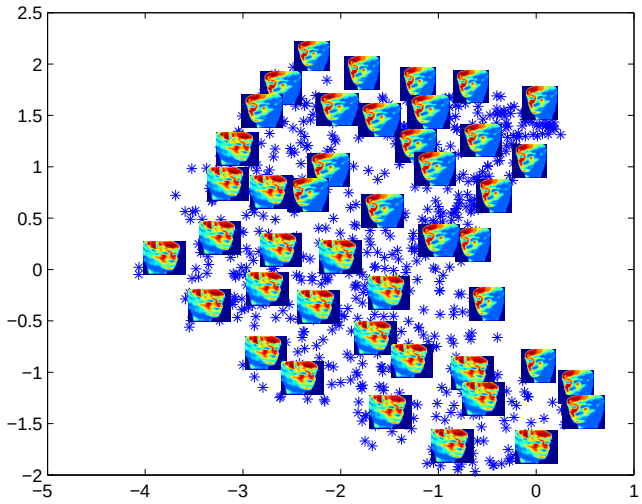

Figure 7.13: 2D embeddings of different pose face images by KDDA

7.5 Conclusion

In this chapter, an active vision system for identifying humans' faces from background and recognizing the faces was presented. Haar-Cascade classifier and precise face detector were used to do the face detection. Feature extraction algorithm, LLE and WLLE have been utilized for finding compact and robust feature descriptor to do face recognition. The proposed robot vision system for human detection and recognition was thoroughly evaluated in experiments, which demonstrated the effectiveness of the face detection module and face recognition module.

Chapter 8

Conclusions and Future work

The work presented in this thesis focused on both fundamental academic exploration of patter recognition algorithms and practical implementation of the algorithms for developing effective neurological therapeutic schemes. In this chapter, the results of the research work described in the previous chapters are summarized and the major contributions of this work are reviewed. Suggestions for future work are also presented.

8.1 Conclusions and Contributions

The thesis has covered advanced engineering technologies like brain imaging and processing technologies, intelligent control designs and advanced robotics as aid in the treatment of several different neurological disorders, including epilepsy, stroke, and autism. In this thesis, an attempt has been made to develop necessary techniques and demonstrate theoretically and empirically that the proposed methods serve as promising technologies for future neurological therapy strategies design.

(i) Part I of the thesis has been dedicated to detection and prevention of epileptic seizures.

- An automatic detection of epilepsy was proposed based on EEG signal processing. The automatic seizure detection consists of feature extraction and classification. In this research, several statistical features were proposed for feature extraction. SVM and BPNN were applied as classifier. These algorithms were evaluated and compared through experiments on two-channels I-EEG data obtained from Swiss mice. The experimental results demonstrated the merits of the proposed methods.
- Upon detection of seizures, we addressed the problem of controlling the synaptic plasticity to constrain bursting activity in epileptic seizures. A closed-loop control strategy was designed for a direct drug injection or electrical stimulation of related brain region on the basis of a good understanding of dynamical changes in seizures onset. The closed-loop system was demonstrated to be globally stable. Simulation studies were carried out to show the effectiveness of the control for stopping the bursting activity in brain with epilepsy. Through this study, we have shown how advanced nonlinear control techniques allow for effective design of drug injection or electrical stimulation schemes for achieving brain states restoration.

(ii) Part II of the thesis has been dedicated to mind robotic rehabilitation of stroke.

- Mind robotic rehabilitation was developed based on non-invasive motor imagery based BCI technology and a human-friendly interactive robot. The mind robotic

rehabilitation was designed for stroke patients to do regular rehabilitation training at home. A human-friendly interactive robot was developed as a visual and motion feedback for BCI system to make the patients more cognitively engaged in rehabilitative training process. For the BCI system, we used a spatial filtering algorithm, CSP, for discriminative feature extraction of EEG signal with left hand movement imagination and right hand movement imagination. Furthermore, a feature fusion of CSP and AR spectral analysis was proposed and proved to have obvious improvement for the performance of BCI system. QDA was utilized as classifier for the combined feature vectors. The proposed feature fusion method was evaluated by both off-line and real-time experiments and compared to single-feature extraction methods. The experimental results demonstrated that the feature fusion method outperformed each of the single-feature extraction algorithms.

(iii) Part III of the thesis has been dedicated to social therapy of autism.

- An interactive robot pet, RoBear, was developed to help autistic children based on a good understanding of autism-related hypothesis of neuroscience and cognitive science, and advanced robotics technology with multimodal HRI. A multimodal HRI framework was proposed, under which the RoBear was able to identify the face and voice and sensitive to the emotional change of the patients working with it. The RoBear was designed to be responsive to the physical and psychological states of the patients and capable of detecting both implicit and

explicit communication from the patients to determine its own behavior. We argue that RoBear is promising for providing individualized and empathetic social companion for children, elderly and socially disabled people, and is especially well suited for social therapy of autistic children.

- Under the multimodal HRI framework mentioned in Chapter 5, an intelligent audio human detection system was introduced to recognize human voice and identify it from background sound. An unsupervised learning algorithm NLE was proposed for sound sources recognition. NLE is a variant of LLE algorithm, which can address the trail and error problem for finding neighborhood in LLE. Additionally, motivated by the scale adaptation of human's perception, several scale invariant metrics were designed to enhance the intrinsic feature extraction performance of NLE. The NLE and SINLE were shown to outperform the original LLE algorithm through the experimental results on both artificial and real-world sound data.

- Under the multimodal HRI framework proposed in Chapter 5, we introduced a real-time vision system for detecting and recognizing human face from real environment. Adaboost-based Haar-Cascade classifier was used for human face detection. ELM was used to further remove the non-face images. For face recognition, we conducted extensive experiments on different face data set, using dimension reduction algorithm like LLE, WLLE and other famous feature extraction algorithms for face image. Furthermore, we did a thorough comparison between the proposed WLLE algorithm and other famous feature extraction algorithms for face image. The experimental results demonstrated that the WLLE algorithm

outperformed the other algorithms, which may be caused by the new neighbor selection criterion we proposed. The WLLE is a promising way to extract useful features for recognition of face images.

8.2 Limitations and Future Work

Based on review of the limitations of this research work, the research topics that are recommended for further investigation are presented.

- Although evidence suggests that brain signal processing techniques and interactive robotics resulted in significant improvements in neurological therapy, the results are currently inconclusive due to the large variations in neurological improvements in both groups and the limited number of patients recruited for current study. Furthermore, the work proposed in this thesis is weak on the experimental validation due to difficulties in obtaining human EEG data and experiment subjects for testing our systems because of some ethic issues. A conclusive result could be drawn from a larger scale study through collaboration with hospitals and other neuroscience research groups. Nevertheless, the outcome of this preliminary study is promising as it demonstrated the role of the engineering approaches in neurological therapy.

- The use of EEG technique is limited by two issue. The first is the requirement of electrically-conductive gel for a good connection between the sensors and the scalp, which is time-consuming and limits the realizable density of sensors on the scalp and EEG recording time. The second limiting issue with typical EEG systems is that they are not portable due to the mass of wires connecting the sensor to computer. Thus,

it would be a future work to design active electrode (also called "dry electrode") with low impedance which does not requires conductive gel, and to develop wireless EEG device with wireless capability for EEG signal acquisition. These improvements of EEG device may lead to the transfer of EEG technique from usage under laboratory settings to daily usage of seamless and minimally obtrusive neural signal acquisition in neurological therapy. Furthermore, we may also investigate more effective algorithms to minimize the number of required EEG electrodes.

- In this thesis, we only focused on utilizing pattern recognition algorithm, in particular, feature extraction algorithm, and interactive robotics for developing novel neurological therapeutic schemes. However, a number of other engineering technologies can be applied to enhance the effectiveness of neurological therapy. These technologies for future study include intelligent control, network communications, advanced classification algorithms, etc. Sensor fusion for brain monitoring is also a future trend of this research. For instance, since the MEG and EEG complement each other, their combined usage may greatly improve our understanding of what is occurring in the brain, and provide more practical brain monitoring for neurological therapy.

- In this thesis, the multimodal HRI for robotic rehabilitation of neurological disorder was developed based on robot audio and vision system and a motor imagery based BCI. Future direction of research includes the detection of attention and emotional states of the patient using BCI for a more holistic approach towards mind robotic rehabilitation in order to address the neuropsychological issues in addition to the physiological aspects of rehabilitation for an optimal therapy. Specifically, for social

therapy of autism, a BCI based emotion detection method should be developed to complement the facial expression based emotion detection to develop empathic robot pet for optimal social training of autistic children. However, a challenging issue is in how to achieve reliable emotion detection accuracy with a small number of EEG sensors for minimally obtrusive brain signal acquisition from autistic children who are reluctant to be physically touched.

Bibliography

[1] B. Obermaier, G. R. Muller, and G. Pfurtscheller, "Virtual keyboard controlled by spontaneous EEG activity," *IEEE Trans. Neural Syst. Rehabil. Eng.*, vol. 11, pp. 422–426, 2003.

[2] J. R. Wolpaw, "Brain-computer interfaces (BCIs) for communication and control: a mini-review," *Suppl. Clin. Neurophysiol.*, vol. 57, pp. 607–613, 2004.

[3] A. B. Gardner, A. M. Krieger, G. Vachtsevanos, and B. Litt, "One-class novelty detection for seizure analysis from intracranial EEG," *Journal of Machine Learning Research*, vol. 7, pp. 1025–1044, 2006.

[4] R. Esteller, "Detection of seizure onset in epileptic patients from intracranial EEG signals," *Ph.D dissertation, Georgia Inst. Technol.*, 2000.

[5] Y. Salant, I. Gath, and O. Henriksen, "Prediction of epileptic seizures from two-channel EEG," *Medical and biolodical Engineering and Computing*, vol. 36, pp. 549–556, 1998.

[6] Z. Rogowski, I. Gath, and E. Bental, "On the prediction of epileptic seizures," *Biological Cybernetics*, vol. 42, pp. 9–15, 1981.

[7] C. M. Light, P. H. Chappell, B. Hudginsz, and K. Engelhart, "Intelligent multifunction myoelectric control of hand prostheses," *J. Med. Eng. Technol.*, vol. 26, pp. 139–146, 2002.

[8] X. Navarro, T. B. Krueger, N. Lago, S. Micera, T. Stieglitz, and P. Dario, "A critical review of interfaces with the peripheral nervous sytem for the control of neuroprostheses and hybrid bionic systems," *J. Peripher. Nerv. Syst.*, vol. 10, pp. 229–258, 2005.

[9] R. Okuno, M. Yoshida, and K. Akazawa, "Compliant grasp in a myoelectric hand prosthesis. Controlling flexion angle and compliance with electromyogram signals," *IEEE Eng. Med. Biol. Mag.*, vol. 24, pp. 48–56, 2005.

[10] M. Zecca, S. Micera, M. C. Carrozza, and P. Dario, "Control of multifunctional prosthetic hands by processing the electromyographic signal," *Crit. Rev. Biomed. Eng.*, vol. 30, pp. 459–485, 2002.

[11] S. I. Tillery and D. M. Taylor, "Signal acquisition and analysis for cortical control of neuroprosthetics," *Curr. Opin. Neurobiol.*, vol. 14, pp. 758–762, 2004.

[12] S. Musallam, B. D. Corneil, B. Greger, H. Scherberger, and R. A. Andersen, "Cognitive control signals for neural prosthetics," *Science*, vol. 305, pp. 258–262, 2004.

[13] G. E. Loeb, R. A. Peck, W. H. Moore, and K. Hood, "BION system for distributed neural prosthetic interfaces," *Med. Eng. Phys.*, vol. 23, pp. 9–18, 2001.

[14] K. V. Shenoy, D. Meeker, S. Cao, S. A. Kureshi, B. Pesaran, C. A. Buneo, A. P. Batista, P. P. Mitra, J. W. Burdick, and R. A. Andersen, "Neural prosthetic control signals from plan activity," *NeuroReport*, vol. 14, pp. 591–596, 2003.

[15] T. Hinterberger, R. Veit, B. Wilhelm, N. Weiskopf, J. J. Vatine, and N. Birbaumer, "Neuronal mechanisms underlying control of a brain-computer interface," *Eur. J. Neurosci.*, vol. 21, pp. 3169–3181, 2005.

[16] F. E. Dudek and M. Spitz, "Hypothetical mechanisms for the cellular and neurophysiologic basis of secondary epileptogenesis: proposed role of synaptic reorganization," *J. Clin. Neurophysiol.*, vol. 14, pp. 90–101, 1997.

[17] N. D. Volkow, B. Rosen, and L. Farde, "Imaging the living human brain: Magnetic resonance imaging and positron emission tomography," *Proc. Natl. Acad. Sci.*, vol. 94, pp. 2787–2788, 1997.

[18] B. J. Casey and M. D. Haan, "Introduction: new methods in developmental science," *Developmental Science*, vol. 5, pp. 265–267, 2002.

[19] D. Purves, G. J. Augustine, D. Fitzpatrick, L. C. Katz, A. S. LaMantia, and J. O. McNamara, *Neurosciences*. De Boeck University Eds., 1999.

[20] S. R. Cherry, J. Sorenson, and M. Phelps, *Physics in Nuclear Medicine*, 3rd ed. W B Saunders, 2003.

[21] M. E. Phelps, E. J. Hoffman, N. A. Mullani, and M. M. Ter-Pogossian, "Application of annihilation coincidence detection to transaxial reconstruction tomography," *Journal of Nuclear Medicine*, vol. 16, no. 3, pp. 210–224, 1975.

[22] A. Villringer and H. Obrig, "Near-infrared spectroscopy and imaging," in *In Brain Mapping: The Methods.* USA: Elsevier Science, 2002, pp. 141–158.

[23] R. Sitaram, Y. Hoshi, and C. Guan, "Near infrared spectroscopy based brain-computer interface," in *Proc. of the International Conference on Experimental Mechanics*, 2005, pp. 434–442.

[24] H. Zhang and C. Guan, "A kernel-based signal localization method for nirs brain-computer," in *18th International Conference on Pattern Recognition (ICPR'06)*, Hong Kong, China, 2006, pp. 1158–1161.

[25] S. Coyle, T. Ward, C. Markham, and G. McDarby, "On the suitability of near-infrared (NIR) systems for nextgeneration brain-computer interfaces," *Physiological Measurements*, vol. 25, pp. 815–822, 2004.

[26] N. Weiskopf, F. Scharnowski, R. Veit, R. Goebel, N. Birbaumer, and K. Mathiak, "Self-regulation of local brain activity using real-time functional magnetic resonance imaging (fMRI)," *J. Physiol. (Paris)*, vol. 98, pp. 357–373, 2004.

[27] M. Maruishi, M. Miyatani, T. Nakao, and H. Muranaka, "Compensatory cortical activation during performance of an attention task by patients with diffuse axonal injury: a functional magnetic resonance imaging study," *NeuroImage*, vol. 21, pp. 1604–1611, 2004.

[28] J. Kong, L. Ma, R. L. Gollub, J. Wei, X. Yang, D. Li, X. Weng, F. Jia, C. Wang, F. Li, R. Li, and D. Zhuang., "A pilot study of functional magnetic resonance imaging of the brain during manual and electroacupuncture stimulation of acupuncture point

(LI-4 Hegu) in normal subjects reveals differential brain activation between methods," *Journal of Alternative and Complementary Medicine*, vol. 8, no. 4, pp. 411–419, 2002.

[29] W. Blume, H. Luders, E. M. C. Tassinari, W. van Emde Boas, and J.Engel, "Glossary of descriptive terminology for ictal semiology: report of the ilae task force on classification and terminology," *Epilepsia*, vol. 42, no. 9, pp. 1212–1218, 2001.

[30] R. S. Fisher, W. van Emde Boas, W. Blume, C. Elger, P. Genton, P. Lee, and J. Jr.Engel, "Epileptic seizures and epilepsy: Definitions proposed by the international league against epilepsy (ILAE) and the international bureau for epilepsy (IBE)," *Epilepsia*, vol. 46, no. 4, pp. 470–472, 2005.

[31] A. B. Geva and D. H. Kerem, "Forecasting generalized epileptic seizures from the eeg signal by wavelet analysis and dynamic unsupervised fuzzy clustering," *IEEE Transaction of Biomed Engineering*, vol. 45, pp. 1205–1216, 1998.

[32] R. Esteller, G. Vachtsevanos, J. Echauz, and B. Litt, "A comparison of fractal dimension algorithms using synthetic and experimental data," in *presented and the IEEE Int. Symp. Circuits and Systems*, Orlando, FL, 1999.

[33] B. Litt, R. Esteller, and J. Echauz, "Epileptic seizures may begin hours in advance of clinical onset: a report of five patients," *Neuron*, vol. 30, pp. 51–64, 2001.

[34] G. D. Cascino, "Epilepsy: contemporary perspectives on evaluation and treatment," *Mayo Clinic Proc*, vol. 69, pp. 1199–1211, 1994.

[35] J. Engel, "Surgery for seizures," *New England Journal of Medcine*, vol. 334, pp. 647–653, 1996.

[36] G. A. Baker, A. Jacoby, D. Buck, C. Stalgis, and D. Monnet, "Quality of life of people with epilepsy: A european study," *Epilepsia*, vol. 38, pp. 353–362, 1997.

[37] J. F. Annegers, S. P. Coan, W. A. Hauser, and J. Leestma, "Epilepsy, vagal nerve stimulation by the NCP system, all-cause mortality, and sudden, unexpected, unexplained death," *Epilepsia*, vol. 41, pp. 549–553, 2000.

[38] B. Litt, A. D'Alessandro, R. Esteller, J. Echauz, and G. Vachtsevanos, "Translating seizure detection, prediction and brain stimulation into implantable devices for epilepsy," in *First International IEEE EMBS Conference on Neural Engineering*, Capri Island, Italy, 2003, pp. 485 – 488.

[39] I. Osorio, M. Frei, B. Manly, S. Sunderam, N. C. Bhavaraju, and S. B. Wilkinson, "An introduction to contingent (closed-loop) brain electrical stimulation for seizure blockage," *Journal of CIinical Neurophysiology*, vol. 18, pp. 533–544, 2001.

[40] M. L. Kringelbach, N. Jenkinson, S. L. F. Owen, and T. Z. Aziz, "Translational principles of deep brain stimulation," *Nature Reviews Neuroscience*, vol. 8, pp. 623–635, 2007.

[41] L. D. Iasemidis, J. C. Sackellares, H. P. Zaveri, and W. J. Williams, "Phase space topography and the Lyapunov exponent of electrocorticograms in partial seizures," *Brain topography*, vol. 2, pp. 187–201, 1990.

[42] M. H. Beers and R. Berkow, *The Merck Manual of Geriatrics*, 3rd ed. New Jersey: Merck Research Laboratories, 2000, proCite field[17]: Eds.

[43] N. Venketasubramanian, L. C. Tan, S. Sahadevan, J. J. Chin, E. S. Krishnamoorthy, C. Y. Hong, and S. M. Saw, "Prevalence of stroke among chinese, malay, and indian singaporeans: A community-based tri-racial cross-sectional survey," *Stroke*, vol. 36, no. 3, pp. 551–556, 2005.

[44] M. W. O'Dell, C.-C. D. Lin, and V. Harrison, "Stroke rehabilitation: Strategies to enhance motor recovery," *Annual Review of Medicine*, vol. 60, no. 1, 2009.

[45] M. Hallett, "The plastic brain," *Annals of Neurology*, vol. 38, no. 1, pp. 4–5, 1995.

[46] L. S. Turkstra, A. L. Holland, and G. A. Bays, "The neuroscience of recovery and rehabilitation: What have we learned from animal research?" *Archives of Physical Medicine and Rehabilitation*, vol. 84, no. 4, pp. 604–612, 2003.

[47] B. Klob, *Brain plasticity and behavior*. Mahwah: Lawrence Erlbaum Associates, 1995.

[48] J. Young and A. Forster, "Review of stroke rehabilitation," *BMJ*, vol. 334, no. 7584, pp. 86–90, 2007.

[49] A. Pollock, G. D. Baer, P. Langhorne, and V. M. Pomeroy, "Physiotherapy treatment approaches for stroke," *Stroke*, vol. 39, no. 2, pp. 519–520, 2008.

[50] H. I. Krebs, J. J. Palazzolo, L. Dipietro, M. Ferraro, J. Krol, K. Rannekleiv, B. T. Volpe, and N. Hogan, "Rehabilitation robotics: Performance-based progressive robot-assisted therapy," *Autonomous Robots*, vol. 15, no. 1, pp. 7–20, 2003.

[51] H. I. Krebs and N. Hogan, "Therapeutic robotics: A technology push," *Proceedings of the IEEE*, vol. 94, no. 9, pp. 1727–1738, 2006, proCite field[16]: Hogan, N.

[52] P. S. Lum, C. G. Burgar, P. C. Shor, M. Majmundar, and M. V. der Loos, "Robot-assisted movement training compared with conventional therapy techniques for the rehabilitation of upper-limb motor function after stroke," *Archives of Physical Medicine and Rehabilitation*, vol. 83, no. 7, pp. 952–959, 2002.

[53] K. K. Ang, C. Guan, K. S. G. Chua, B. T. Ang, C. W. K. Kuah, C. Wang, K. S. Phua, Z. Y. Chin, and H. Zhang, "A clinical evaluation of non-invasive motor imagery-based brain-computer interface in stroke," in *Proceedings of the International Conference of the IEEE Engineering in Medicine and Biology Society (EMBC'08)*, Vancouver, BC Canada, 2008, pp. 4178–4181, proCite field[10]:.

[54] D. G. Amaral, C. M. Schumann, and C. W. Nordahl, "Neuroanatomy of autism," *Trends in Neurosciences*, vol. 31, no. 3, pp. 137–145, 2008.

[55] I. Rapin and R. Tuchman, "Autism: Definition, neurobiology, screening, diagnosis," *Pediatric Clinics of North America*, vol. 55, no. 5, pp. 1129–1146, 2008.

[56] S. M. Myers and C. P. Johnson, "Management of children with autism spectrum disorders," *Pediatrics*, vol. 120, no. 5, pp. 1162–1182, 2007.

[57] G. A. Stefanatos, "Regression in autistic spectrum disorders," *Neuropsychol Rev*, vol. 18, no. 4, pp. 305–319, 2008.

[58] T. J. Leskovec, B. M. Rowles, and R. L. Findling, "Pharmacological treatment options for autism spectrum disorders in children and adolescents," *Harvard Review of Psychiatry*, vol. 16, no. 2, pp. 97–112, 2008.

[59] D. P. Oswald and N. A. Sonenklar, "Medication use among children with autism spectrum disorders," *Journal of Child and Adolescent Psychopharmacology*, vol. 17, no. 3, pp. 348–355, 2007.

[60] D. J. Posey, K. A. Stigler, C. A. Erickson, and C. J. McDougle, "Antipsychotics in the treatment of autism," *J Clin Invest*, vol. 118, no. 1, pp. 6–14, 2008.

[61] J. K. Buitelaar, "Why have drug treatments been so disappointing?" *Novartis Foundation Symposium*, vol. 251, pp. 235–244, 2004.

[62] M. Sigman, S. J. Spence, and A. T. Wang, "Autism from developmental and neuropsychological perspectives," *Annu Rev Clin Psychol*, vol. 2, pp. 327–355, 2006.

[63] M. G. Aman, "Treatment planning for patients with autism spectrum disorders," *J Clin Psychiatry*, vol. 67, no. 12, pp. 38–45, 2005.

[64] A. F. Burgess and S. E. Gutstein, "Quality of life for people with autism: Raising the standard for evaluating successful outcomes," *Child and Adolescent Mental Health*, vol. 12, no. 2, pp. 80–86, 2007.

[65] M. L. Hediger, L. J. England, C. A. Molloy, K. F. Yu, P. Manning-Courtney, and J. L. Mills, "Reduced bone cortical thickness in boys with autism or autism spectrum disorder," *Journal of Autism and Developmental Disorders*, vol. 38, no. 5, pp. 848–856, 2008.

[66] M. J. Brown, T. Willis, B. Omalu, and R. Leiker, "Deaths resulting from hypocalcemia after administration of edetate disodium: 2003-2005," *PEDIATRICS*, vol. 118, no. 2, pp. e534–e536, 2006.

[67] H. Kozima, M. P. Michalowski, and C. Nakagawa, "Keepon - a playful robot for research, therapy, and entertainment," *International Journal of Social Robotics*, vol. 1, pp. 3–18, 2009.

[68] F. Michaud and C. Théberge-Turmel, *Socially intelligent agent.* Dordrecht: Kluwer Academic, 2002, ch. Mobile robotic toys and autism, pp. 125–132.

[69] M. Okada and M. Goan, "Modeling sociable artificial creatures: Findings from the Muu project," in *Proceedings of the 13th international conference on perception and action*, California, USA, July 5-10 2005, p. 55.

[70] B. Scassellati, "Using social robots to study abnormal social development," in *Proceedings of the 5th intenational workshop on epigenetic robotics*, 2005, pp. 11–14.

[71] R. Duckrow and S. Spencer, "Regional coherence and the transfer of ictal activity during seizure onset in the medial temporal lobe," *Electroencephalography And Clinical Neurophysiology*, vol. 82, pp. 415–422, 1992.

[72] K. Lehnertz and C. Elger, "Spatio-temporal dynamics of the primary epileptogenic area in temporal lobe epilepsy characterized by neuronal complexity loss," *Electroencephalography And Clinical Neurophysiology*, vol. 95, pp. 108–117, 1995.

[73] F. R. Tang, S. C. Chia, P. M. Chen, H. Gao, W. L. Lee, T. S. Yeo, J. M. Burgunder, A. Probst, M. K. Sim, and E. A. Ling, "Metabotropic glutamate receptor 2/3 in the hippocampus of patients with mesial temporal lobe epilepsy, of rats and mice after pilocarpine-induced status epilepticus," *Epilepsy Res.*, vol. 59, pp. 167–180, 2004.

[74] F. R. Tang, S. C. Chia, F. L. Jiang, D. L. Ma, P. M. Chen, and Y. C. Tang, "Calcium binding protein containing neurons in sclerotic mouse hippocampus with special reference to their afferents from the medial septum and the entorhinal cortex," *Neuroscience*, vol. 140, pp. 1467–1479, 2005.

[75] R. J. Racine, "Modification of seizure activity by electric stimulation, ii. motor seizure," *Electroencephalogr. Clin. Neurophysiol*, vol. 32, p. 281C294, 1972.

[76] M. A. Navakatikyan, P. B. Colditz, C. J. Burke, T. E. Inder, J. Richmond, and C. E. Williams, "Seizure detection algorithm for neonates based on wave-sequence analysis," *Clinical Neurophysiology*, vol. 117, pp. 1190–1203, 2006.

[77] G. T. Finnerty and J. G. Jefferys, "9-16 Hz oscillation precedes secondary generalization of seizures in the rat tetanus toxin model of epilepsy," *Journal of Neurophysiology*, vol. 103, pp. 356–362, 1997.

[78] P. V. Hese, J. P. Martens, P. Boon, S. Dedeurwaerdere, I. Lemahier, and R. V. de Walle, "Detection of spike and wave discharges in the cortical eeg of genetic absence epilepsy rats from strasbourg," *Physics in Medical Biology*, vol. 48, pp. 1685–1700, 2003.

[79] S. M. Zoldi, A. Krystal, and H. S. Greenside, "Stationarity and redundancy of multichannel eeg data recorded during generalized tonic-clonic seizures," 1999. [Online]. Available: http://www.citebase.org/abstract?id=oai:arXiv.org:chao-dyn/9905004

[80] L. Iasemidis, H. Zaveri, J. Sackellares, W. Williams, and T. Hood, "Nonlinear dynamics of ECoG data in temporal lobe epilepsy," *Electroencephalography and Clinical Neurophysiology*, vol. 5, p. 339, 1988.

[81] M. D'Alessandro, G. Vachtsevanos, A. Hinson, R. Esteller, J. Echauz, and B. Litt, "A genetic approach to selecting the optimal feature for epileptic seizure prediction," in *Proceedings of 23rd Annual EMBS International Conference*, Istanbul, Turkey, 25-28 October 2001, pp. 1703–1706.

[82] K. F. Fong, A. P. Loh, and W. W. Tan, "A frequency domain approach for fault detection," *Accepted for publication in International Journal of Control*, 2009.

[83] W. W. Tan, "A modified least-mean-square algorithm for training neurofuzzy controllers on-line," *ISA Transactions*, vol. 46, no. 2, pp. 181–188, 2007.

[84] J. F. Kaiser, "On a simple algorithm to calculate the "energy" of a signal," in *Proc. 1990 Int. Conf. Acoustis, Speech, Signal Processing*, vol. 1, 1990, pp. 381–384.

[85] S. S. Ge and Y. Cui, "New potential functions for mobile robot path planning," *IEEE Transactions on Robotic and Automation*, vol. 16, no. 5, pp. 615–620, October 2000.

[86] M. M. Polycarpou and M. J. Mears, "Stable adaptive tracking of uncertain systems using nonlinearly parametrized on-line approximators," *International Journal of Control*, vol. 70, pp. 363–384, 1998.

[87] G. V. Luijtellaar, J. Welting, and R. Q. Quiroga, "The reticular thalamic nucleus is involved in left-right EEG synchronization," in *Sleep-Wake research in the Netherlands*. Dutch Society for Sleep-Wake Research, 2000.

[88] A. G. Stein, H. G. Eder, D. E. Blum, A. Drachev, and R. S. Fisher, "An automated drug delivery system for focal epilepsy," *Epilepsy Research*, vol. 39, pp. 103–104, 2000.

[89] H. G. Eder, A. G. Stein, and R. S. Fisher, "Interictal and ictal activity in the rat conbalt/pilocarpine model of epilepsy decreased by local perfusion of diazepam," *Epilepsy Research*, vol. 29, pp. 17–24, 1997.

[90] D. Janigro, "Blood-brain barrier, ion homeostasis and epilepsy: possible implications towards the understanding of ketogenic diet mechanisms," *Epilepsy Research*, vol. 37, pp. 223–232, 1999.

[91] B. J. Gluckman, H. Nguyen, S. L. Weinstein, and S. J. Schiff, "Adaptive electric field control of epileptic seizures," *Journal of Neuroscience*, vol. 21, pp. 590–600, 2001.

[92] C. Koch and I. Segev, *Methods in Neuronal Modeling*. Massachusetts: MIT Press, 1989.

[93] P. Kudela, P. J. Franaszczuk, and G. K. Berger, "Synaptic plasticity in neuronal network models can explain patterns of bursting activity seen in temporal lobe epileptic seizures," in *Proceedings of the 26th Annual International Conference of the IEEE EMBS*, San Francisco, CA, USA, 2004, pp. 715–717.

[94] S. S. Ge, Z. L. Tian, and T. H. Lee, "Nonlinear control of a dynamic model of HIV-1," *IEEE transactions on biomedical engineering*, vol. 52, pp. 353–361, 2005.

[95] S. S. Ge and C. Wang, "Adaptive neural control of uncertain MIMO nonlinear systems," *IEEE Transactions on Neural Networks*, vol. 15, pp. 674–692, 2004.

[96] C. Wang and S. S. Ge, "Adaptive backstepping control of uncertain lorenz system," *International Journal of Bifurcation and Chaos*, vol. 11, pp. 1115–1119, 2001.

[97] C. C. Jouny, P. J. Franaszczuk, and G. K. bergey, "Characterization of epileptic seizure dynamics using gabor atom density," *Clinical Neurophysiology*, vol. 114, pp. 426–437, 2003.

[98] S. S. Ge, "Adaptive control of uncertain lorenz system using decoupled backstepping," *International Journal of Bifurcation and Chaos*, vol. 14, pp. 1439–1445, 2004.

[99] W. H. Young, "On classes of summable functions and their fourier series," *Proc. Roy. Soc. London Ser. A*, vol. 87, pp. 225–229, 1912.

[100] R. Cooper, "Notes on certain inequalities. i." *J. London Math. Soc.*, vol. 2, pp. 17–21, 1927.

[101] ——, "Notes on certain inequalities. ii." *J. London Math. Soc.*, vol. 2, pp. 159–163, 1927.

[102] J. P. LaSalle, "Stability theory for ordinary differential equations," *Journal of Differential Equations*, vol. 4, pp. 57–65, 1968.

[103] T. Yoshizawa, *Stability Theory by Lyapunov's Second Method*. Tokyo, Japan: The mathematical Society of Japan, 1966.

[104] C. Wang and S. S. Ge, "Adaptive synchronization of uncertain chaotic system via backstepping design," *Chaos, Solitons and Fractals*, vol. 12, pp. 1199–1206, 2001.

[105] S. S. Ge and C. Wang, "Uncertain chaotic system control via adaptive neural design," *International Journal of Bifurcation and Chaos*, vol. 12, pp. 1097–1109, 2001.

[106] S. S. Ge, C. C. Hang, T. H. Lee, and T. Zhang, *Stable Adaptive Neural Network Control*. Boston: Kluwer Academic Publisher, 2002.

[107] A. Yesildirek and F. L. Lewis, "Feedback linearization using neural networks," *Automatica*, vol. 31, pp. 1659–1664, 1995.

[108] P. Kudela, P. J. Franaszczuk, and G. K. Berger, "Model of the propagation of synchronous firing in a reduced neuron network," *Neurocomputing*, vol. 26-27, pp. 411–418, 1999.

[109] J. Zhang, R. E. Campbell, A. Y. Ting, and R. Y. Tsien, "Creating new fluorescent probes for cell biology," *Nat Rev Mol Cell Biol.*, vol. 3, no. 12, pp. 906–918, 2002.

[110] N. Demaurex, "Calcium measurements in organelles with ca^{2+} sensitive fluorescent proteins," *Cell Calcium*, vol. 38, no. 3-4, pp. 213–222, 2005.

[111] R. Ashworth, "Approaches to measuring calcium in zebrafish: focus on neuronal development," *Cell Calcium*, vol. 35, no. 5, pp. 393–402, 2004.

[112] A. Miyawaki, O. Griesbeck, R. Heim, and R. Y. Tsien, "Dynamic and quantitative ca^{2+} measurements using improved cameleons," *Proc Natl Acad Sci*, vol. 96, no. 5, pp. 2135–2140, 1999.

[113] O. Gerasimenko and A. Tepikin, "How to measure ca^{2+} in cellular organelles?" *Cell Calcium*, vol. 38, no. 3-4, pp. 201–211, 2005.

[114] B. T. Volpe, D. Lynch, A. Rykman-Berland, M. Ferraro, M. Galgano, N. Hogan, and H. I. Krebs, "Intensive sensorimotor arm training mediated by therapist or robot improves hemiparesis in patients with chronic stroke," *Neurorehabilitation and Neural Repair*, vol. 22, no. 3, pp. 305–310, 2008.

[115] J.-J. Chang, W.-L. Tung, W.-L. Wu, M.-H. Huang, and F.-C. Su, "Effects of robot-aided bilateral force-induced isokinetic arm training combined with conventional rehabilitation on arm motor function in patients with chronic stroke," *Archives of Physical Medicine and Rehabilitation*, vol. 88, no. 10, pp. 1332–1338, 2007.

[116] S. E. Fasoli, H. I. Krebs, J. Stein, W. R. Frontera, R. Hughes, and N. Hogan, "Robotic therapy for chronic motor impairments after stroke: follow-up results," *Archives of Physical Medicine and Rehabilitation*, vol. 85, no. 7, pp. 1106–1111, 2004.

[117] P. S. Lum, C. G. Burgar, and P. C. Shor, "Evidence for improved muscle activation patterns after retraining of reaching movements with the mime robotic system in subjects with post-stroke hemiparesis," *IEEE Transactions on Neural Systems and Rehabilitation Engineering*, vol. 12, no. 2, pp. 186–194, 2004.

[118] G. Pfurtscheller, C. Brunner, A. Schlogl, and F. H. L. da Silva, "Mu rhythm (de)synchronization and eeg single-trial classification of different motor imagery tasks," *NeuroImage*, vol. 31, no. 1, pp. 153–159, 2006.

[119] M. Stavrinou, L. Moraru, L. Cimponeriu, P. D. Stefania, and A. Bezerianos, "Evaluation of cortical connectivity during real and imagined rhythmic finger tapping," *Brain Topography*, vol. 19, no. 3, pp. 137–145, 2007.

[120] D. McFarland, L. Miner, T. Vaughan, and J. Wolpaw, "Mu and beta rhythm topographies during motor imagery and actual movements," *Brain Topography*, vol. 12, no. 3, pp. 177–186, 2000.

[121] G. Pfurtscheller, C. Neuper, C. Brunner, and F. L. da Silva, "Beta rebound after different types of motor imagery in man," *Neuroscience Letters*, vol. 378, no. 3, pp. 156–159, 2005.

[122] S. C. Wriessnegger, J. Kurzmann, and C. Neuper, "Spatio-temporal differences in brain oxygenation between movement execution and imagery: A multichannel near-infrared spectroscopy study," *International Journal of Psychophysiology*, vol. 67, no. 1, pp. 54–63, 2008, doi: DOI: 10.1016/j.ijpsycho.2007.10.004.

[123] N. Birbaumer, "Brain-computer-interface research: Coming of age," *Clinical Neurophysiology*, vol. 117, no. 3, pp. 479–483, 2006.

[124] B. Blankertz, G. Dornhege, M. Krauledat, K.-R. Muller, and G. Curio, "The non-invasive berlin brain-computer interface: Fast acquisition of effective performance in untrained subjects," *NeuroImage*, vol. 37, no. 2, pp. 539–550, 2007.

[125] J. R. Wolpaw, N. Birbaumer, D. J. McFarland, G. Pfurtscheller, and T. M. Vaughan, "Brain-computer interfaces for communication and control," *Clinical Neurophysiology*, vol. 113, no. 6, pp. 767–791, 2002.

[126] J. J. Daly and J. R. Wolpaw, "Brain-computer interfaces in neurological rehabilitation," *The Lancet Neurology*, vol. 7, no. 11, pp. 1032–1043, 2008.

[127] G. M. Friehs, V. A. Zerris, C. L. Ojakangas, M. R. Fellows, and J. P. Donoghue, "Brain-machine and brain-computer interfaces," *Stroke*, vol. 35, no. 11, pp. 2702–2705, 2004.

[128] K. K. Ang, Z. Y. Chin, H. Zhang, and C. Guan, "Filter bank common spatial pattern(fbcsp) in brain computer interface," in *IEEE International Joint Conference on Neural Networks, IEEE World Congress on Computational Intelligence*, 2008, pp. 2390–2397.

[129] G. Pfurtscheller, C. Neuper, D. Flotzinger, and M. Pregenzer, "EEG based discrimination between imagination of right and left hand movement," *Electroenc. Clin. Neurophys.*, vol. 103, no. 5, pp. 1–10, 1997.

[130] C. Guger, H. Ramoser, and G. Pfurtscheller, "Real-time EEG analysis with subject-specific spatial patterns for a brain computer interface (bci)," *IEEE Transactions on Rehabilitation Engineering*, vol. 8, no. 4, pp. 447–456, 2000.

[131] B. Blankertz, R. Tomioka, S. Lemm, M. Kawanabe, and K.-R. Müller, "Optimizting spatial filters for robust EEG single-trial analysis," *IEEE Signal Proc. Magazine*, vol. 25, no. 1, pp. 41–56, 2008.

[132] H. Ramoser, J. Muller-Gerking, and G. Pfurtscheller, "Optimal spatial filtering of single trial eeg during imagined handmovement," *IEEE Transactions on Rehabilitation Engineering*, vol. 8, no. 4, pp. 441–446, 2000.

[133] G. Pfurtscheller, C. Brunner, A. Schlogl, and F. L. da Silva, "Mu rhythm (de)synchronization and EEG single-trial classification of different motor imagery tasks," *NeuroImage*, vol. 33, pp. 153–159, 2006.

[134] J. R. Wolpaw and D. J. McFarland, "Control of a two-dimensional movement signal by a noninvasive brain-computer interface in humans," *Proc. Natl. Acad. Sci. U.S.A.*, vol. 101, pp. 17 849–17 854, 2004.

[135] J. Dolezal, J. Stastny, and P. Sovka, "Modelling and recognition of movement related eeg signal," in *International Conference on Applied Electronics*, 2006, pp. 27–30.

[136] C. Anderson, E. Stolz, and S. Shamsunder, "Discriminating mental tasks using EEG represented by AR models," in *IEEE Engineering in Medicine and Biology Annual Conference*, vol. 2, 1995, pp. 875–876.

[137] J. G. Proakis, C. M. Rader, F. Ling, C. L. Nikias, M. Moonen, and I. K. Proudler, Eds., *Algorithm for statistical signal processing.* Prentice Hall, 2001, pp. 461–462.

[138] J. Li, "Linear discriminant analysis," Department of statistic,The Penn State University, Tech. Rep., 2009.

[139] G. Pfurtscheller and A. Schlogl, "Bci competition II," 2002. [Online]. Available: http://www.bbci.de/competition/ii/

[140] S.-J. Blakemore and U. Frith, *The Learning Brain: Lessons for Education.* London: Wiley-Blackwell, 2005.

[141] B. Hermelin, *Bright splinters of the mind: a personal story of research with autistic savants.* London: Jessica Kingsley, 2001.

[142] M. Thomas and A. Karmiloff-Smith, "Are developmental disorders like cases of adult brain damage? implications from connectionist modelling," *Behavioral and Brain Sciences*, vol. 25, no. 6, pp. 727–788, 2002.

[143] A. Karmiloff-Smith, "Development itself is the key to understanding developmental disorders," *Trends in Cognitive Sciences*, vol. 2, no. 10, pp. 389–398, 1998.

[144] M. Dow, "Example space software renderings." [Online]. Available: http://lcni.uoregon.edu/ mark/Space_software/renderings.html

[145] J. M. Leppänen and C. A. Nelson, "Tuning the developing brain to social signals of emotions," *Nature Reviews Neuroscience*, vol. 10, pp. 37–47, 2008.

[146] P. R. Huttenlocher, "Synaptic density in human frontal cortex - developmental changes and effects of aging," *Brain Research*, vol. 163, no. 2, pp. 195–205, 1979.

[147] P. R. Huttenlocher and A. S. Dabholkar, "Regional differences in synaptogenesis in human cerebral cortex," *Journal of Comparative Neurology*, vol. 387, no. 2, pp. 167–178, 1997.

[148] U. Frith, *Autism: Explaining the enigma*. London: Wiley-Blackwell, 1989.

[149] K. Kaye, *The mental and social life of babies*. Chicago: University of Chicago Press, 1982.

[150] C. Trevarthen, "Intrinsic motives for companionship in understanding: Their origin, development, and significance for infant mental health," *Infant Mental Health*, vol. 22, pp. 95–131, 2001.

[151] K. Dautenhahn, "I could be you: The phenomenological dimension of social understanding," *Cybernetics and Systems*, vol. 25, no. 8, pp. 417–453, 1997.

[152] H. Kozima and A. Ito, *Ecology of language acquisition*. Dordrecht: Kluwer Academic, 2003, ch. From joint attention to lanfuage acquisition, pp. 65–81.

[153] J. Zlatev, "The epigenesis of meaning in human beings, and possibly in robots," *Minds and Machines*, vol. 11, no. 2, pp. 155–195, 2001.

[154] M. Tomasello, *The cultural origins of human cognition*. Cambridge: Harvard University Press, 1999.

[155] S. Baron-Cohen, H. A. Ring, S. Wheelwright, E. T. Bullmore, M. J.Brammer, A. Simmons, and S. C.Williams, "Social intelligence in the normal and autistic brain: an fmri study," *European Journal of Neuroscience*, vol. 11, pp. 1891–1898, 1999.

[156] S.-J. Blakemore, "The social brain in adolescence," *Nature Reviews Neuroscience*, vol. 9, pp. 267–277, 2008.

[157] R. Varley and M. Siegal, "Neural systems involved in 'theory of mind'," *Nature Reviews Neuroscience*, vol. 3, pp. 463–471, 2002.

[158] A. N. Hampton, P. Bossaerts, and J. P. O'Doherty, "Neural correlates of mentalizing-related computations during strategic interactions in humans," in *Proceedings of the National Academy of Sciences of the United States of America*, vol. 105, no. 18, May 2008, p. 6741C6746.

[159] M. L. Ganz, "The lifetime distribution of the incremental societal costs of autism," *Arch Pediatr Adolesc Med*, vol. 161, pp. 343–349, 2007.

[160] G. Montes and J. S. Halterman, "Association of childhood autism spectrum disorders and loss of family income," *Pediatrics*, vol. 121, pp. e821–e826, 2008.

[161] S. S. Ge and C. H. Fua, "Queues and artificial potential trenches for multi-robot formations," *IEEE Transactions on Robotics*, vol. 21, no. 4, pp. 646–656, August 2005.

[162] S. S. Ge, "Social robotics: Integrating advances in engineering and computer science," in *Proc. of the 2007 Electrical Engineering/Electronics, Computer, Telecommunications and Information Technology (ECTI) Int. Conf.*, Chiang Rai, Thailand, May 2007, pp. xvii–xxvi, keynote Speech.

[163] S. S. Ge, A. P. Loh, and F. Guan, "Robust sound localization using lower number of microphones," *International Journal of Information Acquisition*, vol. 2, no. 1, pp. 1–22, 2005.

[164] ——, "3d sound localization based on audio and video," in *Proceedings of Fourth International Conference on Control and Automation*, Montreal, Canada, June 2003, pp. 168–172.

[165] S. S. Ge, C. Wang, and C. C. Hang, "Facial expression imitation in human robot interaction," in *Proceeding of 17th IEEE International Symposium on Robot and Human Interactive Communication. RO-MAN 2008.*, Munich, Germany, Aug. 1-3 2008, pp. 213–218.

[166] A. J. W. van der Kouwe, D. L. Wang, and G. J. Brown, "A comparision of auditory and blind separation techniques for speech segregation," *IEEE Transactions on Speech and Audio Processing*, vol. 9, no. 3, pp. 189–195, 2001.

[167] A. S. Bregman, *Auditory scene analysis : the perceptual organization of sound*. cambridge, Mass: MIT Press, 1990.

[168] J. Chen, B. D. Van-Veen, and K. E. Hecox, "External ear transfer function modeling: a beamforming approach," *Journal of the Audio Engineering Society*, vol. 4, pp. 1933–1944, 1992.

[169] J. Blauert, *Spatial Hearing - Revised Edition: The Psychophysics of Human Sound Localization*, J. Blauert, Ed. Cambridge, MA: The MIT Press, October 1996.

[170] S. T. Roweis and L. K. Saul, "Nonlinear dimensionality reduction by locally linear embedding," *Science*, vol. 290, pp. 2323–2326, 2000.

[171] S. S. Ge, F. Guan, A. P. Loh, and C. H. Fua, "Feature representation based on intrinsic structure discovery in high dimensional space," in *Proceedings of the 2006 IEEE International Conference on Robotics and Automation*, Orlando, Florida, USA, May 2006, pp. 3399–3404.

[172] K. Fukunaga and L. Hostetler, "Optimization of k-nearest neighbor density estimates," *IEEE Trans. Inf. Theory*, vol. 19, no. 3, pp. 320–326, 1973.

[173] R. D. Short and K. Fukunaga, "The optimal distance measure for nearest neighbor classification," *IEEE Trans. Inf. Theory*, vol. 27, no. 5, pp. 622–627, 1981.

[174] K. Fukunaga and T. E. Flick, "An optimal global nearest neighbor metric," *IEEE Trans. Pattern Anal. Mach. Intelligence*, vol. 6, no. 3, pp. 314–318, 1984.

[175] P. R. Schrater, D. C. Knill, and E. P. Simoncell, "Perceiving visual expansion without optic flow," *Nature*, vol. 410, pp. 816–819, 2001.

[176] P. N. Yianilos, "Normalized forms for two common metrics, Technical Memorandum," December 1991.

[177] D. Haussler, "Decision theoretic generalizations of the pac model for neural net and other learning applications," *Information and Computation*, vol. 100, no. 1, pp. 78–150, 1990.

[178] M.-H. Yang, D. J. Kriegman, and N. Ahuja, "Detecting faces in images: a survey," *IEEE Transactions on Pattern Analysis and Machine Intelligence*, vol. 24, no. 1, pp. 34 –58, January 2002.

[179] W. Zhao, R. Chellappa, P. J. Phillips, and A. Rosenfeld, "Face recognition: A literature survey," *ACM Computing Surveys*, vol. 35, no. 4, pp. 399–458, 2003.

[180] P. Viola and M. Jones, "Rapid object detection using a boosted cascade of simple features," in *Conference on Computer Vision and Pattern Recognition*, 2001, pp. 511–518.

[181] ——, "Robust real-time face detection," *International Journal of Computer Vision*, vol. 57, no. 2, pp. 137–154, 2004.

[182] C. S. Zhang, J. Wang, N. Y. Zhao, and D. Zhang, "Reconstruction and analysis of multi-pose face images based on nonlinear dimensionality reduction," *Pattern Recognition*, vol. 37, no. 2, pp. 325–336, February 2004.

[183] C. H. Lee, J. S. Kim, and K. H. Park, "Automatic human face location in a complex background using motion and color information," *Pattern Recognition*, vol. 29, no. 11, pp. 1877–1889, November 1996.

[184] Y. Dai and Y. Nakano, "Face-texture model based on sgld and its application in face detection in a color scene," *Pattern Recognition*, vol. 29, no. 6, pp. 1007–1017, June 1996.

[185] B. L. Zhang, H. Zhang, and S. S. Ge, "Face recognition by applying wavelet subband representation and kernel associative memory," *IEEE Transactions on Neural Networks*, vol. 15, no. 1, pp. 166 – 177, January 2004.

[186] S. S. Ge, Y. Yang, T. H. Lee, and C. Wang, "Facial expression recognition and tracking for intelligent human-robot interaction," *Journal of Intelligent Service Robotics - Special Issue*, vol. 1, no. 2, pp. 143–157, 2008.

[187] Y. Pan, S. S. Ge, and A. A. Mamun, "Weighted locally linear embedding for dimension reduction," *Pattern Recognitioin*, vol. 42, pp. 798–811, 2009.

[188] S. Z. Li, S. Member, and Z. Zhang, "Floatboost learning and statistical face detection," *IEEE Transactions on Pattern Analysis and Machine Intelligence*, vol. 26, no. 9, pp. 1112–1123, 2004.

[189] C. Huang, H. Ai, Y. Li, and S. Lao, "Vector boosting for rotation invariant multi-view face detection," *IEEE Transactions On Pattern Analysis and Machine Intelligence*, vol. 29, no. 4, pp. 671–686, 2007.

[190] I. Haritaoglu, D. Harwood, and L. S. Davis, "W4: Real-time surveillance of people and their activities," *IEEE Transactions On Pattern Analysis and Machine Intelligence*, vol. 22, no. 8, pp. 809–830, 2000.

[191] G. Luca, L. Marcenaro, and C. S. Regazzoni, "Automatic detection and indexing of video-event shots for surveillance applications," *IEEE Transactions on Multimedia*, vol. 4, no. 4, pp. 459–471, December 2002.

[192] S. Z. Li, L. Zhou, Z. Zhang, A. Blake, H. Zhang, and H. Shum, "Statistical learning of multi-view face detection," in *Proceedings of the 7th European Conference on Computer Vision (ECCV)*, 2002, pp. 67–81.

[193] S. Z. Li, Z. Zhang, and H. Zhang, "Learning to detect multi-view faces in real-time," in *Proceeding of the 2nd international conference on development and learning (ICDL'02)*, 2002.

[194] B. Froba and A. Ernst, "Fast frontal-view face detection using a multi-path decision tree," in *International Conference on Audio- and Video-based Biometric Person Authentification (AVBPA)*, 2003, pp. 921–928.

[195] L. Y. Li, W. M. Huang, I. Y. H. Gu, and Q. Tian, "Statistical modeling of complex background for foreground object detection," *IEEE Transactions On Image Processing*, vol. 13, no. 11, pp. 1459–1472, 2004.

[196] "Open source computer vision library," Intel Corporation, 2001. [Online]. Available: www.cs.unc.edu/Research/stc/FAQs/OpenCV/OpenCVReferenceManual.pdf

[197] R. E. Schapire, "The boosting approach to machine learning an overview," in *MSRI Workshop on Nonlinear Estimation and Classification*, Berkeley, California, March 19-29 2001, pp. 709–715.

[198] Y. Ito, "Approximation of functions on a compact set by finite sums of a sigmoid function without scaling," *Neural Networks*, vol. 4, pp. 817–826, 1991.

[199] K. Hornik, "Approximation capabilities of multilayer feedforward networks," *Neural Networks*, vol. 4, pp. 251–257, 1991.

[200] Y. Ito, "Approximation of continuous functions on $\mathbf{R}^d$ by linear combinations of shifted rotations of a sigmoid function with and without scaling," *Neural Networks*, vol. 5, pp. 105–115, 1992.

[201] M. Leshno, V. Y. Lin, A. Pinkus, and S. Schocken, "Multilayer feedforward networks with a nonpolynomial activation function can approxiamate any function," *Neural Networks*, vol. 6, pp. 861–867, 1993.

[202] H. A. Rowley, S. Baluja, and T. Kanade, "Neural network-based face detection," *IEEE Transactions On Pattern Analysis and Machine intelligence*, vol. 20, pp. 23–38, 1998.

[203] ——, "Rotation invariant neural network-based face detection," in *Proceeding of IEEE Computer Society Conference on Computer Vision and Pattern Recognition(CVPR'98)*, Santa Barbara, CA, USA, June 23-25 1998, pp. 38–44.

[204] G.-B. Huang, Q.-Y. Zhu, and C.-K. Siew, "Extreme learning machine: Theorey and applications," *Neurocomputing*, vol. 70, pp. 489–501, 2006.

[205] G. B. Huang, L. Chen, and C. K. Siew, "Universal approximation using incremental constructive feedforward networks with random hidden nodes," *IEEE Transactions On Neural Networks*, vol. 17, no. 4, pp. 879–892, 2006.

[206] D. Serre, *Matrices: Theory and Applications*. Springer-Verlag New York, Inc, 2002.

[207] C. R. Rao and S. K. Mitra, *Generalized Inverse of Matrices and Its applications*. New York: John Wiley & Sons, Inc, 1971.

[208] D. B. Graham and N. Allinson, "Umist face database," 1998. [Online]. Available: http://images.ee.umist.ac.uk/danny/database.html

[209] F. Guan, L. Y. Li, S. S. Ge, and A. P. Loh, "Robust human detection and identification by using stereo and thermal images in human robot interaction," *International Journal of Information Acquisition*, vol. 4, no. 2, pp. 161–183, 2007.

[210] D. Huang and C. Xiang, "A novel LDA algorithm based on approximate error probability with application to face recognition," in *ICIP 2006*, 2006, pp. 653–656.

[211] C. Xiang, X. Fan, and T. H. Lee, "Face recognition using recursive fisher linear discriminant," *IEEE Transactions on Image Processing*, vol. 15, no. 8, pp. 2097–2105, 2006.

[212] B. Scholkopf, A. Smola, and K. R. Muller, "Nonlinear component analysis as a kernel eigenvalue problem," *Neural Computation*, vol. 10, no. 5, pp. 1299–1319, 1998.

[213] J. Lu, K. N. Plataniotis, and A. N. Venetsanopoulos, "Face recognition using kernel direct discriminant analysis algorithms," *IEEE Transactions on Neural Networks*, vol. 14, no. 1, pp. 117–126, 2003.

[214] J. Yang, A. F. Frangi, J. yu Yang, D. Zhang, and Z. Jin, "KPCA plus LDA: A complete kernel fisher discriminant framework for feature extraction and recognition," *IEEE Transactions on Pattern Analysis and Machine Intelligence*, vol. 27, no. 2, pp. 230–244, 2005.

[215] S. T. Roweis and L. K. Saul, "Think globally, fit locally: Unsupervised learning of low dimensional manifolds." *Journal of Machine Learning Research*, vol. 4, pp. 119–155, June 2003.

[216] C. Y. Zhou and Y. Q. Chen, "Improving nearest neighbor classification with cam weighted distance," *Pattern Recognition*, vol. 39, pp. 1–11, 2006.

[217] E. Pekalska, A. Harol, R. Duin, B. Spillmann, and H. Bunke, "Non-euclidean or non-metric measures can be informative," in *Structural, Syntactic, and Statistical Pattern Recognition*, 2006, pp. 871–880.

[218] D. B. Graham and N. M. Allinson, "Characterizing virtual eigensignatures for general purpose face recognition," in *Face Recognition: From Theory to Applications, NATO ASI Series F, Computer and Systems Sciences*, H. Wechsler, P. J. Phillips, V. Bruce, F. Fogelman-Soulie, and T. S. Huang, Eds., 1998, vol. 163, pp. 446–456.

[219] J. Tenenbaum, V. de Silva, and J. C. Langford, "A global geometric framework for nonlinear dimensionality reduction," *Science*, vol. 290, pp. 2319–2323, 2000.

[220] M. Belkin and P. Niyogi, "Laplacian eigenmaps for dimensionality reduction and data representation," *Neural Computation*, vol. 15, no. 6, pp. 1373–1396, 2003.

Appendix A

Local Linear Embedding (LLE)

The problem LLE attempts to solve is: given a set $X = [x_1, x_2, \ldots, x_N]$, where $x_i (i = 1, \ldots, N)$ is i^{th} node on a high dimensional manifold embedded in R^D, i.e., $x_i \in R^D$, and then find a set $Y = [y_1, y_2, \ldots, y_N]$ in R^d, where $d \ll D$ such that the intrinsic structure in X can be represented by that of Y. This can be done using three major steps.

A.1 Neatest Neighborhood Construction

We firstly attempt to express data point x_i as a linear combination of its k nearest neighbors $x_j,\ j = 1, 2, \ldots, k$.

$$\hat{x}_i = \sum_{j \in \Omega_i} w_{ij} x_j, \tag{A.1}$$

where Ω_i is the neighborhood of sample x_i. The neighborhoods can be constructed according to a KNN rule or to consist of all points inside a ball around x_i with radius ϵ (known as ϵ-neighborhoods [220]). In the original algorithm the standard Euclidean metric based KNN is used to select the nearest neighbors. However, many other novel approaches can be

utilized for constructing neighborhoods to form new method.

A.2 Optimization of Reconstruction Weights

Once the data point x_i is expressed as a linear combination of its k nearest neighbors $x_j,\ j = 1, 2, \ldots, k$, the optimal weight matrix w_{ij} for data reconstruction can be obtained by minimizing the approximation error cost function

$$\epsilon(W_i) \quad = \quad \sum_i d_W \left(x_i, \sum_{j \in \Omega_i} w_{ij} x_j \right)^2, \tag{A.2}$$

subject to the constraints

$$j \notin \Omega_i \Rightarrow w_{ij} \quad = \quad 0 \tag{A.3}$$

$$\sum_{j \in \Omega_i} w_{ij} \quad = \quad 1, \tag{A.4}$$

where $w_i = [w_{i1}, \ldots, w_{ik}]$ is the weights connecting sample x_i to its neighbors. The function $d_W(\cdot, \cdot)$ is an appropriate distance measure. The first constraint says that only data points in the neighborhood of data point x_i should be used in the reconstruction of $\hat{x}_i$, while the second constraint imposes invariance to translation.

To see how a closed form solution can be obtained, we use Euclidean metric as $d_W(\cdot, \cdot)$ for example. In order to use a Lagrange multiplier η_i, we rewrite the approximation error cost function (A.2) as:

$$\begin{aligned} \epsilon(W_i) &= \|x_i - \hat{x}_i\| \\ &= \left\| x_i \sum_{j \in \Omega_i} w_{ij} - \sum_{j \in \Omega_i} (w_{ij} x_j) \right\| \\ &= \sum_{j \in \Omega_i} w_{ij} \sum_{k \in \Omega_i} w_{ik} (x_i - x_j)^T (x_i - x_k). \end{aligned} \tag{A.5}$$

By defining

$$C_i(j,k) = (x_i - x_j)^T(x_i - x_k) \tag{A.6}$$

and applying a Lagrange multiplier η_i, the approximation error becomes

$$\epsilon(W_i) = \sum_{j\in\Omega_i} w_{ij} \sum_{k\in\Omega_i} w_{ik} C_i(j,k) + \eta_i(\sum_{j\in\Omega_i} w_{ij} - 1). \tag{A.7}$$

The optimal weights are found by requiring the partial derivatives with respect to each weight w_{ij} to be zero,

$$\frac{\partial\epsilon(W_i)}{\partial w_{ij}} = 2\sum_{k\in\Omega_i} w_{ik} C_i(j,k) + \eta_i = 0,\ \forall j \in \Omega_i. \tag{A.8}$$

By setting the value of η_i, the desired solution w_i is found by simply solving the equations,

$$\sum_{k\in\Omega_i} C_i(j,k) w_{ik} = 1, \tag{A.9}$$

and then re-scale the weights so that they sum to one.

In unusual cases, it can arise that the matrix (A.6) is singular or nearly singular. In that case, the least square problem for finding the weights does not have a unique solution. As such, in order to guarantee numerical stability we regulate C by

$$C_i(j,k) \leftarrow C_i(j,k) + \eta_r I, \tag{A.10}$$

where $\eta_r << \text{trace(C)}$ is a small constant to be defined as part of the algorithm. I is identical matrix.

A.3 Mapping to Low-dimensional Embedding

The final step of LLE is to compute a low dimensional embedding of the high dimensional inputs x_i based on the reconstruction weights w_{ij}. The high dimensional data are mapped

into the low dimensional space R^d by requiring reconstruction to work as well as possible. This leads to another minimization problem [171]. The low dimensional outputs $y_i,\ i = 1, 2, \ldots, N$ are found by minimizing the cost function,

$$\Phi(Y) = \sum_i d_W \left(y_i, \sum_{j \in \Omega_i} w_{ij} y_j \right)^2, \tag{A.11}$$

where $Y = [y_1, \ldots, y_N]$ consists of the data points embedded into the low dimensional space. This minimization problem is not well-posed without further constraints. Zero mean and unity covariance is used in the LLE algorithm to make the problem well-posed. In other words Y should obey the constraints

$$\sum_{i=1}^{N} y_i = \mathbf{0} \tag{A.12}$$

$$\frac{1}{N} Y Y^T = \mathbf{I}, \tag{A.13}$$

where $\mathbf{0}$ is a vector with all elements being zero, and $\mathbf{I}$ is a identical matrix. The first constraint is to assure that coordinates y_i can be translated by a constant displacement without affecting the cost, while the second constraint imposes unit covariance of the embedding vectors.

For the case that $d_W(\cdot, \cdot)$ is the Euclidean metric, rewrite cost function on matrix form as:

$$\begin{aligned} \Phi(Y) &= \mathrm{Tr}\left[(\mathrm{Y} - \mathrm{YW})^{\mathrm{T}}(\mathrm{Y} - \mathrm{YW})\right] \\ &= \mathrm{Tr}\left[(\mathrm{Y} - \mathrm{YW})(\mathrm{Y} - \mathrm{YW})^{\mathrm{T}}\right] \\ &= \mathrm{Tr}\left[\mathrm{Y}(\mathrm{I} - \mathrm{W})(\mathrm{I} - \mathrm{W})^{\mathrm{T}}\mathrm{Y}^{\mathrm{T}}\right] \\ &= \mathrm{Tr}\left[\mathrm{YMY}^{\mathrm{T}}\right], \end{aligned} \tag{A.14}$$

where the symmetric matrix

$$M = (I - W)(I - W)^T. \tag{A.15}$$

The minimum of $\Phi(Y)$ in Equation (A.14) subject to the constraint of Equation (A.13) can be obtained by finding the d smallest eigenvectors of M. The minimal value of $\Phi(Y)$ equals the sum of the eigenvalues of M. Notice that

$$M\mathbf{1} = (I - W)(I - W)^T\mathbf{1} = 0, \tag{A.16}$$

due to the requirement $\sum_{j\in\Omega_i} w_{ij} = 1$. Therefore the smallest eigenvalue is automatically zero with corresponding eigenvector $\mathbf{1}$. Since the eigenvectors are mutually orthogonal, it fulfills the constraint of Equation (A.12). To summarize, the d dimensional embedding $Y \in R^{d\times N}$ consists of eigenvector number $2, \ldots, d+1$ as its rows.

Appendix B

Author's Publications

Journal and Magazine:

[**1**] **Y. Pan**, S. S. Ge, and A. A. Mamun, "Weighted Locally Linear Embedding for Dimension Reduction", *Pattern Recognition*, vol. 42, no. 5, pp. 798-811, 2009.

[**2**] S. S. Ge, F. Guan, **Y. Pan** and A.P. Loh, "Neighborhood Linear Embedding for Intrinsic Structure Discovery", *Machine Vision and Applications*, (online first) DOI:10.1007/s00138-008-0169-4, available online: http://dx.doi.org/10.1007/s00138-008-0169-4, 2008.

[**3**] S. S. Ge, **Y. Pan**, " Breathing Life into Machines" (COVER STORY), *INNOVATION: the Magazine of Research and Technology*, vol. 8, no. 3, pp. 12-13, 2008.

Conference:

[**1**] **Y. Pan**, S. S. Ge, and A. A. Mamun, "Nonlinear Control of Synaptic Plasticity Model for Constraining Bursting Activity in Epileptic Seizures", *Proceedings of the 2007*

American Control Conference, New York City, USA , pp. 2012-2017, 2006.

[**2**] **Y. Pan**, S. S. Ge, F. R. Tang and A. A. Mamun, " Detection of Epileptic Spike-Wave Discharges Using SVM", *Proceedings of the 2007 IEEE International Conference on Control Applications*, Suntec City, Singapore, pp. 467-472, 2007.

[**3**] S. S. Ge, **Y. Pan**, A. A. Mamun, "Methodologies on Brain-Machine Interaction", *Proceedings of 17th World Conference, The International Federation of Automatic Control (IFAC) 2008*, Seoul, Korea, pp. 13779-13784, July 6-11, 2008.

[**4**] **Y. Pan**, S. S. Ge, A. A. Mamun and E. Brekke, "Sound Source Recognition for Human Robot Interaction", *Proceedings of 17th IEEE International Symposium on Robot and Human Interactive Communication (RO-MAN 2008)*, Munich, Germany, pp. 604 - 609, 1-3 Aug. 2008.

[**5**] **Y. Pan**, S. S. Ge, A. A. Mamun and F. R. Tang, "Detection of Seizures in EEG Signal using Weighted Locally Linear Embedding and SVM classifier", *3rd IEEE International Conference on Cybernetics and Intelligent Systems (CIS) 2008*, Chengdu, China, pp. 358 - 363, 21-24 Sept. 2008.

[**6**] **Y. Pan**, S. S. Ge and H. He, "Face Recognition Using ALLE and SIFT for Human Robot Interaction", Advances in Robotics, FIRA RoboWorld Congress, vol. 5744, Lecture Notes in Computer Science, pp. 53-62, Springer, 2009.

[**7**] S. S. Ge, **Y. Pan**, Q. Zhang, and L. Chen, "Equivalent Relationship of Feedforward Neural Networks and Real-Time Face Detection System", Advances in Robotics, FIRA RoboWorld Congress, vol. 5744, Lecture Notes in Computer Science, pp. 301-310,

Springer, 2009.

[8] **Y. Pan**, S. S. Ge, H. He, L. Chen, "Face Detection for Human Robot Interaction of Social Robots", accepted by IEEE RO-MAN 2009.

[9]**Y. Pan**, S. S. Ge, Q. Z. Goh, and K. S. Hong, "Mind Robotic Rehabilitation based on Non-Invasive Motor Imagery Brain Computer Interface", *submitted to 2010 IEEE International Conference on Robotics and Automation.*